

Reply to Reviews for "Greenland Ice Sheet discharge from 2000 to 2018"

K. D. Mankoff & Co-Authors

Comments from reviewers are in normal font and differentiated from the replies that use a **bold colored font**. Most changes are tracked in the document showing changes between versions, but latexdiff sometimes fails with reference changes, so many references to the new Mouginot et al. (2019) are not highlighted. In addition, changes to graphics and the bibliography are not highlighted.

This single PDF contains the reply to the reviewers, the revised document highlighting most of the changes, and then the revised document without changes highlighted.

Contents

1	Reply to Editor	2
2	Reply to Reviewer #1 Ellyn Enderlin (Referee) doi:10.5194/essd-2019-29-RC1	2
2.1	Major Comments	2
2.2	Minor Comments	3
3	Reply to Reviewer #2 doi:10.5194/essd-2019-29-RC2	4
3.1	Major Comments	4
3.1.1	Treatment of Velocity Data	4
3.1.2	Temporal Averaging	6
3.1.3	Automated Flux Gate Selection Algorithm	6
3.2	Minor Comments	7
4	References	11
5	Revised Document Showing Changes	12
6	Revised Document	48

1 Reply to Editor

We are happy to read these reviews due to their general support of our work and constructive suggestions. Our revised text has addressed all of the reviewer comments and we also reply explicitly to each comment below.

We have removed two figures (the velocity and thickness histograms) because the information contained in those is also contained in the 2D velocity v. thickness histogram.

2 Reply to Reviewer #1 Ellyn Enderlin (Referee) [doi:10.5194/essd-2019-29-RC1](https://doi.org/10.5194/essd-2019-29-RC1)

2.1 Major Comments

Since one of the major arguments the authors make is that the use of flux gates that are picked in an automated way is superior over manually-traced gates, I'd like a bit more thorough description of the method used to pick the flux gates. I follow that you apply a 5000m buffer to all ice inland of the terminus but it is less clear what you mean when you say you "select" fast-flowing ice. Do you essentially place the flux gate at the 100m/yr flow contour? If this is the case, then I imagine that in some regions the flux gate is closer than 5000m from the terminus but the rest of section 3.2 suggests that the gates are a fixed location of 5000m inland of the terminus. The addition of a schematic to illustrate the method would be helpful because the few panels in Figure 1 have arcuate geometries that seem independent of flow speed.

We have clarified the text, but to answer the question here, when we "select" fast-flowing ice we do not place a gate at a 100 m yr⁻¹ contour - we use a 2D raster mask for all ice with speed > 100 m yr⁻¹. Then, from this subset, we find the ice edge. The ice edge is the contour line only where the fast ice is near the ocean mask, not all segments of the contour where the fast ice is bounded by slow ice, or land. We then buffer the edge 5000 m in all directions (over slow ice, into the fjord or coastal sea, etc.) creating an oval-like shape around each terminus. We then crop this circular-ish feature by the fast ice mask from the previous step. The result is an arc segment from the circular-ish feature that transects only the fast ice. We call this the gate.

For the interpolation/extrapolation of speed and thickness, why did you use linear interpolation techniques? For the speeds, linear interpolation may introduce considerable aliasing effects, particularly if there are large data gaps around times of rapid change (like the peak in speed in the SE in 2005).

We used a linear interpolation to fill in velocity because we opted for simplicity where possible. Aliasing may be introduced, and we now note that in the text. The method used by King et al. (2018) improves on our method in some situations, but we feel it is not appropriate in others – using past-as-predictor in a changing system means the changes may not be treated properly. Specifically, Jakobshavn no longer appears to be following the annual cycle, so a model that is based on statistical monthly behavior may not be appropriate.

For the thickness data, why did you use the average of the last 3 years with data to estimate thickness for 2017-2018? Was flow relatively steady during this time? Are your results considerably influenced if you would use only the last 1-2 years or expand to include a longer time period? For the speeds you simply use the closest observation at the ends of the time series. Why use a different approach for thickness?

We back- and forward-fill speed (extend rather than extrapolate) because speed has a highly variable second derivative so extrapolation will introduce larger errors than extension. That is, extrapolation is sensitive to the last trend, while extension, which effectively assumes steady state, is safer for the points back-filled in the early 1990s.

We used linear for thickness interpolation because that was the best fit among the four relationships (linear & \log_{10} for velocity & speed) we explored. We could get a much better correlation coefficient if we used discharge for the dependent variable as in Enderlin et al. (2014), but we were unable to justify that decision because the relationship is then a form of self-correlation – velocity exists in both terms and they are highly co-dependent, but the correlation coefficient test assumes variables are independent.

We chose to use a 3-year smooth after examining the rate of change of 2-year or 1-year. We chose this as a subjective value. It does not have a large effect on the early part of the time series – rates of change are low in the 90's.

2.2 Minor Comments

p. 3, l. 11: Replace “200 m per pixel” with “200m pixel”

Done.

p. 7, l. 5: If I understand this correctly, then all of your discharge uncertainty is from thickness uncertainty. Is this correct?

Correct. We now explain in the text (and show in the supplemental material) that proportional velocity uncertainty is an order of magnitude less than proportional thickness uncertainty. Adding velocity uncertainty and treating it as random w.r.t. thickness uncertainty would add a small amount to the total uncertainty. Because we are already conservative in our uncertainty estimate, we choose to ignore this small additional uncertainty.

p. 7, l. 24: Remove “both”

Done.

p. 8, l. 3: Is there a particular reason why you use 150Gt/yr as the cutoff here? Is this the estimated balance discharge?

No, this was simply a rounded estimate (from 148 Gt yr⁻¹) of the current discharge. This text has been removed.

p. 8, l. 15-21: The numbers presented in this section indicate that the flux is the area-normalized volume flow rate. Is this correct? I think that most readers would stumble in this section since it is not apparent from the start that the flux is normalized. I normally think of flux as a volume flow rate and I was perplexed by the seemingly contradictory statements in the first sentence until I looked at the flux units.

We used "volume flow rate" incorrectly when it was "mass flow rate". Mass flux by definition is area normalized with dimensions [mass time⁻¹ length⁻²]. Flux is not flow rate. We explicitly use the term "mass flow rate" throughout the document when referring to a product with dimensions [mass time⁻¹]. We have removed this section based comments from both reviewers.

p. 9, l. 19: The Enderlin et al. (2014) paper used bed elevations from radar picks. Examination of the original interpreted data for Koge Bugt suggest the bed was much deeper than the updated (and BedMachine) dataset. It is likely that the Bamber et al. (2013) bed map used the same radar data as Enderlin et al. (2014). (This comes up again on p. 11, l. 5.)

Thank you for clarifying and we have revised the text accordingly.

p. 9, l. 26: The use of Khan et al. (2016) surface elevation adjustments may also play a role since the Enderlin et al. (2014) elevations are directly extracted from DEMs and Operation IceBridge lidar timeseries.

Correct, and we have revised the text to reflect this.

3 Reply to Reviewer #2 [doi:10.5194/essd-2019-29-RC2](https://doi.org/10.5194/essd-2019-29-RC2)

3.1 Major Comments

3.1.1 Treatment of Velocity Data

On Page 10, line 5, the authors state that the signal to noise ratio may be reduced at the individual glacier level but that this noise is not apparent in the total ice sheet discharge time series. I disagree with this assertion and will highlight an example that I think demonstrates the need for a more careful treatment of outliers.

We agree with the reviewer that our use of unprocessed velocity data was not sufficient. In the revised text we now have a "Invalid Velocity" in addition to a "Missing Velocity" section and exclude outliers based on a standard deviation test.

We want to produce the best possible discharge product but at the same time we must rely on upstream data producers and cannot recreate them all from first principles. If we did, our results would certainly be less accurate than the existing products. We therefore have decided to do some additional processing of upstream products as you suggest (and as we already did for the ice thickness data). We also hope to make extensive use of the ESSD "Living Data" option and when updated velocity products are released, presumably each at higher fidelity, we will incorporate those.

Unfortunately, it seems extremely difficult to develop a filter that flags noise but not real speed-up events. With velocity products now spanning shorter and shorter durations, they will begin to capture the noisy and dynamic true velocity of glaciers, which sometimes do exhibit 10 or 100 % speed-ups over short time periods. We also note that while you have highlighted a case where there is a low point between two high, in general the noise is high, and filtering reduces discharge. This implies that either the velocity errors are not evenly distributed, or true velocity increases are being filtered, because we know from glacier behavior that short-term changes are almost always speed-up events and not slow-down events.

The filter we selected (30 point moving mean, removing 2-sigma outliers, run 3x) appears to remove all outliers, but likely removes some real velocity spikes too. Our treatment reduces GIS annual average discharge by ~1% in most years, up to 4% in years with high discharge, and more in the 1980s when the data is noisy. We explain this in the revised text and add a section to the Appendix showing the same (filtered) time-series from the main paper text, but un-filtered.

Distinct spikes are apparent in the Greenland total graph (Figure 6) from the ~monthly data in 2011 and 2013. These seem to be primarily the result of similar spikes in the SE sector (Figure 7). In the SE in 2011, there is a rapid fall of ~50 Gt (30%) and a subsequent rise again of ~40 Gt all within a ~3-month period, which is physically improbable.

Looking more closely at the top 7 individual glacier plots in Figure 8, we see that the sector spike in 2011 is an artifact of discharge at Køge Bugt Glacier (located in the SE), which increases from a baseline of < 20 Gt/yr to over 40 Gt/yr in 1-2 months. Given the usage of annual surface elevations used in this study, this change must then be due to velocity, and would require an acceleration of over 100% in a very short time period. Below are velocity time series taken from Joughin et al. (2018) (<https://doi.org/10.5194/tc-12-2211-2018>), which shows no such dramatic acceleration during that time. From my quick glance at the individual glacier discharge data accompanying this manuscript, several other glaciers also occasionally exhibit large, abrupt changes that I suspect are untreated outliers.

Similarly, the next SE sector spike in 2013 is not present in either Køge Bugt or Kangerlussuaq Glacier, which are the largest two glaciers in this sector. This would mean that the remaining glaciers in the SE sector (which I estimate from the figure to roughly account for an average ~100 Gt/yr) would have to compensate for the ~50 Gt/yr increase. I'm skeptical of this because, to my knowledge, such an abrupt and short-lived acceleration in 2013 has not been previously documented.

These examples show that although signal noise at individual glaciers will typically be mitigated in the total ice sheet time series, large outliers at the more prominent glaciers will propagate to the sector-wide time series and also possibly to the total time series and impact annual averages. The outlier problem is amplified when linear temporal averaging is applied using noisy data points. I think the data quality could be improved by a simple low-pass filter, which would also make the individual glacier time series more robust for those who may use the data for local studies. It may be helpful to reference the velocity

maps/mosaics associated with outlying points to assess if the pixels are particularly noisy at that time.

We agree and have applied a filter prior to the linear temporal averaging step.

3.1.2 Temporal Averaging

How are annual averages computed from the nonuniform time series? I suspect that the series are resampled at uniform intervals prior to averaging, but this is not explicitly described in the manuscript. Even if resampled at equal intervals, the use of linear interpolation for missing time periods means that there is an inherent sampling bias that the authors should estimate, though it may be small. This could be done using the reference period with dense temporal coverage.

We explored two temporal filling options:

- 1. Annual average of samples**
- 2. Resample to daily resolution with linear interpolation, then compute annual average**

We use method 2, similar to Joughin et al. (2018) and now state this explicitly. The difference between the methods is small in most years. The average across all years is < 5 % and the median < 3%. In theory and when using clean or modeled discharge estimates as in King et al. (2018), the error should be ~6% at worst, because seasonal discharge variability is ~6% (King et al. 2018).

We have updated the text to clarify this method and its possible effects.

3.1.3 Automated Flux Gate Selection Algorithm

I'd like to see more details on the algorithm included in the manuscript, especially since the automated algorithm is the key strength of this work. Some details are commented throughout the code samples, but it requires digging. I suggest a methods section describing the algorithm development that at minimum addresses:

#1 If and how frequent manual adjustments are needed due to continued retreat (terminus retreats behind 5km upstream of GIMP-determined terminus).

No adjustments are needed because we set gates using the baseline period, years 2015, 2016, and 2017. There has been no retreat (that we have detected) > 5 km since then. We state that although the gates can be moved, and are for Fig. 2, they are not for the rest of the work.

#2 The treatment of unconfined, radially-draining catchments – do they require additional corrections as shape and direction of dominant flow change?

No. The gate is defined 1x and, in this work, is stationary. It is true that over time some edge pixels might cross the threshold from greater than or equal to 100 m yr⁻¹ to less than 100 m yr⁻¹, and then slower ice would be included in the discharge estimate. Similarly, some ice initially excluded due to flow less than 100 m yr⁻¹ may increase,

but not be included. We assume these edge cases are insignificant. Gate location and flow direction are independent. At each time step we calculate gate-orthogonal flow. This was described at the end of the discussion section (wrong location) in the submitted document. The text has now been moved to the methods section, but is again discussed briefly at the end of the discussion section.

#3 Brief description of treatment of floating ice shelves. By termini selection, do you mean grounding ice mask from BedMachine/GIMP or glacier front?

We have added text explaining that we are referring to grounding line mask.

#4 the algorithm ever require “unfiltering” originally excluded pixels after gate migration? For example, though most glaciers accelerate toward the terminus, if a pixel 5 km upstream of a slow moving near-terminus pixel exceeds the 100 m/yr threshold, is it still excluded, or retroactively filled along the gate? I suspect this would only happen in some instances at radially-draining glaciers.

Gates do not migrate. There is an additional case opposite to the one you describe above. If a fast terminus does not have fast ice upstream of it, the gate would not be positioned there. We have performed a limited manual inspection of the algorithm at each step and have observed one of these situations. I found one small glacier on the north west coast that had fast ice near the ice edge, but no fast ice inland, and therefore no gate. Given the size of this glacier - just a few pixels wide, I let the algorithm exclude it. Similarly, I examined the initial fast ice mask for locations where the mask does not reach the coast where I would expect it to. I did not see anywhere where this occurred. These two examinations were not exhaustive.

We are reasonably confident we have gates where anyone else ever placed gates manually, and then some more.

3.2 Minor Comments

Title and use of ‘2000-2018’ period: The figures and the description that the period studied as ‘18 year’ (abstract) indicate that the time series extends through the end of 2017 and excludes data from 2018. While the use of 2000 ‘to’ 2018 could be taken to mean ‘up until’ 2018, ‘2000 to 2018’ and ‘20XX to 2017’ are interchangeably used throughout the manuscript and it is confusing to the reader which exact period is being referenced. For example, an average discharge from 2010 to 2017 is mentioned on line 6 of the abstract. Based on the usage of the title, is this taken to mean the average was calculated over the period 2010 through 2016, excluding 2017? Similarly, on page 7, line 27, a sector average is described over the 2007 to 2017 period. If the terminology is consistent and this does indeed refer to 2007 through 2016, why is 2017 excluded in these instances? Otherwise, please consider either replacing ‘2000 to 2018’ with ‘2000 through 2017’, or editing the remaining ‘to 2017’ references for consistency.

We apologize for the inconsistency and typos. We’ve decided that "through 2017" is the clearest phrasing and have changed all text to reflect this.

Page 2, Equation 1: Perhaps specify that A is area (even though it's intuitive) so that all terms are defined.

Done.

Page 2, Line 5: "...and Q is the volumetric flow rate". This makes it sound like Q should be in Equation 1. Are you defining now for later use? If the term is not used again it might be best to omit.

Q is in Eq. 1, but we've changed the text. Q is now the discharge flux (although the section of the text about discharge flux has been removed). Flux integrated over gate area equals flow rate.

Page 3, Line 2: Contribute should be "contribution"

Done.

Page 5, Line 20: The use of 917 kg/m³ density value should be noted again in the discussion when comparing to previous studies as it could be another, albeit small, source of difference.

We mention the density value we use twice in the methods, and once point out that others may use a reduced value if considering firm or crevasses. We don't see why anyone would use a value more dense than 917 kg m⁻³. This suggests the difference between our estimates and others who did use a reduced density is even larger than we show here.

Because there are so many different reasons others may have different estimates, we disagree with the need to explicitly mention density in the discussion, especially since that would not be likely to explain any differences, but rather increase differences.

3.4.1 Missing Velocity Do the reported stamps refer to the time span midpoint, or the first date of the time span (first image)?

We use the middle of the time spans when provided and now clarify this.

Page 6, Line 23: "This thickness adjustment adds 21 Gt to our baseline-period discharge estimate..." Should be Gt/yr?

Yes, fixed.

Is this adjustment, described in Table A2 and as applied to the final estimates in Figure 6, added as a fixed value to the full time series or does the magnitude of the adjustment vary through time ?

The thickness adjustment adds that amount relative to the unadjusted baseline discharge. We highlight this value to show the approximate impact of the thickness adjustment on discharge. The baseline discharge is never included in the time series (it is only used to place gates, there is no velocity product included elsewhere that spans 3 years). The 21 Gt yr⁻¹ value is different at each time for the following two reasons (recall discharge \propto thick * velocity): 1) the adjusted thickness is further adjusted

temporally with Khan et al. (2016), and more importantly, 2) velocity is variable in time.

3.4.3 Ice Discharge Uncertainty: Is the temporal variability in coverage considered in error estimates? I would expect discharge estimates for a given time with, for example, only ~20% coverage to have a larger uncertainty than a time point with full coverage.

Our uncertainty treatment is simplistic but conservative (because we treat all errors as systematic not random). You are correct that reduced coverage may have larger uncertainty, but it is also a function of time since any given pixel was last observed. 10% coverage with a 100% coverage one week on either side can be linearly filled with high confidence. 50% coverage with 100% coverage a few months away may have more uncertainty.

We do not quantify the effect of gap filling in the error estimate in units of Gt. We do provide the coverage in the data we release so that others can use coverage as they want - perhaps as a proxy for quality, uncertainty, remove all points < C coverage, etc.

4.2 Ice discharge (volumetric flow rate) Page 7, line 26: If 169 Gt/yr is 54% of total ice sheet discharge, this yields a total ice sheet discharge of ~313 Gt/yr. On line 28, 70 Gt/yr representing 32% of total ice sheet contribution would indicate that total ice sheet discharge is ~219 Gt/yr. These values are inconsistent with each other and with the preceding paragraph. Can some text be added here to clarify what these percentages represent?

When calculating the contribution of a region to the total, we incorrectly removed that region from the total. This has been fixed.

4.3 Volumetric flux: I found this section confusing. By normalizing discharge by cross-sectional area, the authors are effectively describing interannual changes in velocity (since density is constant through time). I think it would be easier to follow if described in velocity terms, but it may not be necessary to include this section at all.

It should have been "mass flux" not "volumetric flux".

Density is constant but thickness is not, so this estimate is not describing only inter-annual changes in velocity. Because thickness changes slowly in this work, it is approximately describing intra-annual changes in velocity. Discharge mass flux (like discharge mass flow rate) is a function of both velocity and ice thickness. If the velocity remains the same but the ice thins by a factor of two, the discharge flow rate would decrease by a factor of two, but the discharge flux would remain steady.

After considering issues with this section raised by both Ellyn Enderlin and Reviewer #2 we have opted to remove it.

Page 8, line 18: 2013 maximum should be 2011 (as previously stated on page 7, line 24).

Flux is different than flow rate, and the year of maximum flow rate is not the same as

the year of maximum flux. This section has been removed.

Page 9, line 29: “The King et al. (2018) 2005 peak discharge is 524 +/- 9 Gt dropping to 461 +/- 9 Gt in 2008 – a decrease of ~63 Gt. In our work, the 2005 peak is 515 +/- 50 Gt, dropping to 495 +/- 50 Gt in 2008 – a decrease of only ~20 Gt.”

This comparison should be altered to either (1) compare annual averages between both studies, or (2) compare absolute max and min value between 2005 and 2008 from the ~monthly estimates (which look to be about 550 - 480 = 70 Gt from Fig. 6). The annual changes from King et al. (2018), plotted in red in Figure 1 from that paper, show an annual change of ~20 Gt, which is comparable with these results.

You are correct, and we are happy to have it pointed out to us that our results are not significantly different from the other recent discharge estimate. We have revised this text.

Figure 2: The heatmap is an excellent addition to the manuscript and packs a lot of information into a very readable figure. Interesting to see sensitivity to cutoff velocities increases with upstream gate distance.

We are not sure why there is increased sensitivity to cutoff velocities with upstream gate distance. One hypothesis is that farther upstream, the slower velocities are more strongly influenced by SMB processes. That is, a 10 m yr⁻¹ pixel 9000 m upstream would take 900 years to reach the ice edge (if it did not accelerate...).

Figure 8 and discussion of 7 largest discharging glaciers: I accessed the individual glacier discharge data available on the data portal and calculated that ‘IKERTIVAQ_M’ glacier contributes a period average discharge of ~14 Gt/yr, which is larger than the average contribution from Nioghalvfjærdsbrae. Why was this glacier excluded from the top 7? If instead this is a reference to the top 7 glaciers spread throughout each sector rather than absolute largest 7, then consider adding a word on this for clarification.

The top five glaciers are clearly Sermeq Kujalleq (Jakobshavn Isbræ), Helheim, Kangerlussuaq, Køge Bugt C. and Zachariae Isstrøm. After that, it is sensitive to the definition of "top". We used the mean of the last year. Using the last point, the mean of the last year, the mean of the last three years, and the sum of the last five years all give different results. We now clarify the method in the text. We note that the gate labeled "Ikertivaq M" spans both the M and S sector from Mouginot et al. (2019) and appears as one large gate, while all other glaciers described here as the "top" are individual outlet glaciers.

Page 24, line 17: Is the gate number 263 or 264? Both values are used throughout the manuscript.

Updated and fixed due to updated input data.

Table A2: Are these values given for the reference period (2015-2017)?

Yes and clarified.

4 References

- Bamber, J. L., J. A. Griggs, R. T. W. L. Hurkmans, J. A. Dowdeswell, S. P. Gogineni, I. Howat, J. Mouginot, J. Paden, S. Palmer, E. Rignot, and D. Steinhage (2013). “A new bed elevation dataset for Greenland”. *The Cryosphere*. 7 (2), 499–510. DOI: [10.5194/tc-7-499-2013](https://doi.org/10.5194/tc-7-499-2013).
- Enderlin, E. M., I. M. Howat, S. Jeong, M.-J. Noh, J. H. van Angelen, and M. R. van den Broeke (2014). “An improved mass budget for the Greenland Ice Sheet”. *Geophysical Research Letters*. 41 (3), 866–872. DOI: [10.1002/2013GL059010](https://doi.org/10.1002/2013GL059010).
- Joughin, I., B. E. Smith, and I. Howat (July 2018). “Greenland Ice Mapping Project: ice flow velocity variation at sub-monthly to decadal timescales”. *The Cryosphere*. 12 (7), 2211–2227. ISSN: 1994-0424. DOI: [10.5194/tc-12-2211-2018](https://doi.org/10.5194/tc-12-2211-2018).
- Khan, S. A., I. Sasgen, M. Bevis, T. van Dam, J. L. Bamber, J. Wahr, M. Willis, K. H. Kjær, B. Wouters, V. Helm, B. Csatho, K. Fleming, A. A. Bjørk, A. Aschwanden, P. Knudsen, and P. K. Munneke (Sept. 2016). “Geodetic measurements reveal similarities between post-Last Glacial Maximum and present-day mass loss from the Greenland ice sheet”. *Science Advances*. 2 (9), e1600931–e1600931. ISSN: 2375-2548. DOI: [10.1126/sciadv.1600931](https://doi.org/10.1126/sciadv.1600931).
- King, M. D., I. M. Howat, S. Jeong, M. J. Noh, B. Wouters, B. Noël, and M. R. van den Broeke (Dec. 2018). “Seasonal to decadal variability in ice discharge from the Greenland Ice Sheet”. *The Cryosphere*. 12 (12), 3813–3825. ISSN: 1994-0424. DOI: [10.5194/tc-12-3813-2018](https://doi.org/10.5194/tc-12-3813-2018).
- Mouginot, J. and E. Rignot (2019). *Glacier catchments/basins for the Greenland Ice Sheet*. DOI: [10.7280/d1wt11](https://doi.org/10.7280/d1wt11).

5 Revised Document Showing Changes

Greenland Ice Sheet ~~solid ice discharge from 2000 to 2018~~1986 through 2017

Kenneth D. Mankoff¹, Willam Colgan¹, Anne Solgaard¹, Nanna B. Karlsson¹, Andreas P. Ahlstrøm¹, Dirk van As¹, Jason E. Box¹, Shfaqat Abbas Khan², Kristian K. Kjeldsen¹, Jeremie Mouginot³, and Robert S. Fausto¹

¹Department of Glaciology and Climate, Geological Survey of Denmark and Greenland (GEUS), Copenhagen, Denmark

²DTU Space, National Space Institute, Department of Geodesy, Technical University of Denmark, Kgs. Lyngby, Denmark

³Department of Earth System Science, University of California, Irvine, CA, USA

Correspondence: Ken Mankoff (kdm@geus.dk)

Abstract. We present a ~~new 18-year (2000 to 2018)~~1986 through 2017 estimate of Greenland Ice Sheet ice discharge. Our data include all ~~discharging~~ ice that flows faster than 100 m yr⁻¹ and are generated through an automatic and adaptable method, as opposed to conventional hand-picked gates. We position gates near the present-year termini and estimate problematic bed topography (ice thickness) values where necessary. In addition to using annual time-varying ice thickness, our time series uses velocity maps that begin with ~~monthly estimates and sparse spatial~~ sparse spatial and temporal coverage and ends with ~~~6-day estimates and~~ near-complete spatial coverage ~~-. The recent average (and six-day updates to velocity. The 2010 to through 2017)-average~~ ice discharge through the flux-gates is ~~~500-488 ± 50-49~~ Gt yr⁻¹. The 10 % uncertainty stems primarily from uncertain ice bed location (ice thickness). We attribute the ~50 Gt yr⁻¹ differences among our results and previous studies to our use of updated bed topography from BedMachine v3. Discharge ~~increases-is approximately steady from 1986 to 2000,~~ increases sharply from 2000 to 2005, then ~~appears approximately steady-is approximately steady again.~~ However, regional and glacier variability is more pronounced, with ~~decreases at all major discharging-recent decreases at most major~~ glaciers and in all but one ~~sector-region~~ offset by increases in the NW ~~sector-region~~. As part of the journal's living archive option, all input data, code, and results from this study will be updated when new input data are accessible and made freely available at doi:10.22008/promice/data/ice_discharge.

15 1 Introduction

The mass of the Greenland ice sheet is decreasing (e.g. Fettweis et al. (2017); van den Broeke et al. (2017); Wiese et al. (2016); Khan et al. (2016)). Most ice sheet mass loss – as iceberg discharge, submarine melting, ~~meltwater runoff, and basal ablation~~ and meltwater runoff – enters the fjords and coastal seas, and therefore ice sheet mass loss directly contributes to sea-level rise (WCRP Global Sea Level Budget Group, 2018; Moon et al., 2018; Nerem et al., 2018; Chen et al., 2017). Greenland's total ice loss can be estimated through a variety of independent methods, for example 'direct' mass change estimates from GRACE (Wiese et al., 2016) or by using satellite altimetry to estimate surface elevation change, which is then converted into mass change (using a firn model, e.g. Khan et al. (2016)). However, attributing-partitioning the mass loss ~~into-iceberg-between~~

ice discharge (D) and surface mass balance (SMB) remains challenging (c.f. Rignot et al. (2008) and Enderlin et al. (2014)). Correctly assessing mass loss, as well as the attribution of this loss (SMB or D) is critical to understanding the process-level response of the Greenland ice sheet to climate change, and thus improving models of future ice-sheet changes and associated sea-level rise (Moon et al., 2018).

- 5 The total mass of an ice-sheet, or a drainage basin, changes if the mass gain (SMB inputs, primarily snowfall) is not balanced by the mass loss (D and SMB outputs, the latter generally meltwater runoff). This change is typically termed ice-sheet mass balance (MB) and the formal expression for this rate of change in mass is (e.g. Cuffey and Paterson (2010)),

$$\frac{dM}{dt} = \rho \int_A b dA - \int_g Q dg, \quad (1)$$

where ρ is the average density of ice, b is ~~the surface an area~~ mass balance, and Q is the ~~volumetric flow rate~~ discharge flux.

- 10 The left hand side of the equation is the rate of change of mass, the first part term on the right hand side is the area A integrated surface mass balance (SMB), and the second term is the ~~volumetric discharge~~ D mass flow rate that drains through gate g , ~~or discharge (D)~~. Equation 1 is often simplified to

$$MB = SMB - D \quad (2)$$

- 15 where MB is the mass balance, and referred to as the "input-output" method (e.g. Khan et al. (2015)). Virtually all studies agree on the trend of Greenland mass balance, but large discrepancies persist in both the magnitude and attribution. Magnitude discrepancies include, for example, Kjeldsen et al. (2015) reporting a mass imbalance of -250 ± 21 Gt yr⁻¹ during 2003 to 2010, Ewert et al. (2012) reporting -181 ± 28 Gt yr⁻¹ during 2003 to 2008, and Rignot et al. (2008) reporting a mass imbalance of -265 ± 19 Gt yr⁻¹ during 2004 to 2008. Some of ~~this difference~~ these differences may be due to different ice sheet area masks used in the ~~study~~ studies. Attribution discrepancies include, for example, Enderlin et al. (2014) attributing the majority
20 (64 %) of mass loss to changes in SMB during the 2005 to 2009 period but Rignot et al. (2008) attributing the majority (85 %) of mass loss to changes in D during the 2004 to 2008 period.

- Discharge may be calculated through several methods, including ~~volumetric mass~~ flow rate through gates (e.g. Enderlin et al. (2014); King et al. (2018)), or solving as a residual from independent mass balance terms (e.g. Kjær et al. (2012); Kjeldsen et al. (2015)). The gate method that we use in this study incorporates ice thickness and an estimated vertical velocity profile
25 from the observed surface velocity to calculate the discharge. ~~The term discharge refers to the ice volumetric flow rate at or close to the grounding line.~~ A typical formulation of discharge across a gate D_g is,

$$D_g = \rho V H w, \quad (3)$$

where ρ is ~~depth-averaged density~~ the average density of ice, V is ~~depth-averaged~~ depth-average gate-perpendicular velocity, H is the ice thickness, and w is the gate width. Uncertainties in V and H naturally ~~influences~~ influence the estimated discharge.

At fast-flowing outlet glaciers, V is typically assumed to be equal at all ice depths, and observed surface velocities can be directly translated into depth-averaged velocities (as in Enderlin et al. (2014); King et al. (2018)). To ~~avoid added~~ minimize uncertainty from SMB or basal ~~process~~ mass balance corrections downstream of a flux gate, the gate should be at the grounding line of the outlet glacier. Unfortunately, uncertainty in ~~radar-derived~~ bed elevation (translating to ice thickness uncertainty) increases toward the grounding line.

Conventional methods of gate selection involve hand-picking gate locations, generally as linear features (e.g. Enderlin et al. (2014)) or visually approximating ice-orthogonal gates at one point in time (e.g. King et al. (2018)). Manual gate definition is ~~suboptimal~~ sub-optimal. For example, the largest discharging glaciers draw from an upstream radially-diffusing region that may not easily be represented by a single linear gate. Approximately flow-orthogonal curved gates may not be flow-orthogonal on the multi-decade time scale due to changing flow directions. Manual gate selection makes it difficult to update gate locations, corresponding with glacier termini retreat or advance, in a systematic and reproducible fashion. We therefore adopt an algorithmic approach to generate gates based on a range of criteria.

Here, we present a ~~time-evolving~~ discharge dataset based on gates selected in a reproducible fashion by a new algorithm. Relative to previous studies, we employ ice velocity observation over a longer period with higher temporal frequency and denser spatial coverage. ~~Our expanded data set permits estimates of discharge at high frequency from all Greenland ice sheet outlet glaciers.~~ We use ice velocity from ~~2000 to 2018~~ 1986 through 2017 including six-day velocities for the last ~500 days of the time series, and discharge at 200 m ~~per~~ pixel resolution capturing all ice flowing faster than 100 m yr^{-1} that crosses glacier termini into fjords.

2 Input data

Historically, discharge gates were selected along well-constrained flight-lines of airborne radar data (Enderlin et al., 2014). Recent advances in ice thickness estimates through NASA Operation IceBridge (Millan et al., 2018), NASA Oceans Melting Greenland (OMG; Fenty et al. (2016)), fjord bathymetry (Tinto et al., 2015), and methods to estimate thickness from surface properties (e.g. McNabb et al. (2012); James and Carrivick (2016)) have been combined into digital bed elevation models such as BedMachine v3 (Morlighem et al., 2017b, a) or released as independent datasets (Millan et al., 2018). From these advances, digital bed elevation models have become more robust at tidewater glacier termini and grounding lines. The incorporation of flight-line ice thickness data into higher-level products that include additional methods and data means gates are no longer limited to flight-lines (e.g. King et al. (2018)).

Ice velocity data are available with increasing spatial and temporal resolution (e.g. vijay2019, *resolving?*). Until recently, ice velocity mosaics were limited to once per year during winter (Joughin et al., 2010), and they are still temporally limited, often to annual resolution, prior to 2000 (e.g. Mougnot et al. (2018b, c)). Focusing on recent times, ice-sheet wide velocity mosaics from the Sentinel 1A & 1B are now available every six days (<http://PROMICE.org>). The increased availability of satellite data has improved ice velocity maps both spatially and temporally thereby decreasing the

need to rely on spatial and temporal interpolation of velocities from annual/winter mosaics (Andersen et al., 2015; King et al., 2018).

The discharge gates in this study are generated using only surface speed and an ice mask. We use the MEaSURES Greenland Ice Sheet Velocity Map from InSAR Data, Version 2 (Joughin et al., 2010, 2015, updated 2018), hereafter termed "MEaSURES 0478" due to the National Snow and Ice Data Center (NSIDC) date set ID number. We use the BedMachine v3 (Morlighem et al., 2017b, a) ice mask.

For ice thickness estimates, we use surface elevation from GIMP (Howat et al. (2014, 2017); NSIDC data set ID 0715), adjusted through time with surface elevation change from Khan et al. (2016). ~~We use and~~ bed elevations from BedMachine v3 replaced by Millan et al. (2018) where available. Ice ~~catchment sector and region~~ delineation is from Mouginot and Rignot (2019) ~~and Rignot and Mouginot (2012) (see Supplemental Material)~~. Ice velocity data are obtained from a variety of products including Sentinel 1A & 1B derived by PROMICE (see ~~Supplemental Material for Sentinel velocity information~~ Appendix), MEaSURES 0478, ~~and~~ MEaSURES 0646 (Howat, 2017), ~~Mouginot et al. (2018b), and Mouginot et al. (2018c)~~. Official glacier names come from Bjørk et al. (2015). Other glacier names come from Mouginot and Rignot (2019). See Table 1 for an overview of data sets used in this work.

~~Our compilation includes 235. This work uses 308~~ different velocity maps, biased toward the last 500 days of the time series when six-day ice velocities become available from the Sentinel-1 satellites. The temporal distribution (~~apparent from the plots~~) ~~is is 1 to a few velocity map per year from 1986 to 2000,~~ 9 to 13 velocity maps per year from 2000 through 2015, 24 in 2016, and 55 in 2017.

Table 1. Summary of data sources used in this work. ~~First column is the physical property covered by the data. Second column is the informal name used in this work to reference this data source. Third column is (are) the reference(s).~~

Property	Name used in this paper	Reference
Basal Topography	BedMachine	Morlighem et al. (2017b, a)
Basal Topography for Southeast		Millan et al. (2018)
Surface Elevation	GIMP 0715	Howat et al. (2014, 2017)
Surface Elevation Change	Surface Elevation Change	Khan et al. (2016)
Baseline Velocity	MEaSURES 0478	Joughin et al. (2015, updated 2018)
Velocity	Sentinel	Appendix
Velocity	MEaSURES 0646	Howat (2017)
Velocity	pre-2000	Mouginot et al. (2018b, c)
Sectors & Regions	Sectors & Regions	Mouginot and Rignot (2019)
Names		Bjørk et al. (2015); Mouginot and Rignot (2019)

3 Methods

3.1 Terminology

We use the following terminology, most displayed in Fig. 1:

- 5 – "Pixels" are individual 200 m x 200 m raster discharge grid cells. We use the nearest neighbor when combining data sets that have different grid properties.
- "Gates" are contiguous (including diagonal) clusters of pixels.
- "~~Catchments~~Sectors" are spatial areas that have 0, 1, or > 1 gate(s) plus any upstream source of ice that flows through the gate(s), and come from Mouginit and Rignot (2019)~~and Rignot and Mouginit (2012) (See Supplemental Material).~~
- 10 – "~~Sectors~~Regions" are groups of ~~catchments~~sectors, also from Mouginit and Rignot (2019), and labeled by approximate geographic region.
- The "baseline" period is the average 2015, 2016, and 2017 winter velocity from MEaSURES 0478.
- "Coverage" is the percentage of total, ~~sector, catchment~~region, sector, or gate discharge observed at any given time. By definition coverage is 100 % during the baseline period. From the baseline data, the ~~contribute~~contribution to total discharge of each pixel is calculated, and coverage is reported for all other maps that have missing observations (Fig. A2). Total estimated discharge is always reported because missing pixels are gap-filled (see "Missing and invalid data" section below).
- 15 – "Fast-flowing ice" is defined as ice that flows more than 100 m yr⁻¹.
- Names are reported using the official Greenlandic names from Bjørk et al. (2015) if a nearby name exists, then Mouginit and Rignot in parentheses.
- 20 Although we refer to solid ice discharge, and it is in the solid phase when it passes the gates and eventually reaches the termini, submarine melting does occur at the termini and some of the discharge enters the fjord as liquid water (Enderlin and Howat, 2013).

3.2 Gate location

Gates are algorithmically generated for fast-flowing ice (greater than 100 m yr⁻¹) close to the ice sheet terminus determined by the baseline-period data. We ~~define the termini using~~ apply a 2D inclusive mask to the baseline data for all ice flowing faster than 100 m yr⁻¹. We then select the mask edge where it is near the BedMachine ice mask (not including ice shelves), which effectively provides grounding line termini. We buffer the termini 5000 m in all directions creating ovals around the termini and once again ~~only select~~ down-select to fast-flowing ice pixels. ~~Our~~ This procedure results in gates 5000 m upstream from the

baseline terminus that bisect the baseline fast-flowing ice. We manually mask some land- or lake-terminating glaciers which are initially selected by the algorithm due to fast flow and mask issues.

We select a 100 m yr^{-1} speed cutoff because slower ice, taking longer to reach the terminus, is more influenced by SMB. For the influence of this threshold on our results see the Discussion section [below](#) and Fig. 2.

5 We select gates at 5000 m upstream from the baseline termini, which means that gates are likely $> 5000 \text{ m}$ from the termini further back in the historical record (Murray et al., 2015; Wood et al., 2018). The choice of a 5000 m buffer follows from the fact that ~~a low-as-possible distance-to-terminus is desirable to avoid it is near-terminus and thus avoids~~ the need for (minor) SMB corrections downstream, yet is not too close to the terminus where discharge results are sensitive to the choice of distance-to-terminus value (Fig. 2), which may be indicative of bed (ice thickness) errors.

10 3.3 [Discharge Thickness](#)

~~We calculate discharge per pixel using density (917 kg m^{-3}), ice speed from satellite imagery, pixel width, and ice thickness derived from time-varying surface elevation and a fixed bed elevation (Eq. 3). We assume that any change in surface elevation corresponds to a change in ice thickness and thereby neglect basal uplift, erosion, and melt, which combined are orders of magnitude less than surface melting (e.g. Cowton et al. (2012); Cowton et al. (2007)). We also assume depth-averaged ice velocity is equal to the~~ [derive thickness from surface velocity and bed elevation. We use GIMP 0715 surface elevations in all locations, and the BedMachine bed elevations in most locations, except southeast Greenland where we use the Millan et al. \(2018\) bed. The GIMP 0715 surface elevations are all time-stamped per pixel. We adjust the surface through time by linearly interpolating elevation changes from Khan et al. \(2016\), which covers the period from 1995 to 2016. We use the average of the first and last three years for earlier and later times, respectively. Finally, from the fixed bed and temporally varying surface, we calculate the time-dependent ice thickness at each gate pixel.](#)

3.4 [Missing and/or invalid data](#)

The baseline data provides velocity at all gate locations by definition ([Fig. ??](#)), but individual non-baseline velocity maps often have missing [or invalid](#) data. Also, thickness provided by BedMachine is clearly incorrect in some places (e.g. fast-flowing ice that is 10 m thick, Fig. 3). We define invalid data and fill in missing data as described below.

25 3.4.1 [Invalid velocity](#)

[We flag invalid \(outlier\) velocities by treating each pixel as an individual time series, applying a 30 point rolling window, flagging values more than 2 standard deviations outside the mean, and repeating this filter three times. We also drop the 1972 to 1985 years from Mouginot et al. \(2018b\) because there is low coverage and extremely high variability when using our algorithm.](#)

30 [This outlier detection method appears to correctly flag outliers \(see Appendix for un-filtered time series graphs\), but likely also flags some true short-term velocity increases. The effect of this filter is a \$\sim 1\%\$ reduction in discharge most years, but more](#)

in years with high discharge – a reduction of 3.2 % in 2013, 4.3 % in 2003, and more in the 1980s when the data is noisy. Any analysis using this data and focusing on individual glaciers or short-term changes (or lack there-of) should re-evaluate the upstream data sources.

3.4.2 Missing velocity

5 We generate an ice speed time series by assigning the PROMICE, MEaSURES 0478, ~~and~~MEaSURES 0646, and pre-2000
products to their respective reported time stamps (even though these are time-span products), or to the middle of their time
span when they cover a long period such as the annual maps from Mouginot et al. (2018b, c). We ignore that any individual
velocity ~~data set (map) and even point (pixel) map or pixel~~ has a time span, not a time stamp. Velocities are sampled only
where there are gate pixels. Missing pixel velocities are linearly interpolated in time, except for missing data at the beginning
10 ~~or end~~ of the time series which are ~~backward- and forward-filled (respectively)~~ back- and forward-filled with the temporally-
nearest value for that pixel (Fig. A2). We do not spatially interpolate missing velocities because the spatial changes around a
missing data point are most likely larger than the temporal changes. We visually represent the discharge contribution of directly
observed pixels, termed coverage (Fig. A2) as time series graphs and opacity of dots and error bars in the figures. Therefore,
the gap-filled discharge contribution at any given time is equal to 100 minus the coverage. Discharge is always reported as
15 estimated total discharge even when coverage is less than 100 %.

3.4.3 Invalid thickness

~~We derive thickness from surface and bed elevation. We use GIMP 0715 surface elevations in all locations, and the BedMachine
bed elevations in most locations, except southeast Greenland where we use the Millan et al. (2018) bed. The GIMP 0715 surface
elevations are all time-stamped per pixel. We adjust the surface through time by linearly interpolating elevation changes from
20 Khan et al. (2016), which covers the period from 2000 to 2016. We linearly interpolate the average of the last three years to
later times. Finally, from the fixed bed and temporally varying surface, we calculate the time-dependent ice thickness at each
gate pixel.~~

The thickness data ~~generated as described above (Fig. ??)~~ are unlikely to be valid at all appear to be incorrect in some
locations. For example, many locations have fast-flowing ice (~~Fig. ??~~), but report ice thickness as 10 ~~or less m~~ m or less (Fig.
25 3, left panel). We accept all ice thickness greater than 20 m and construct from this a thickness versus \log_{10} speed relationship.
For all ice thickness less than or equal to 20 m thick (~~at each pixel location~~) we adjust thickness based this relationship (~~Figs.~~
~~?? and Fig. 3, right~~ panel). We selected the 20 m thickness cutoff after visually inspecting the velocity distribution (Fig. 3,
~~right-left~~ panel). This thickness adjustment adds ~~21 Gt~~ 20 Gt yr⁻¹ to our baseline-period discharge estimate with no adjustment.
In the ~~Supplemental Material Appendix~~ and Table A2 we discuss the discharge contribution of these adjusted pixels, and a
30 comparison among this and other thickness adjustments.

3.4.4 Ice Discharge Uncertainty

3.5 Discharge

We calculate discharge per pixel using density (917 kg m^{-3}), filtered and filled ice speed, projection-corrected pixel width, and adjusted ice thickness derived from time-varying surface elevation and a fixed bed elevation (Eq. 3). We assume that any change in surface elevation corresponds to a change in ice thickness and thereby neglect basal uplift, erosion, and melt, which combined are orders of magnitude less than surface melting (e.g. Cowton et al. (2012); Cowton et al. (2007)). We also assume depth-averaged ice velocity is equal to the surface velocity.

We calculate discharge using the gate-orthogonal velocity at each pixel and at each timestamp – all velocity estimates are gate-orthogonal at all times, regardless of gate position, orientation, or changing glacier velocity direction over time.

Annual averages are calculated by linearly interpolating to daily, then estimating annual. The difference between this method and averaging only the observed samples is $\sim 3\%$ median (5% average, and a maximum of 10% when examining the entire ice sheet and all years in our data). It is occasionally larger at individual glaciers when a year has few widely-space samples of highly variable velocity.

3.5.1 Discharge Uncertainty

A longer discussion related to our and others treatments of errors and uncertainty is in the Appendix, but here we describe how we estimate the uncertainty related to the ice discharge following a simplistic approach. This yields an uncertainty of the total ice discharge of approximately 10% throughout the time series.

At each pixel we estimate the maximum discharge, D_{\max} , from

$$D_{\max} = \rho(V + \sigma_V)(H + \sigma_H)W, \quad (4)$$

and minimum discharge, D_{\min} , from

$$D_{\min} = \rho(V - \sigma_V)(H - \sigma_H)W, \quad (5)$$

where ρ is ice density, V is baseline velocity, σ_V is the baseline velocity error, H is ice thickness, σ_H is the ice thickness error, and W is the width at each pixel. Included in the thickness term is surface elevation change through time (dH/dt) and its uncertainty ($\sigma_{dH/dt}$). However, because $\sigma_H \gg \sigma_V$ and $\sigma_H \gg \sigma_{dH/dt}$, both σ_V and $\sigma_{dH/dt}$ terms are ignored. When data sets do not come with error estimates we treat the error as 0.

We use $\rho = 917 \text{ kg m}^{-3}$ because the gates are near the terminus in the ablation zone and ice thickness estimates should not include snow or firn, although regionally ice density may be $< 917 \text{ kg m}^{-3}$ due to crevasses. We ignore the velocity error σ_V and the elevation change error σ_H because the proportional thickness error (σ_H/H) is an order of magnitude larger than the proportional velocity error (σ_V/V) yet both contribute linearly to the discharge. Similarly, $\sigma_H \gg \sigma_{dH/dt}$. W is

location-dependent due to the errors between our working map projection (EPSG 3413) and a more accurate spheroid model of the earth surface. We adjust linear gate width by up to ~4% in the north and ~-2.5% in the south of Greenland (area errors are up to 8%). On a pixel by pixel basis we used the provided thickness uncertainty for each dataset. Where we modified the thickness ($H < 20$ m), we prescribe an uncertainty of 0.5 times the adjusted thickness. Subsequently, the uncertainty on individual glacier-, ~~catchment-~~sector-, ~~region-~~, or ice sheet scale is obtained by summarizing, but not reducing by the square of the sums, the uncertainty related to each pixel. ~~An in-depth discussion related to treatment of errors and uncertainty is in the Supplementary Information-~~

~~We are conservative with our thickness error estimates, by assuming the uncertainty range is from D_{min} to D_{max} and not reducing by the sum-of-squares of sectors or regions.~~

10 4 Results

4.1 Gates

Our ~~discharge gate algorithm generates 5981~~ gate placement algorithm generates 6002 pixels making up ~~264-276~~ gates, assigned to ~~172-176~~ ice-sheet sectors following from Mouginot and Rignot (2019). Previous similar studies have used 230 gates (King et al., 2018) and 178 gates (Enderlin et al., 2014).

15 The widest gate (~47 km) is Sermersuaq (Humboldt Gletsjer), the 2nd widest (~34 km) is Sermeq Kujalleq (Jakobshavn Isbræ). 23 additional glaciers have gate lengths longer than 10 km. The minimum gate width is 3 pixels (600 m) by definition in the algorithm.

The average ~~thickness at unadjusted gates is 407~~ unadjusted thickness gates is 405 m with a standard deviation of ~~259-260~~. The average thickness ~~at gates with erroneous values adjusted is 440~~ after adjustment is 439 m with a standard deviation of ~~226-225~~. A histogram of unadjusted and adjusted thickness at all gate locations is shown in Fig. ~~??~~, ~~speed at all gate locations is shown in Fig. ??~~, and a combined 2D histogram in Fig. 3.

4.2 ~~Ice discharge (volumetric flow rate)~~Discharge

Our ice discharge dataset (Fig. 4) reports a total discharge of ~~468-438~~ $\pm 47-43$ Gt in 1986, ~~has a minimum of 421~~ ± 42 Gt ~~in 1995, increases to 452~~ ± 45 in 2000 ~~and 515~~, ~~further to 504~~ $\pm 50-49$ Gt/yr in 2005, after which annual discharge remains approximately steady at ~~495 to 520~~ ~~484 to 503~~ $\pm \sim 50$ Gt/yr during the 2005 to 2017 period. Annual maxima in ice discharged occurred in 2005 (~~515-504~~ $\pm 50-49$ Gt/yr), 2011 (~~521-499~~ $\pm 53-50$ Gt/yr), and ~~2013 (519-2014 (503~~ $\pm 53-51$ Gt/yr). ~~Discharge in both 2016 and 2017 was less than 500 Gt each year-~~

At the ~~sector region~~ scale, the SE glaciers (see Fig. 1 for ~~sectors regions~~) are responsible for ~~148 to 169~~ ~~139 to 167~~ ($\pm 12-11$ %) Gt yr⁻¹ of discharge (~~42 to 54~~ ~~30 to 34~~ % of ice-sheet wide discharge) over the ~~2007-1986~~ to 2017 period. By comparison, the predominantly land-terminating NO, NE and SW together were ~~responsible for only ~70 Gt yr⁻¹~~ ~~also responsible for 131 to 168~~ of discharge (~~32 ~31~~ % of ice-sheet wide discharge) during this time (Fig. 5). The discharge from most ~~sectors regions~~ has

been approximately steady or declining for the past decade. The NW is the only sector-region exhibiting a persistent increase in discharge ;~~From ~90 to 115~~ ~~From ~89 to 113~~ Gt yr⁻¹ (~~22-21~~ % increase) over the ~~2000 to 2018~~ 1998 through 2017 period (+ ~1 Gt yr⁻¹ or + ~~0.9~~ ~1 % yr⁻¹). This persistent increase in NW discharge ~~is offsetting offsets~~ declining discharge from other regions. The largest contributing sector-region, SE, contributed a high of ~~175-167 ± 20 Gt in 2003~~ 19 Gt in 2005, but dropped to ~~148 (154)~~ 149 (155) ± 18 Gt in 2016 (2017). ~~The last time the SE sector was persistently below 150 Gt yr⁻¹ was in the early 2000s.~~

~~In the NO, NE and SW sectors, which contribute a minority of ice-sheet discharge, low coverage (large data gaps) is evident in the coverage chart (Fig. 5, only NO of these three sectors is shown for clarity), and as linear trends with data point centers and error bars transparent. These indicators of gap-filling are also evident in the NW sector but only in 2014 & 2015. They are more clearly evident in the NE, NO, and SW with adjusted scaling (Fig. ?? in Supplemental Material is the same as Fig. 5 but with a logarithmic y-axis).~~

Focusing on the top ~~seven contributors~~ eight contributors (mean of last year) at the individual sector or glacier scale (Fig. 6), Sermeq Kujalleq (Jakobshavn Isbræ) has slowed down from an annual average high of ~~~55-52~~ Gt yr⁻¹ in 2012 to ~45 Gt yr⁻¹ in 2016 and ~38 Gt yr⁻¹ in 2017. ~~The 2012-2017, likely due to ocean cooling (Khazendar et al., 2019). We exclude Ikertivaq from the top 8 because that gate spans multiple sectors and outlets, while the other top dischargers are each a single outlet. The 2013 to 2016 slowdown of Sermeq Kujalleq (Fig. 6) is compensated by the many glaciers that make up the NW sector-region (Fig. 5). The large 2017 reduction in discharge at Sermeq Kujalleq is partially offset by a large increase in the 2nd largest contributor, Helheim Gletsjer (Fig. 6).~~

4.3 Volumetric flux

~~Thinning and accelerating ice may balance each other to maintain a steady volume flow rate, but the same thinning and accelerating ice would increase flux due to the decreased cross-sectional flux area. Since the flux is proportional to gate size (height) and ice velocity, it is highly dependent on gate location. Volume flow rate is roughly steady since 2005, and increased ~12 % between the 2001 minimum (461 Gt yr⁻¹) and 2013 maximum (521 Gt⁻¹). During this same period the flux increased 16 % from a 2001 minimum (0.80 Gt yr⁻¹ km⁻²) to a 2011 maximum (0.95 Gt yr⁻¹ km⁻²). Flux exhibits a similar year-to-year variability as discharge (volume flow rate) but the flux signal is overlaid on a continuously accelerating trend line, equal to the inverse of the thinning rate.~~

5 Discussion

Different ice discharge estimates among studies likely stem from three categories: 1) changes in true discharge, 2) different input data (ice thickness and velocity), and 3) different assumptions and methods used to analyze data. Improved estimates of true discharge is the goal of this and many other studies, but changes in true discharge (category 1) can happen only when a work extends a time series into the future because historical discharge is fixed. Thus, any inter-study discrepancies in historical discharge must be due to category 2 (different data) or category 3 (different methods). Most studies use both updated data and

new or different methods, but do not always provide sufficient information to disentangle the two. This is inefficient. To more quantitatively discuss inter-study discrepancies, it is imperative to explicitly consider all three potential causes of discrepancy. Only when results are fully reproducible – meaning all necessary data and code are available (c.f. Mankoff and Tulaczyk (2017); Rezvanbehbahani et al. (2017)) – can new works confidently attribute discrepancies relative to old works. Therefore, in addition to providing new discharge estimates, we attempt to examine discrepancies among our estimates and other recent estimates. Without access to code and data from previous studies, it is challenging to take this examination beyond a qualitative discussion.

The algorithm-generated gates we present offer some advantages over traditional hand-picked gates. Our gates are shared publicly, are generated by `a`-code that can be audited by others, and are easily adjustable within the algorithmic parameter space. This **adjustability** allows both sensitivity testing of gate location (Fig. 2) and allows gate positions to systematically evolve with glacier termini (not done here, ~~because we also report flux which is sensitive to gate location, in addition to flow rate~~). The total ice discharge we estimate is ~10 % less than the total discharge of two previous estimates (Enderlin et al., 2014; Rignot et al., 2008), and similar to that of King et al. (2018), who attributes their discrepancy with Enderlin et al. (2014) to the latter using only summer velocities, which have higher annual average values than seasonally-comprehensive velocity products. The gate locations also differ among studies, and glaciers with baseline velocity less than 100 m yr⁻¹ are not included in our study due to our velocity cutoff threshold, but this should not lead to substantially different discharge estimates (Fig. 2).

Our gate selection algorithm also does not place gates in northeast Greenland at Storstrømmen, Bredebræ, or their confluence, because during the baseline period that surge glacier was in a slow phase. We do not manually add gates at these glaciers. The last surge ended in 1984 (Reeh et al., 1994; Mougnot et al., 2018a), prior to the beginning of our time series, and these glaciers are therefore not likely to contribute substantial discharge even in the early period of discharge estimates.

We instead attribute the majority of our discrepancy with Enderlin et al. (2014) to the use of differing bed topography in southeast Greenland. When we compare our top ten highest discharging glaciers in 2000 with those reported by Enderlin et al. (2014), we find that the Køge Bugt discharge reported by Enderlin et al. (2014) is ~31 Gt, but our estimate is only ~16 Gt (and ~17 Gt in King et al. (2018)). The Bamber et al. (2013) bed elevation dataset most likely that likely uses the same bed data employed by Enderlin et al. (2014) has a major bed-depression-in-depression in the central Køge Bugt bed. This region of enhanced ice thicknesses is not present in the BedMachine dataset that we and King et al. (2018) employ (Fig. B1). If the Køge Bugt gates of Enderlin et al. (2014) are in this location, then those gates overlie Bamber et al. (2013) ice thicknesses that are about twice those reported in BedMachine v3. With all other values held constant, this results in roughly twice the discharge. Although we do not know whether BedMachine or Bamber et al. (2013) is more correct, conservation of mass suggests that a substantial subglacial depression should be evident as either depressed surface elevation or velocity (Morlighem et al., 2016).

We are unable to attribute the remaining discrepancy between our discharge estimates and those by Enderlin et al. (2014), ~~but agree with King et al. (2018) that~~. It is likely a combination of differing seasonal velocity sampling may be the cause (King et al., 2018), our evolving surface elevation from Khan et al. (2016), or other previously-unpublished algorithmic or data differences, of which many possibilities exist.

Our ice discharge estimates agree well with the most recently published discharge data (King et al., 2018), with one notable difference. The King et al. (2018) 2005 peak discharge is 524 ± 9 Gt dropping to 461 ± 9 Gt in 2008 — a decrease of ~ 63 Gt. In our work, the 2005 peak is 515 ± 50 Gt, dropping to 495 ± 50 Gt in 2008 — a decrease of only ~ 20 Gt estimate (King et al., 2018), except that our discharge is slightly less. We note that our uncertainty estimates include the King et al. (2018) estimates, but the opposite does not appear to be true. We suggest the discrepancy in 2005 to 2008 discharge decrease results from differing approaches to temporal interpolation during a period of highly transient discharge. The minor differences are likely due to different methods. King et al. (2018) use seasonally varying ice thicknesses, derived from seasonally varying surface elevations, and a Monte Carlo method to temporally interpolate missing velocity data to produce discharge estimates.

In comparison, we use linear interpolation of both yearly surface elevation estimates and temporal data gaps. It is not clear whether linear or higher-order statistical approaches are best-suited for interpolation during the non-linear discharge changes seen between 2005 and 2008. Our use of unmodified velocity products (except for linear gap-filling) also highlights some of the imperfections in those products. It is not visible in the total discharge graph, but when viewing individual glaciers (Fig. 6) the signal to noise ratio decreases, and any individual outlying data point should be treated with caution, as annual cycles begin to shift, as is the case with Sermeq Kujalleq (Jakobshavn Isbræ) after 2015. There are benefits and deficiencies with both methods. Linear interpolation may alias large changes if there are no other observations nearby in time. Statistical models of past glacier behavior may not be appropriate when glacier behavior changes.

We calculate the gate-orthogonal velocity at each pixel and at each timestamp, meaning all velocity estimates are gate-orthogonal at all times, regardless of gate position, orientation, or changing glacier velocity direction over time. It is unlikely that discharge estimates using gates that are only approximately flow-orthogonal and time-invariant (King et al., 2018) have large errors due to this, because it is unlikely that glacier flow direction changes significantly, but this our gate-orthogonal treatment may be the cause of some differences among our approach and other works. Discharge calculated using non-orthogonal methodology would overestimate true discharge.

6 Data Availability availability

This work in its entirety is available at doi:10.22008/promice/data/ice_discharge (Mankoff, 2019a). The glacier-scale, catchment sector, region, and Greenland summed ice sheet discharge dataset is available at doi:10.22008/promice/data/ice_discharge/d/v0.0.1 (Mankoff, 2019c), where it will be updated as more velocity data become available. The gates can be found at doi:10.22008/promice/data/ice_discharge/gates/v0.0.1 (Mankoff, 2019d), the code at doi:10.22008/promice/data/ice_discharge/code/v0.0.1 (Mankoff, 2019b), and the surface elevation change at doi:10.22008/promice/data/DTU/surface_elevation_change/v1.0.0 (Khan, 2017).

7 Conclusions

We have presented a novel dataset of flux gates and ~~2000 to 2018~~ 1986 through 2017 glacier-scale ice discharge estimate for the Greenland ice sheet. These data are underpinned by an algorithm that both selects gates for ice flux and then computes ice discharges.

5 Our results are similar to the most recent discharge estimate (King et al., 2018) but begin in 1986 - although there is low coverage and few samples prior to 2000. From our discharge estimate we show that over the past ~~20~~ 30 years, ice sheet discharge ~~rose to just~~ was $\sim 430 \text{ Gt yr}^{-1}$ prior to 2000, rose to over 500 Gt yr^{-1} from 2000 to 2005, and has held roughly steady since 2005 at near 500 Gt yr^{-1} . However, when viewed at a ~~sector or glacier region or sector~~ scale, the system appears more dynamic with spatial and temporal increases and decreases canceling each other out to produce the more stable ice sheet
10 discharge. We note that there does not appear to be any dynamic connection among the ~~sectors~~ regions, and any increase in one ~~sector~~ region that was offset by a decrease in another has likely been due to chance. If in coming years ~~changes occur and the signals happen to~~ when changes occur the signals have matching signs, then ice sheet discharge ~~will~~ would decrease or increase, rather than remain fairly steady.

The application of our flux-gate algorithm shows that ice-sheet wide ~~iceberg~~ discharge varies by ~~50~~ 30 Gt yr^{-1} ~~between the minimum and maximum of the upstream buffer distance (i.e. distance between the flux gates and the glacier termini) and the lateral velocity cut-off of flux gates due only to gate position, or~~ 40 Gt ~~due to gate position and cutoff velocity~~ (Fig. 2). This variance ~~—due only to gate position and shape—~~ is approximately equal to the uncertainty associated with ice-sheet wide discharge estimates reported in many studies (e.g. Rignot et al. (2008); Andersen et al. (2015); Kjeldsen et al. (2015)). ~~The ice discharge we present here is similar to recent estimates by King et al. (2018) where our time series overlap.~~ We highlight
20 a major discrepancy with the ice discharge data of Enderlin et al. (2014) and we suspect this discharge discrepancy – most pronounced in southeast Greenland – is associated with the choice of digital bed elevation model, specifically a deep hole in the ~~Bamber et al. (2013)~~ bed at Køge Bugt.

~~The flux gates, discharge data, and the algorithm used to generate the gates, discharge, and all figures, are freely available. This publication aims to take advantage of this ESSD journal "living data" process to maintain an evolving data set.~~ Transparency in data and methodology are critical to move beyond a focus of estimating discharge quantities, towards more operational mass loss products with realistic errors and uncertainty estimates. The convention of devoting a ~~critical~~ paragraph, or even page, to methods ~~now appears to be~~ is insufficient given the complexity ~~and~~ pace, pace, and importance of Greenland ice sheet research. Therefore the flux gates, discharge data, and the algorithm used to generate the gates, discharge, and all figures from this manuscript are freely available. We hope that the flux gates, data, and code we provide here is a step toward helping
30 others both improve their work and discover the errors in ours.

Acknowledgements. Author Contribution: KDM conceived of the algorithm approach, and wrote the code. KDM, WIC, and RSF iterated over the algorithm results and methods. ASO provided the velocity data. SAK supplied the surface elevation change data. ~~JM provided the catchments.~~ All authors contributed to the scientific discussion, writing, and editing of the manuscript. The authors declare that they have

no conflict of interest. Data from the Programme for Monitoring of the Greenland Ice Sheet (PROMICE) were provided by the Geological Survey of Denmark and Greenland (GEUS) at <http://www.promice.org>. Parts of this work were funded by the INTAROS project under the European Union's Horizon 2020 research and innovation program under grant agreement No. 727890.

References

- Andersen, M. L., Stenseng, L., Skourup, H., Colgan, W., Khan, S. A., Kristensen, S. S., Andersen, S. B., Box, J. E., Ahlstrøm, A. P., Fettweis, X., and Forsberg, R.: Basin-scale partitioning of Greenland ice sheet mass balance components (2007 – 2011), *Earth and Planetary Science Letters*, 409, 89–95, <https://doi.org/10.1016/j.epsl.2014.10.015>, 2015.
- 5 Bamber, J. L., Griggs, J. A., Hurkmans, R. T. W. L., Dowdeswell, J. A., Gogineni, S. P., Howat, I., Mouginot, J., Paden, J., Palmer, S., Rignot, E., and Steinhage, D.: A new bed elevation dataset for Greenland, *The Cryosphere*, 7, 499–510, <https://doi.org/10.5194/tc-7-499-2013>, 2013.
- Bjørk, A. A., Kruse, L. M., and Michaelsen, P. B.: Brief Communication: Getting Greenland’s glaciers right – a new dataset of all official Greenlandic glacier names, *The Cryosphere*, 9, 2215–2218, <https://doi.org/10.5194/tc-9-2215-2015>, 2015.
- 10 Chen, X., Zhang, X., Church, J. A., Watson, C. S., King, M. A., Monselesan, D., Legresy, B., and Harig, C.: The increasing rate of global mean sea-level rise during 1993–2014, *Nature Climate Change*, 7, 492–495, <https://doi.org/10.1038/nclimate3325>, <http://dx.doi.org/10.1038/nclimate3325>, 2017.
- Cowton, T., Nienow, P., Bartholomew, I. D., Sole, A., and Mair, D. W. F.: Rapid erosion beneath the Greenland ice sheet, *Geology*, 40, 343–346, <https://doi.org/10.1130/G32687.1>, 2012.
- 15 Cuffey, K. M. and Paterson, W. S. B.: *The physics of glaciers*, Academic Press, fourth edn., 2010.
- Dall, J., Kusk, A., Nielsen, U., and Merryman Boncori, J. P.: Ice velocity mapping using TOPS SAR data and offset tracking, in: *FRINGE* 2015, vol. 731, 2015.
- Enderlin, E. M. and Howat, I. M.: Submarine melt rate estimates for floating termini of Greenland outlet glaciers (2000 – 2010), *Journal of Glaciology*, 59, 67–75, <https://doi.org/10.3189/2013JoG12J049>, 2013.
- 20 Enderlin, E. M., Howat, I. M., Jeong, S., Noh, M.-J., van Angelen, J. H., and van den Broeke, M. R.: An improved mass budget for the Greenland Ice Sheet, *Geophysical Research Letters*, 41, 866–872, <https://doi.org/10.1002/2013GL059010>, 2014.
- Ewert, H., Groh, A., and Dietrich, R.: Volume and mass changes of the Greenland ice sheet inferred from ICESat and GRACE, *Journal of Geodynamics*, 59-60, 111–123, <https://doi.org/10.1016/j.jog.2011.06.003>, <http://dx.doi.org/10.1016/j.jog.2011.06.003>, 2012.
- Fenty, I., Willis, J., Khazendar, A., Dinardo, S., Forsberg, R., Fukumori, I., Holland, D., Jakobsson, M., Moller, D., Morison, J., Münchow, A., Rignot, E. J., Schodlok, M. P., Thompson, A. F., Tinto, K., Rutherford, M., and Trenholm, N.: Oceans Melting Greenland: Early Results from NASA’s Ocean-Ice Mission in Greenland, *Oceanography*, 29, 72–83, <https://doi.org/10.5670/oceanog.2016.100>, 2016.
- 25 Fettweis, X., Box, J. E., Agosta, C., Amory, C., Kittel, C., Lang, C., Van As, D., Machguth, H., and Gallée, H.: Reconstructions of the 1900–2015 Greenland ice sheet surface mass balance using the regional climate MAR model, *The Cryosphere*, 11, 1015–1033, <https://doi.org/10.5194/tc-11-1015-2017>, <http://dx.doi.org/10.5194/tc-11-1015-2017>, 2017.
- 30 Howat, I.: MEaSURES Greenland Ice Velocity: Selected Glacier Site Velocity Maps from Optical Images, Version 2, <https://doi.org/10.5067/VM5DZ20MYF5C>, used all subsets; Accessed 2018-11-15. NASA National Snow and Ice Data Center Distributed Active Archive Center, 2017.
- Howat, I., Negrete, A., and Smith, B.: MEaSURES Greenland Ice Mapping Project (GIMP) Digital Elevation Model, Version 1, <https://doi.org/10.5067/NV34YUIXLP9W>, used all subsets; Access date unknown. NASA National Snow and Ice Data Center Distributed
- 35 Active Archive Center, 2015.

- Howat, I., Negrete, A., and Smith, B.: MEaSURES Greenland Ice Mapping Project (GIMP) Digital Elevation Model from GeoEye and WorldView Imagery, Version 1, <https://doi.org/10.5067/H0KUYVF53Q8M>, used all subsets; Accessed 2018-10-28. NASA National Snow and Ice Data Center Distributed Active Archive Center, 2017.
- Howat, I. M., Negrete, A., and Smith, B. E.: The Greenland Ice Mapping Project (GIMP) land classification and surface elevation data sets, *The Cryosphere*, 8, 1509–1518, <https://doi.org/10.5194/tc-8-1509-2014>, <http://dx.doi.org/10.5194/tc-8-1509-2014>, 2014.
- Hoyer, S. and Hamman, J. J.: xarray: N-D labeled Arrays and Datasets in Python, *Journal of Open Research Software*, 5, <https://doi.org/10.5334/jors.148>, <http://dx.doi.org/10.5334/jors.148>, 2017.
- Hunter, J. D.: Matplotlib: A 2D graphics environment, *Computing In Science & Engineering*, 9, 90–95, 2007.
- James, W. H. M. and Carrivick, J. L.: Automated modelling of spatially-distributed glacier ice thickness and volume, *Computers & Geosciences*, <https://doi.org/10.1016/j.cageo.2016.04.007>, 2016.
- Joughin, I., Smith, B., Howat, I., and Scambos, T.: MEaSURES Greenland Ice Sheet Velocity Map from InSAR Data, Version 2, <https://doi.org/10.5067/OC7B04ZM9G6Q>, used all subsets; Accessed 2019-03-10. NASA National Snow and Ice Data Center Distributed Active Archive Center, 2015, updated 2018.
- Joughin, I., Smith, B. E., and Howat, I.: Greenland Ice Mapping Project: ice flow velocity variation at sub-monthly to decadal timescales, *The Cryosphere*, 12, 2211–2227, <https://doi.org/10.5194/tc-12-2211-2018>, <http://dx.doi.org/10.5194/tc-12-2211-2018>, 2018.
- Joughin, I. R., Smith, B., Howat, I. M., Scambos, T. A., and Moon, T.: Greenland flow variability from ice-sheet-wide velocity mapping, *Journal of Glaciology*, 56, 415–430, <https://doi.org/10.3189/002214310792447734>, 2010.
- Khan, S. A.: Greenland Ice Sheet Surface Elevation Change, https://doi.org/10.22008/promice/data/DTU/surface_elevation_change/v1.0.0, submitted. GEUS Data Center, 2017.
- Khan, S. A., Wahr, J., Stearns, L. A., Hamilton, G. S., van Dam, T., Larson, K. M., and Francis, O.: Elastic uplift in southeast Greenland due to rapid ice mass loss, *Geophysical Research Letters*, 34, <https://doi.org/10.1029/2007gl031468>, <http://dx.doi.org/10.1029/2007GL031468>, 2007.
- Khan, S. A., Aschwanden, A., Bjørk, A. A., Wahr, J., Kjeldsen, K. K., and Kjær, K. H.: Greenland ice sheet mass balance: a review, *Reports on Progress in Physics*, 78, 046 801, <https://doi.org/10.1088/0034-4885/78/4/046801>, <http://dx.doi.org/10.1088/0034-4885/78/4/046801>, 2015.
- Khan, S. A., Sasgen, I., Bevis, M., van Dam, T., Bamber, J. L., Wahr, J., Willis, M., Kjær, K. H., Wouters, B., Helm, V., Csatho, B., Fleming, K., Bjørk, A. A., Aschwanden, A., Knudsen, P., and Munneke, P. K.: Geodetic measurements reveal similarities between post-Last Glacial Maximum and present-day mass loss from the Greenland ice sheet, *Science Advances*, 2, e1600 931–e1600 931, <https://doi.org/10.1126/sciadv.1600931>, <http://dx.doi.org/10.1126/sciadv.1600931>, 2016.
- Khazendar, A., Fenty, I. G., Carroll, D., Gardner, A., Lee, C. M., Fukumori, I., Wang, O., Zhang, H., Seroussi, H., Moller, D., Noël, B. P. Y., van den Broeke, M. R., Dinardo, S., and Willis, J.: Interruption of two decades of Jakobshavn Isbrae acceleration and thinning as regional ocean cools, *Nature Geoscience*, 12, 277–283, <https://doi.org/10.1038/s41561-019-0329-3>, <http://dx.doi.org/10.1038/s41561-019-0329-3>, 2019.
- King, M. D., Howat, I. M., Jeong, S., Noh, M. J., Wouters, B., Noël, B., and van den Broeke, M. R.: Seasonal to decadal variability in ice discharge from the Greenland Ice Sheet, *The Cryosphere*, 12, 3813–3825, <https://doi.org/10.5194/tc-12-3813-2018>, <http://dx.doi.org/10.5194/tc-12-3813-2018>, 2018.

- Kjeldsen, K. K., Korsgaard, N. J., Bjørk, A. A., Khan, S. A., Box, J. E., Funder, S., Larsen, N. K., Bamber, J. L., Colgan, W., Broeke, M. v. d., Siggaard-Andersen, M.-L., Nuth, C., Schomacker, A., Andresen, C. S., Willerslev, E., and Kjær, K. H.: Spatial and temporal distribution of mass loss from the Greenland Ice Sheet since AD 1900, *Nature*, 528, 396–400, <https://doi.org/10.1038/nature16183>, 2015.
- Kjær, K. H., Khan, S. A., Korsgaard, N. J., Wahr, J., Bamber, J. L., Hurkmans, R., Van Den Broeke, M. R., Timm, L. H., Kjeldsen, K. K., Bjørk, A. A., Larsen, N. K., Jørgensen, L. T., Færch-Jensen, A., and Willerslev, E.: Aerial Photographs Reveal Late20th-Century Dynamic Ice Loss in Northwestern Greenland, *Science*, 337, 569 – 573, <https://doi.org/10.1126/science.1220614>, 2012.
- Kluyver, T., Ragan-Kelley, B., Pérez, F., Granger, B., Bussonnier, M., Frederic, J., Kelley, K., Hamrick, J., Grout, J., Corlay, S., Ivanov, P., Avila, D., Abdalla, S., and Willing, C.: Jupyter Notebooks – a publishing format for reproducible computational workflows, 2016.
- Kusk, A., Boncori, J. P. M., and Dall, J.: An automated System for Ice Velocity Measurement from SAR, in: EUSAR 2018; 12th European Conference on Synthetic Aperture Radar, pp. 1–4, VDE, 2018.
- Mankoff, K. D.: Greenland Ice Sheet Discharge 2000 to 2018: All Data, https://doi.org/10.22008/promice/data/ice_discharge, submitted. GEUS Data Center, 2019a.
- Mankoff, K. D.: Greenland Ice Sheet Discharge 2000 to 2018: Code, https://doi.org/10.22008/promice/data/ice_discharge/code/v0.0.1, submitted. GEUS Data Center, 2019b.
- Mankoff, K. D.: Greenland Ice Sheet Discharge 2000 to 2018: Discharge, https://doi.org/10.22008/promice/data/ice_discharge/d/v0.0.1, submitted. GEUS Data Center, 2019c.
- Mankoff, K. D.: Greenland Ice Sheet Discharge 2000 to 2018: Gates, https://doi.org/10.22008/promice/data/ice_discharge/gates/v0.0.1, submitted. GEUS Data Center, 2019d.
- Mankoff, K. D. and Tulaczyk, S. M.: The past, present, and future viscous heat dissipation available for Greenland subglacial conduit formation, *The Cryosphere*, 11, 303–317, <https://doi.org/10.5194/tc-11-303-2017>, 2017.
- McKinney, W.: Data Structures for Statistical Computing in Python, in: Proceedings of the 9th Python in Science Conference, edited by van der Walt, S. and Millman, J., pp. 51 – 56, 2010.
- McNabb, R. W., Hock, R., O’Neel, S., Rasmussen, L. A., Ahn, Y., Braun, M., Conway, H., Herreid, S., Joughin, I. R., Pfeffer, W. T., Smith, B., and Truffer, M.: Using surface velocities to calculate ice thickness and bed topography: a case study at Columbia Glacier, Alaska, USA, *Journal of Glaciology*, 58, 1151–1164, <https://doi.org/10.3189/2012JoG11J249>, 2012.
- Millan, R., Rignot, E., Mouginot, J., Wood, M., Bjørk, A. A., and Morlighem, M.: Vulnerability of Southeast Greenland glaciers to warm Atlantic Water from Operation IceBridge and Ocean Melting Greenland data., *Geophysical Research Letters*, 45, 2688–2696, <https://doi.org/10.1002/2017gl076561>, <http://dx.doi.org/10.1002/2017GL076561>, 2018.
- Moon, T., Ahlstrøm, A., Goelzer, H., Lipscomb, W., and Nowicki, S.: Rising Oceans Guaranteed: Arctic Land Ice Loss and Sea Level Rise, *Current Climate Change Reports*, <https://doi.org/10.1007/s40641-018-0107-0>, <http://dx.doi.org/10.1007/s40641-018-0107-0>, 2018.
- Morlighem, M., Rignot, E., and Willis, J.: Improving Bed Topography Mapping of Greenland Glaciers Using NASA’s Ocean Melting Greenland (OMG) Data, *Oceanography*, 29, 62–71, <https://doi.org/10.5670/oceanog.2016.99>, 2016.
- Morlighem, M., Williams, C., Rignot, E., An, L., Arndt, J. E., Bamber, J., Catania, G., Chauché, N., Dowdeswell, J. A., Dorschel, B., Fenty, I., Hogan, K., Howat, I., Hubbard, A., Jakobsson, M., Jordan, T. M., Kjeldsen, K. K., Millan, R., Mayer, L., Mouginot, J., Noël, B., O’Cofaigh, C., Palmer, S. J., Rysgaard, S., Seroussi, H., Siegert, M. J., Slabon, P., Straneo, F., van den Broeke, M. R., Weinrebe, W., Wood, M., and Zinglensen, K.: IceBridge BedMachine Greenland, Version 3, <https://doi.org/10.5067/2CIX82HUV88Y>, used all subsets; Accessed 2018-10-28, 2017a.

- Morlighem, M., Williams, C. N., Rignot, E., An, L., Arndt, J. E., Bamber, J. L., Catania, G., Chauché, N., Dowdeswell, J. A., Dorschel, B., Fenty, I., Hogan, K., Howat, I. M., Hubbard, A., Jakobsson, M., Jordan, T. M., Kjeldsen, K. K., Millan, R., Mayer, L., Mouginot, J., Noël, B. P. Y., Cofaigh, C. Ó., Palmer, S., Rysgaard, S., Seroussi, H., Siegert, M. J., Slabon, P., Straneo, F., van den Broeke, M. R., Weinrebe, W., Wood, M., and Zinglensen, K. B.: BedMachine v3: Complete bed topography and ocean bathymetry mapping of Greenland from multi-beam echo sounding combined with mass conservation, *Geophysical Research Letters*, <https://doi.org/10.1002/2017gl074954>, 2017b.
- Mouginot, J. and Rignot, E.: Glacier catchments/basins for the Greenland Ice Sheet, <https://doi.org/10.7280/d1wt11>, <https://dash.lib.uci.edu/stash/dataset/doi:10.7280/D1WT11>, 2019.
- Mouginot, J., Rignot, E., Scheuchl, B., and Millan, R.: Comprehensive Annual Ice Sheet Velocity Mapping Using Landsat-8, Sentinel-1, and RADARSAT-2 Data, *Remote Sensing*, 9, 364, <https://doi.org/10.3390/rs9040364>, <http://dx.doi.org/10.3390/rs9040364>, 2017.
- Mouginot, J., Bjørk, A. A., Millan, R., Scheuchl, B., and Rignot, E.: Insights on the Surge Behavior of Storstrømmen and L. Bistrup Bræ, Northeast Greenland, Over the Last Century, *Geophysical Research Letters*, 45, 11, 197–11,205, <https://doi.org/10.1029/2018gl079052>, 2018a.
- Mouginot, J., Rignot, E., Millan, R., Wood, M., and Scheuchl, B.: Annual Ice Velocity of the Greenland Ice Sheet (1972-1990), <https://doi.org/10.7280/d1mm37>, <https://dash.lib.uci.edu/stash/dataset/doi:10.7280/D1MM37>, v5, 2018b.
- Mouginot, J., Rignot, E., Scheuchl, B., Millan, R., and Wood, M.: Annual Ice Velocity of the Greenland Ice Sheet (1991-2000), <https://doi.org/10.7280/d1gw91>, <https://dash.lib.uci.edu/stash/dataset/doi:10.7280/D1GW91>, v6, 2018c.
- Murray, T., Scharrer, K., Selmes, N., Booth, A. D., James, T. D., Bevan, S. L., Bradley, J., Cook, S., Llana, L. C., Drocourt, Y., and et al.: Extensive retreat of Greenland tidewater glaciers, 2000–2010, *Arctic, Antarctic, and Alpine Research*, 47, 427–447, <https://doi.org/10.1657/aaar0014-049>, <http://dx.doi.org/10.1657/AAAR0014-049>, 2015.
- Nerem, R. S., Beckley, B. D., Fasullo, J. T., Hamlington, B. D., Masters, D., and Mitchum, G. T.: Climate-change-driven accelerated sea-level rise detected in the altimeter era, *Proceedings of the National Academy of Sciences*, 115, 2022–2025, <https://doi.org/10.1073/pnas.1717312115>, <http://dx.doi.org/10.1073/pnas.1717312115>, 2018.
- Neteler, M., Bowman, M. H., Landa, M., and Metz, M.: GRASS GIS: a multi-purpose Open Source GIS, *Environmental Modelling & Software*, 31, 124–130, <https://doi.org/10.1016/j.envsoft.2011.11.014>, 2012.
- Oliphant, T. E.: *A guide to NumPy*, vol. 1, Trelgol Publishing USA, 2006.
- Pérez, F. and Granger, B. E.: IPython: a System for Interactive Scientific Computing, *Comput. Sci. Eng.*, 9, 21–29, <http://ipython.scipy.org>, 2007.
- PROJ contributors: PROJ coordinate transformation software library, Open Source Geospatial Foundation, <https://proj4.org/>, 2018.
- Rathmann, N. M., Hvidberg, C. S., Solgaard, A. M., Grinsted, A., Gudmundsson, G. H., Langen, P. L., Nielsen, K. P., and Kusk, A.: Highly temporally resolved response to seasonal surface melt of the Zachariae and 79N outlet glaciers in northeast Greenland, *Geophysical Research Letters*, 44, 9805–9814, <https://doi.org/10.1002/2017gl074368>, <http://dx.doi.org/10.1002/2017GL074368>, 2017.
- Reeh, N., Bøggild, C., and Oerter, H.: Surge of Storstrømmen, a large outlet glacier from the Inland Ice of North-East Greenland, *Grønlands Geologiske Undersøgelse Rapport* 162, pp. 201–209, 1994.
- Rezvanbehbahani, S., Stearns, L. A., Kadivar, A., Walker, J. D., and van der Veen, C. J.: Predicting the Geothermal Heat Flux in Greenland: A Machine Learning Approach, *Geophysical Research Letters*, 44, 12, 271–12,279, <https://doi.org/10.1002/2017gl075661>, <http://dx.doi.org/10.1002/2017GL075661>, 2017.

- Rignot, E. J. and Mouginot, J.: Ice flow in Greenland for the International Polar Year 2008-2009, *Geophysical Research Letters*, 39, n/a–n/a, <https://doi.org/10.1029/2012GL051634>, 2012.
- Rignot, E. J., Box, J. E., Burgess, E. W., and Hanna, E.: Mass balance of the Greenland ice sheet from 1958 to 2007, *Geophysical Research Letters*, 35, <https://doi.org/10.1029/2008GL035417>, 2008.
- 5 Schulte, E., Davison, D., Dye, T., and Dominik, C.: A multi-language computing environment for literate programming and reproducible research, *Journal of Statistical Software*, 46, 1–24, 2012.
- Seabold, S. and Perktold, J.: Statsmodels: Econometric and statistical modeling with python, in: 9th Python in Science Conference, 2010.
- Strozzi, T., Luckman, A., Murray, T., Wegmuller, U., and Werner, C.: Glacier motion estimation using SAR offset-tracking procedures, *IEEE Transactions on Geoscience and Remote Sensing*, 40, 2384–2391, <https://doi.org/10.1109/tgrs.2002.805079>, <http://dx.doi.org/10.1109/TGRS.2002.805079>, 2002.
- 10 Tange, O.: GNU Parallel - The Command-Line Power Tool, ;login: The USENIX Magazine, 36, 42–47, <https://doi.org/10.5281/zenodo.16303>, <http://www.gnu.org/s/parallel>, 2011.
- Tinto, K. J., Bell, R. E., Cochran, J. R., and Münchow, A.: Bathymetry in Petermann fjord from Operation IceBridge aerogravity, *Earth and Planetary Science Letters*, 422, 58–66, <https://doi.org/10.1016/j.epsl.2015.04.009>, 2015.
- 15 van den Broeke, M., Box, J., Fettweis, X., Hanna, E., Noël, B., Tedesco, M., Van As, D., Van De Berg, W. J., and Van Kampenhout, L.: Greenland Ice Sheet Surface Mass Loss: Recent Developments in Observation and Modeling, *Current Climate Change Reports*, <https://doi.org/10.1007/s40641-017-0084-8>, <http://dx.doi.org/10.1007/s40641-017-0084-8>, 2017.
- Van Rossum, G. and Drake Jr, F. L.: Python reference manual, Centrum voor Wiskunde en Informatica Amsterdam, 1995.
- Vijay, S., Khan, S. A., Kusk, A., Solgaard, A. M., Moon, T., and Bjørk, A. A.: Resolving seasonal ice velocity of 45 Greenlandic
20 glaciers with very high temporal details, *Geophysical Research Letters*, <https://doi.org/10.1029/2018gl081503>, <http://dx.doi.org/10.1029/2018GL081503>, 2019.
- WCRP Global Sea Level Budget Group: Global sea-level budget 1993–present, *Earth System Science Data*, 10, 1551–1590, <https://doi.org/10.5194/essd-10-1551-2018>, <http://dx.doi.org/10.5194/essd-10-1551-2018>, 2018.
- Wiese, D. N., Yuan, D.-N., Boening, C., Landerer, F. W., and Watkins, M. M.: JPL GRACE Mascon Ocean, Ice, and Hydrology Equivalent
25 HDR Water Height RL05M.1 CRI Filtered Version 2, <https://doi.org/10.5067/TEMSC-2LCR5>, dataset accessed [2017-12-14], 2016.
- Wood, M., Rignot, E., Fenty, I., Menemenlis, D., Millan, R., Morlighem, M., Mouginot, J., and Seroussi, H.: Ocean-induced melt triggers glacier retreat in Northwest Greenland, *Geophysical Research Letters*, <https://doi.org/10.1029/2018gl078024>, <http://dx.doi.org/10.1029/2018GL078024>, 2018.
- Zwally, H. J., Giovinetto, M. B., Beckley, M. A., and Saba, J. L.: Antarctic and Greenland Drainage Systems, http://icesat4.gsfc.nasa.gov/cryo_data/ant_grn_drainage_systems.php, GSFC Cryospheric Sciences Laboratory, 2012.
- 30

Figures

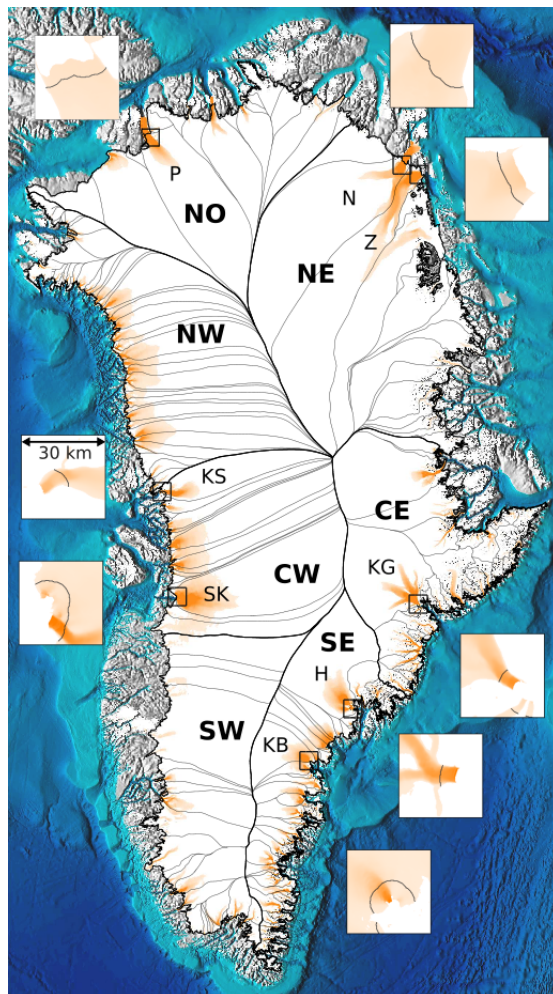


Figure 1. Overview showing fast-flowing ice (orange, greater than 100 m yr^{-1}) and the gates for the ~~seven~~ top eight discharging glaciers (Fig. 6). Gates are shown as black lines in inset images. Each inset is $30 \times 30 \text{ km}$ and all have the same color scaling, but different than the main map. Insets pair with nearest label and box. On the main map, ~~sectors~~ regions from ~~Mouginot et al. (2017)~~ Mouginot and Rignot (2019) are designated by thicker black lines and large bold labels. ~~Catchments~~ Sectors (same source) are delineated with thinner gray lines, and the top discharging ~~catchments~~ glaciers are labeled with smaller font. H = Helheim Gletsjer, KB = (Køge Bugt), KG = Kangerlussuaq Gletsjer, KS = Kangilliup Sermia (Rink Isbræ), N = (Nioghalvfjærdsbræ), P = Petermann Gletsjer, SK = Sermeq Kujalleq (Jakobshavn Isbræ), and Z = Zachariae Zachariae Isstrøm. Basemap terrain (gray), ocean bathymetry (blues), and ice mask (white) come from BedMachine.

~~Histogram of thickness at gate pixels showing both unadjusted (BedMachine & Millan et al. (2018)) and adjusted (this study) thickness as described in the text.~~

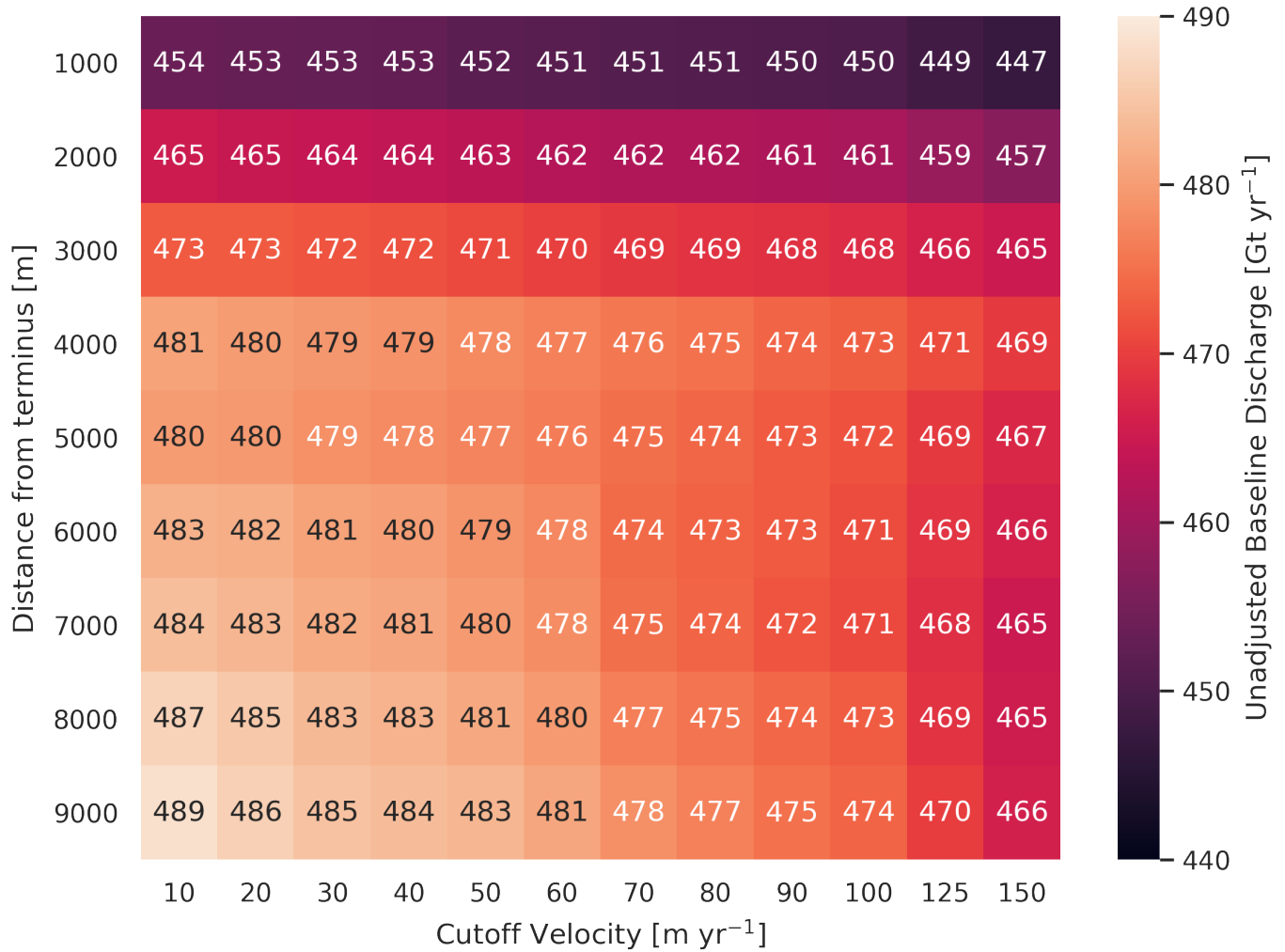


Figure 2. Heatmap and table showing ice sheet discharge as a function of gate buffer distance and ice speed cutoff. The colors of the numbers change for readability.

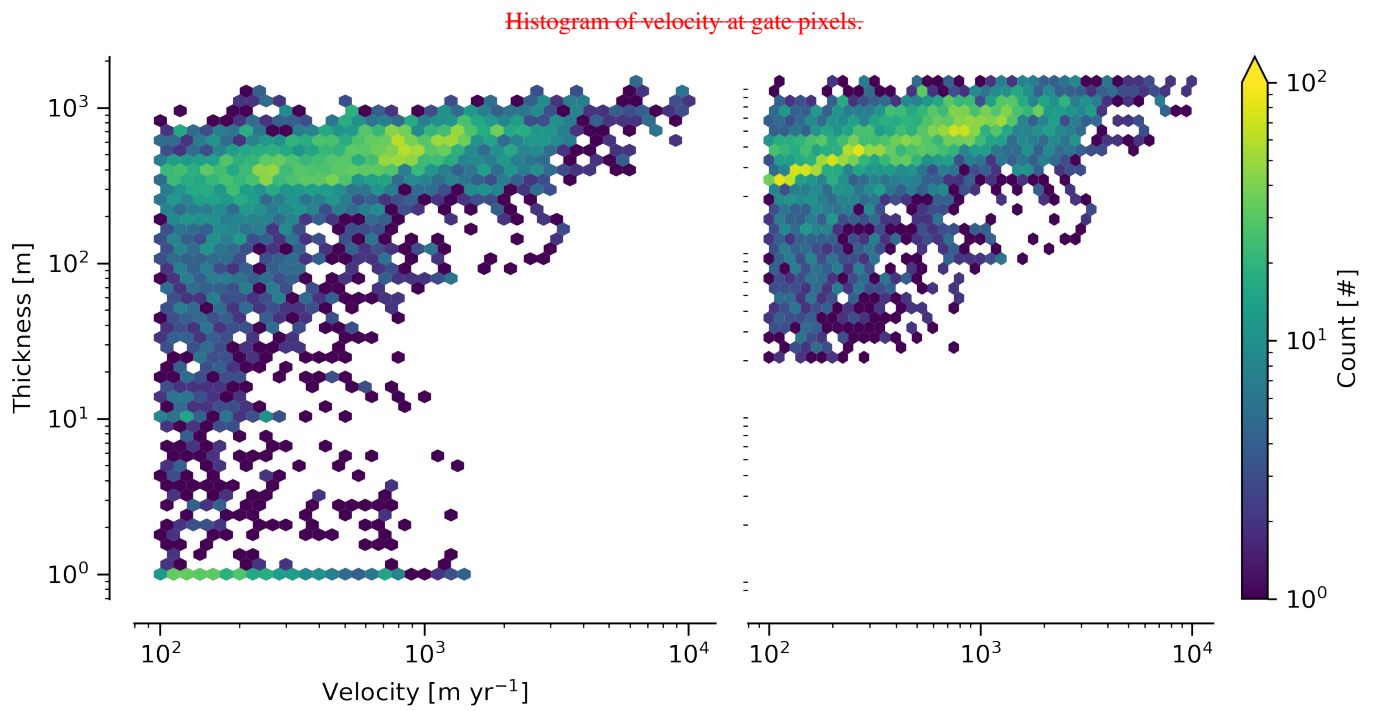


Figure 3. 2D histogram of velocity and thickness at all gate pixels. Left panel: Unadjusted (BedMachine & Millan et al. (2018)) thickness. Right panel: Adjusted (as described in the text) thickness.

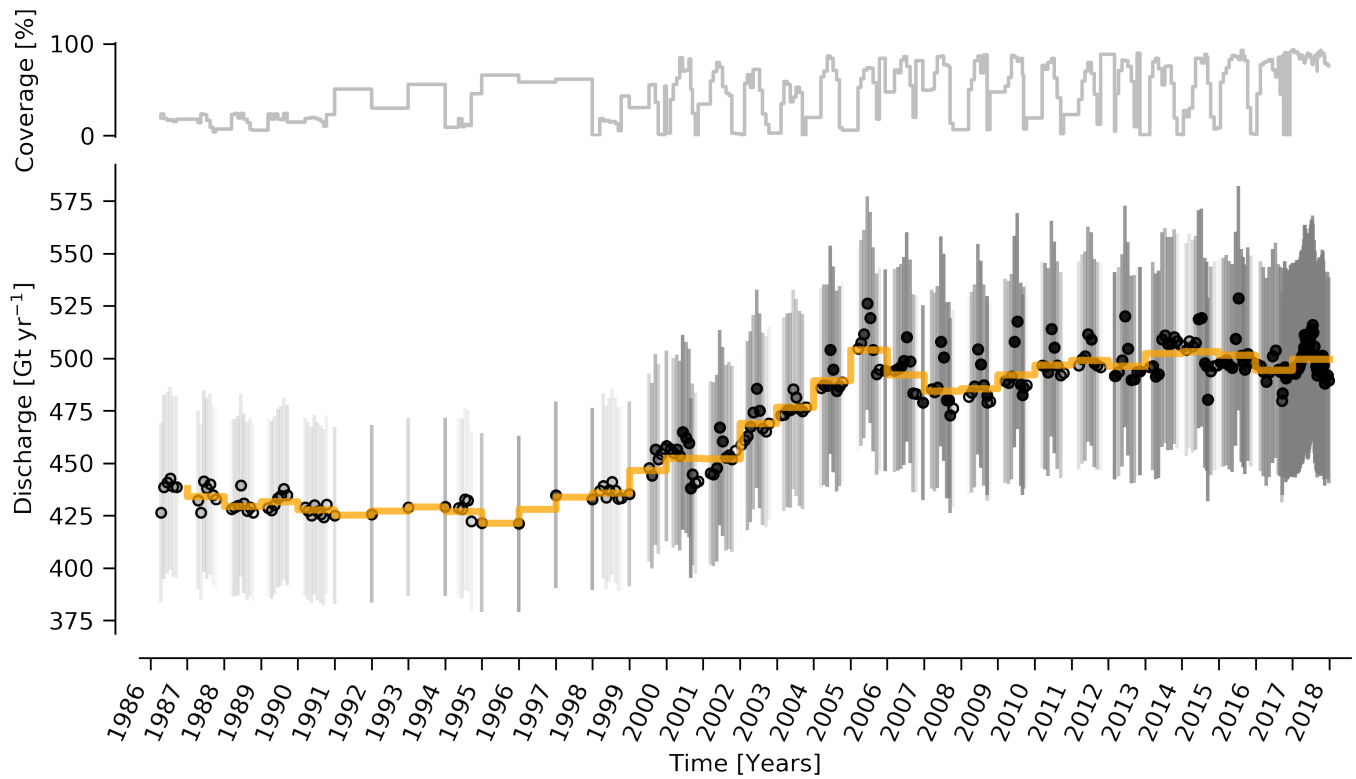


Figure 4. Bottom panel: Time series of ice discharge from the Greenland ice sheet. Dots represent when observations occurred. Orange stepped line is annual average. Coverage (percentage of total discharge observed at any given time) is shown in top panel, and also by opacity of dot interior and error bars on lower panel. When coverage is < 100 %, total discharge is estimated and shown by linearly interpolating missing coverage.

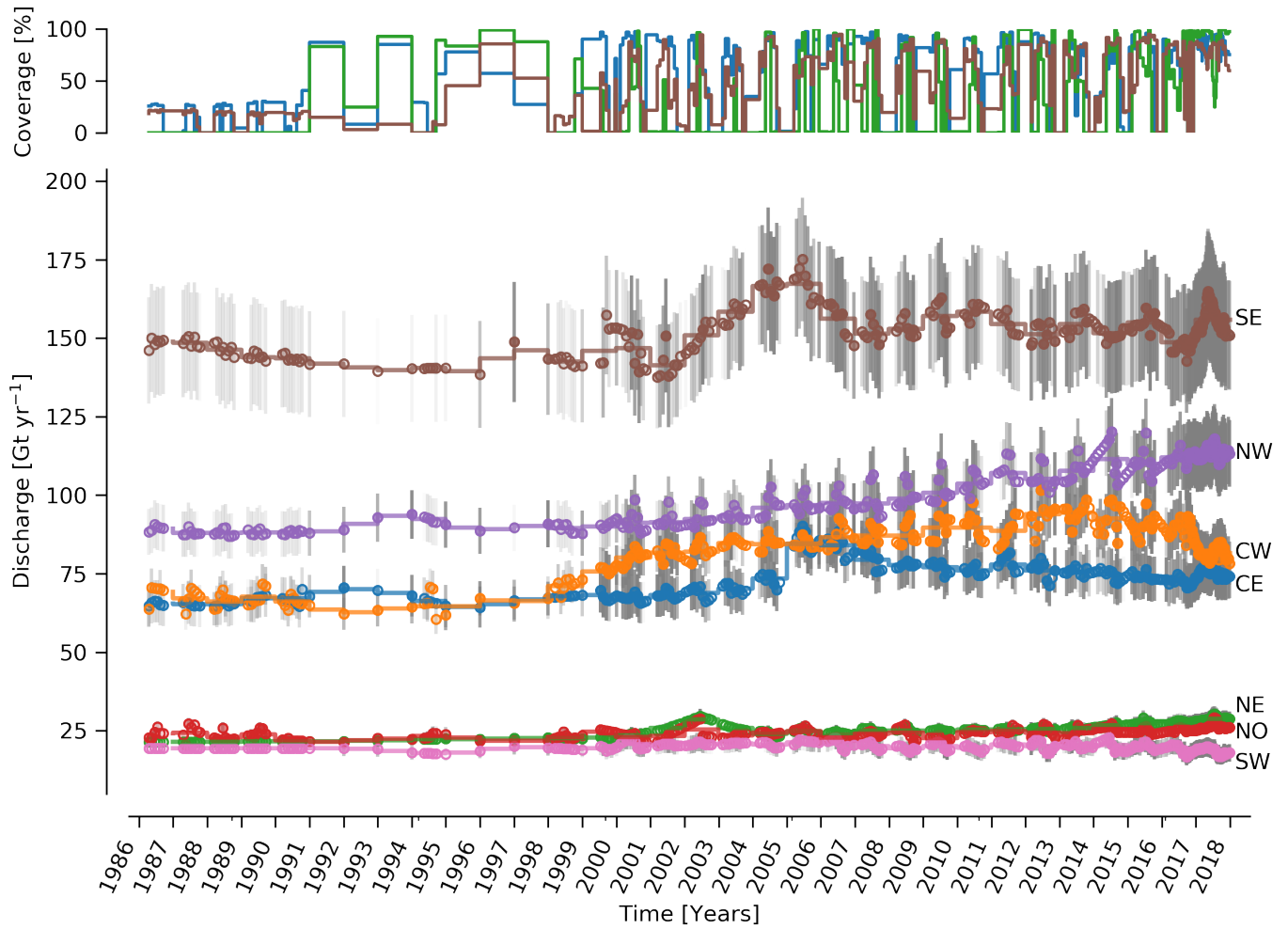


Figure 5. Bottom panel: Time series of ice discharge by [sector](#)[region](#). Same graphical properties as Fig. 4. Top panel: The [sector](#)[region](#) with highest coverage (CE), lowest coverage (NE), and coverage for [sector](#)[the region](#) with highest discharge (SE) are shown. Coverage for other [sectors](#)[regions](#) not shown to reduce clutter.

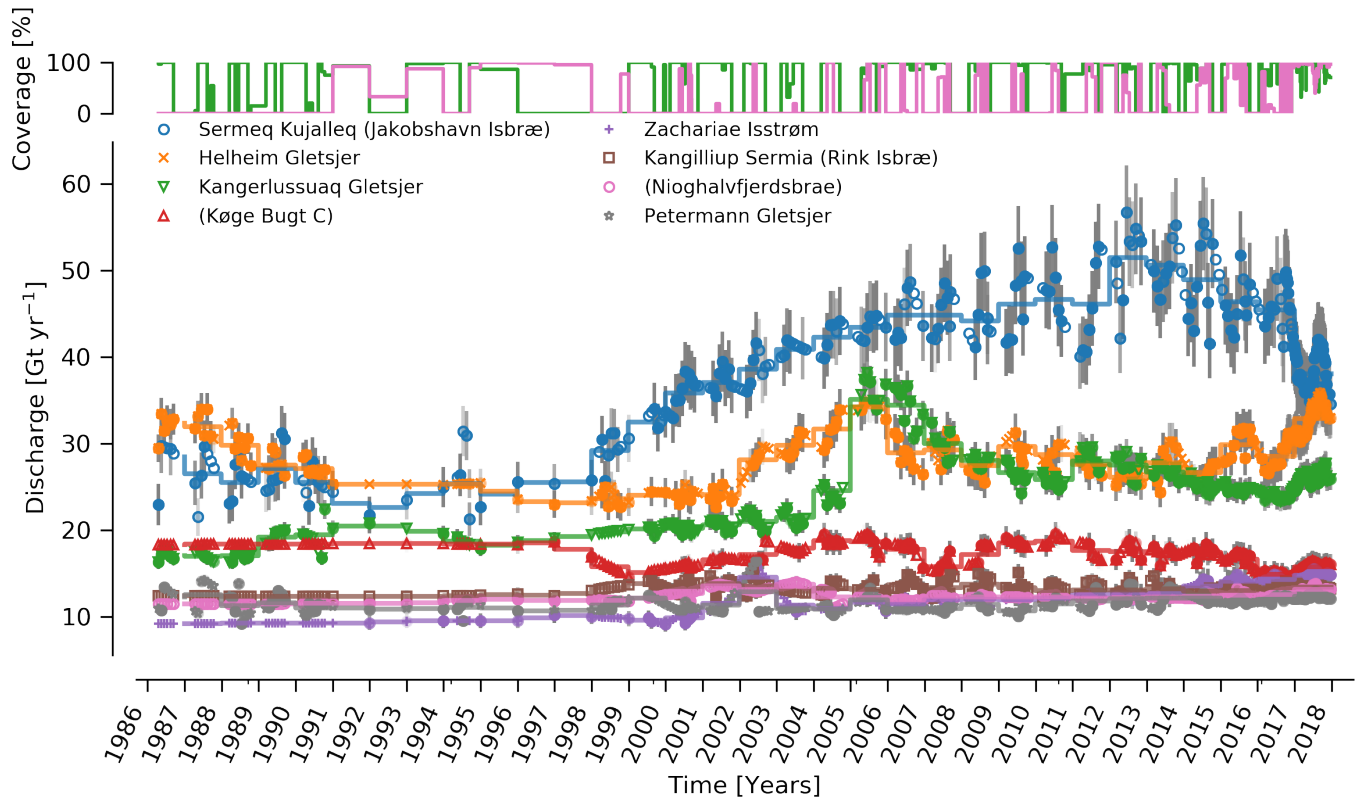


Figure 6. Bottom panel: Time series of ice discharge showing top seven-eight (mean of last year) discharging glaciers. Same graphical properties as Fig. 4. Only highest-an example high (Kangerlussuaq Gletsjer) and lowest-low (Nioghalvfjerdsbrae) coverage shown to reduce clutter.

Appendix A: Errors and Uncertainties

Here we describe our error and uncertainty treatments. We begin with a brief philosophical discussion of common uncertainty treatments, our general approach, and then the influence of various decisions made throughout our analysis, such as gate location and treatments of unknown thicknesses.

5 Traditional and mathematically valid uncertainty treatments divide errors into two classes: systematic (bias) and random. The primary distinction is that systematic errors do not decrease with more samples, and random errors decrease as the number of samples or measurements increases. The question is then which errors are systematic and which are random. A common treatment is to decide that errors within a ~~sector~~-~~region~~ are systematic, and among ~~sectors~~-~~regions~~ are random. This approach has no physical basis - two glaciers a few 100 m apart but in different ~~sectors~~-~~regions~~ are assumed to have random errors, but
10 two glaciers 1000s of km apart but within the same ~~sector~~-~~region~~ are assumed to have systematic errors. ~~In reality, it may be~~ It is more likely the case that all glaciers ~~<W km wide, or>D m deep, less wide than some width or more deep than some depth~~ have systematic errors even if ~~some~~-~~they~~ are on opposite sides of the ice sheet, ~~at least when the~~-~~if~~ ice thickness is estimated with the same method (i.e. the systematic error is likely caused by the sensor and airplane, not the location of the glacier).

The decision to have R random samples (where R is the number of ~~sectors~~-~~regions~~, usually ~ 18 based on ~~the Zwally sectors~~ (Zwally et al., 2012)~~Zwally et al. (2012)~~) is also arbitrary. Mathematical treatment of random errors means that even if the error is 50 %, 18 measurements reduces it to only 11.79 %.

This ~~effect~~-~~reduction~~ is unlikely to be physically meaningful. Our ~~171 sectors, 263 gates and 5980~~-~~176 sectors, 276 gates and 6002~~ pixels means that even if errors were 100 % for each, we could reduce it to ~~7.6, 6.2, 7.5, 6.0~~, or 1.3 % respectively. We note that the area error introduced by the common EPSG:3413 map projection is ~~+8~~-~~5~~ % in the north and ~~-6~~-~~8~~ % in the south, ~~and~~
20 ~~while it may be considered in other works, it is~~. While this error is mentioned in some other works (e.g. Joughin et al. (2018)) it is often not explicitly mentioned.

We do not have a solution for the issues brought up here, except to discuss them explicitly and openly so that those, and our own, error treatments are clearly presented and understood to likely contain errors themselves.

A1 Invalid Thickness

25 We assume ice ~~velocities are correct and ice~~-thicknesses < 20 m are incorrect where ice speed is > 100 m yr⁻¹. Of ~~5980~~-~~pixels, 5380~~-~~6002~~ pixels, ~~5366~~ have valid thickness, and ~~600~~-~~(10~~-~~636~~ (~~12~~ %)) have invalid thickness. However, the speed at the locations of the invalid thicknesses is generally much less (and therefore the assumed thickness is less), and the influence on discharge is less than an average pixel with valid thickness (Table A1).

When aggregating by gate, there are ~~263~~-~~276~~ gates. Of these, ~~186~~-~~(70~~-~~187~~ (~~68~~ %)) have no bad pixels and ~~77~~-~~(30~~-~~89~~ (~~32~~ %))
30 have some bad pixels, ~~53~~-~~65~~ have > 50 % bad pixels, and ~~49~~-~~(19~~-~~61~~ (~~22~~ %)) are all bad pixels.

We adjust these thickness using a poor fit (correlation coefficient: 0.3) of the \log_{10} of the ice speed to thickness where the relationship is known (thickness > 20 m). We set errors equal to one half the thickness (i.e. $\sigma_H = \pm 0.5 H$). We also test the sensitivity of this treatment to simpler treatments, and have the following ~~four~~-~~five~~ categories:

Table A1. Statistics of pixels with and without valid thickness. Numbers represent speed [m yr⁻¹] except for the "count" row.

	Good Pixels	Bad Pixels
count	5366	636
mean	821	266
std	1040	235
min	100	101
25%	230	129
50%	487	171
75%	972	281
max	10044	1423

NoAdj No adjustments made. Assume BedMachine thickness are all correct.

NoAdj+Millan Same as NoAdj, but using Millan et al. (2018) ~~thickness~~ bed where available.

300 If a gate has some valid pixel thicknesses, set the invalid thicknesses to the minimum of the valid thicknesses. If a gate has no valid thickness, set the thickness to 300 m.

5 **400** Set all thickness < 50 m to 400 m

Fit Use the thickness v. speed relationship described above.

Table A2 shows the estimated baseline discharge to these four treatments:

Table A2. Effect of different thickness adjustments on baseline discharge

Treatment	Discharge [Gt]
NoAdj	472 ± 49
NoAdj+Millan	480 ± 49
300	488 ± 49
400	495 ± 51
Fit	492 ± 51

Finally, Figure A1 shows the geospatial locations, concentration, and speed of gates with and without bad pixels.

A2 Missing Velocity

10 ~~The velocity products come with their own uncertainty value at each location. Here we clarify our temporal gap-filling of missing velocities.~~

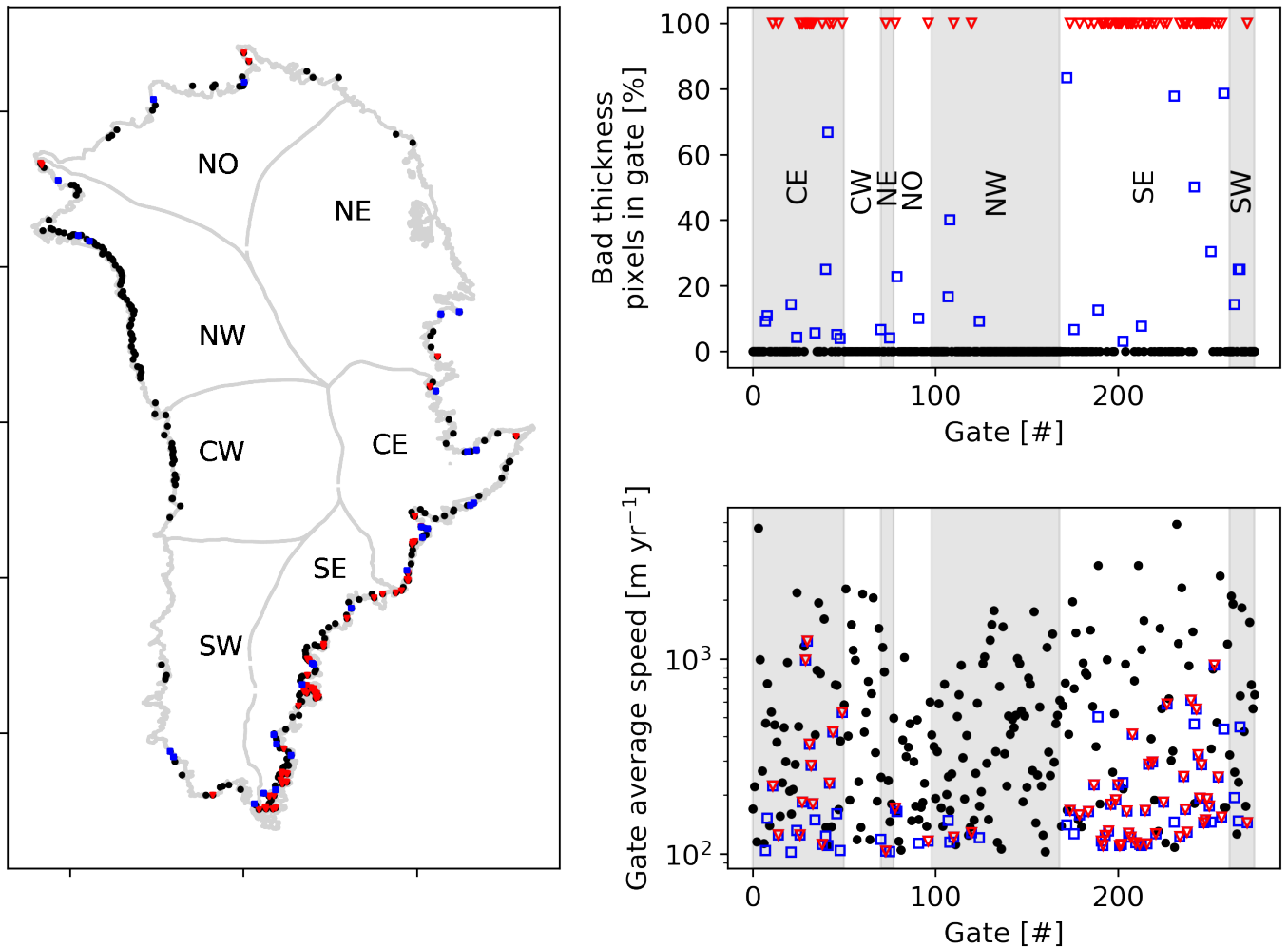


Figure A1. Gate locations and thickness quality. Left: locations of all gates. Black dots represent gates with 100 % valid thickness pixels, blue with partial, and red with none. Top right: Percent of bad pixels in each of the 264-276 gates, arranged by region. Bottom panel: Average speed of gates. Color same as left panel.

We estimate discharge at all pixel locations for any time when there exists any velocity product. Not every velocity product provides velocity estimates at all locations, and we fill in where there are gaps by linear interpolating velocity at each pixel in time. We calculate coverage, the discharge-weighted percent of observed velocity at any given time (Figure A2), and display coverage as 1) line plots over ~~some of~~ the time series graphs, 2) opacity of the error bars and 3) opacity of the infilling of time series dots. Linear interpolation and discharge-weighted coverage is illustrated in Figure A2, where pixel A has a velocity value at all three times, but pixel B has a filled gap at time t_3 . The concentration of valid pixels is 0.5, but the weighted concentration, or coverage, is $9/11$ or ~ 0.82 . When displaying these three discharge values, t_1 and t_4 would have opacity of 1 (black), and t_3 would have opacity of 0.82 (dark gray).

This treatment is applied at the pixel level and then ~~averaged~~ weight-averaged to the gate, ~~catchment, sector, sector, region,~~ and ice sheet results.

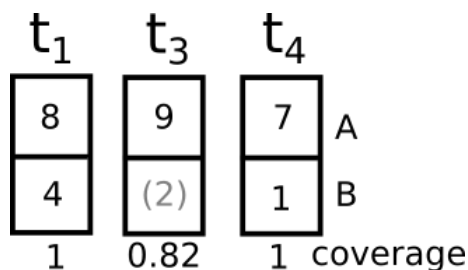


Figure A2. Schematic demonstrating coverage. Velocities are filled with linear interpolation in time, and coverage is weighted by discharge. t columns represent the same two gate pixels (A & B) at three time steps, where t_n are linearly spaced, but t_2 is not observed anywhere on the ice sheet and therefore not included. Numbers in boxes represents example discharge values. Gray parenthetical number is filled, not sampled, in pixel B at time t_3 . Weighted filling computes the coverage as $9/11 = 0.81$, instead of 0.5 (half of the pixels at time t_3 have observations).

A3 ~~Errors from map projection~~ Filtered Velocity

Our work takes place in a projected coordinate system (EPSG 3413) and therefore errors are introduced between the "true" earth spheroid (which is itself an approximation) and our projected coordinates system. We address these by calculating the projection error due to EPSG 3413 which is approximately +8 % in Northern Greenland and -6 % in Southern Greenland, and multiplying variables by a scaling factor if the variables do not already take this into account. Velocities are "true velocities" and not scaled. Here we show the same time series as in Figs. 4, 5, and 6 but without any velocity filtering applied.

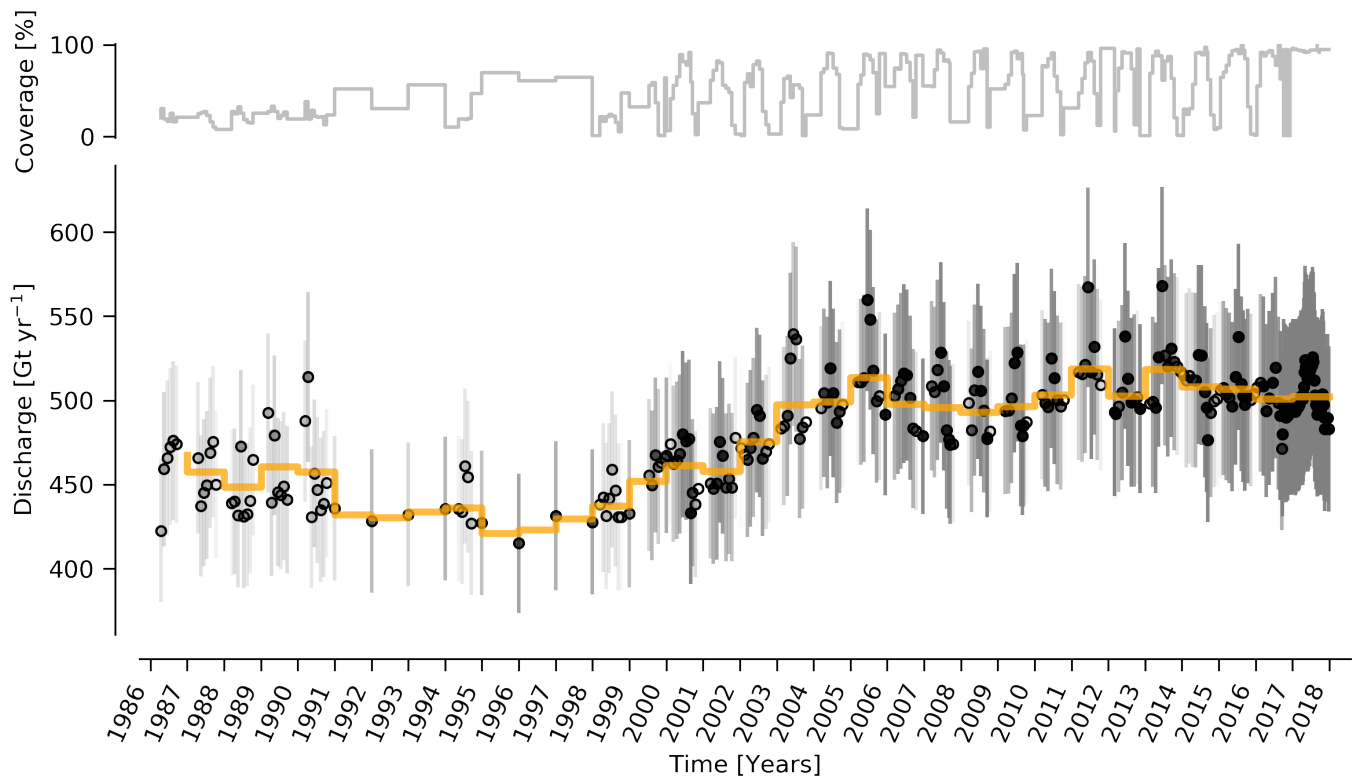


Figure A3. [Same as Fig. 4](#) but [the nominal 200-m gate width is scaled](#) [without the velocity filter.](#) [Note different y-axis](#)

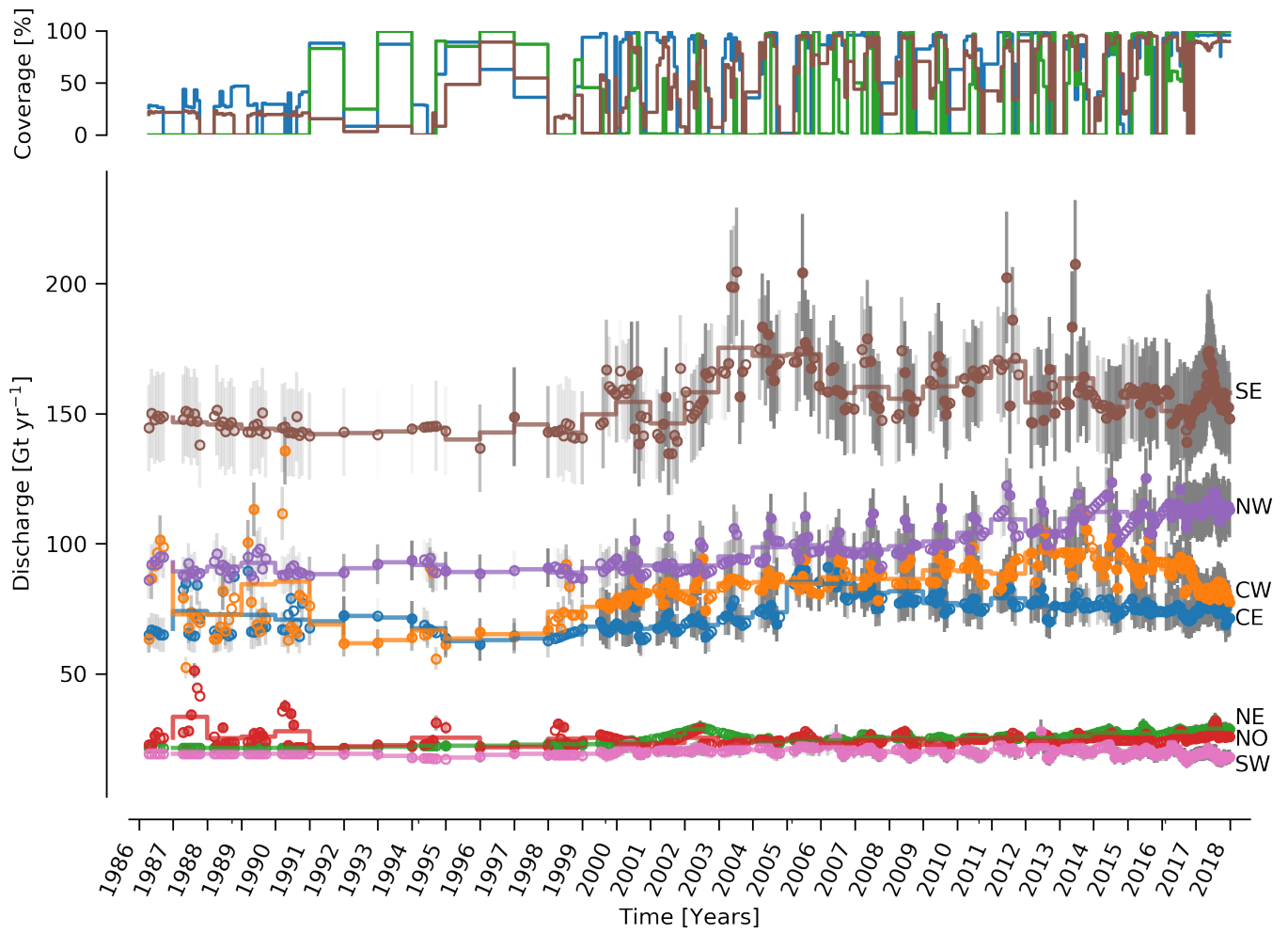


Figure A4. Same as Fig. 5 but without the velocity filter. Note different y-axis

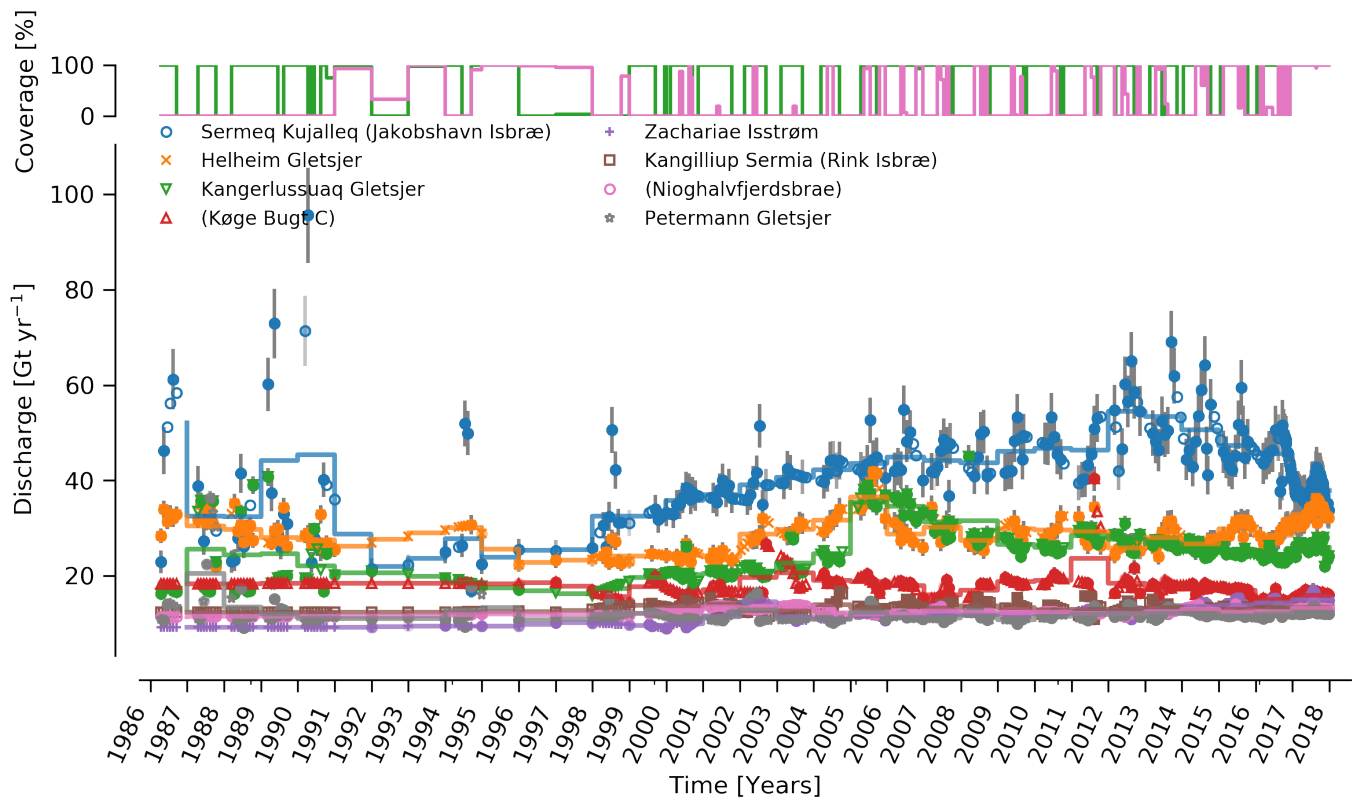


Figure A5. Same as Fig. 6 but without the velocity filter. Note different y-axis

Appendix B: ~~Køge Bugt Bamber~~

Appendix B: Køge Bugt Bed Change between Bamber et al. (2013) and Morlighem et al. (2017b)

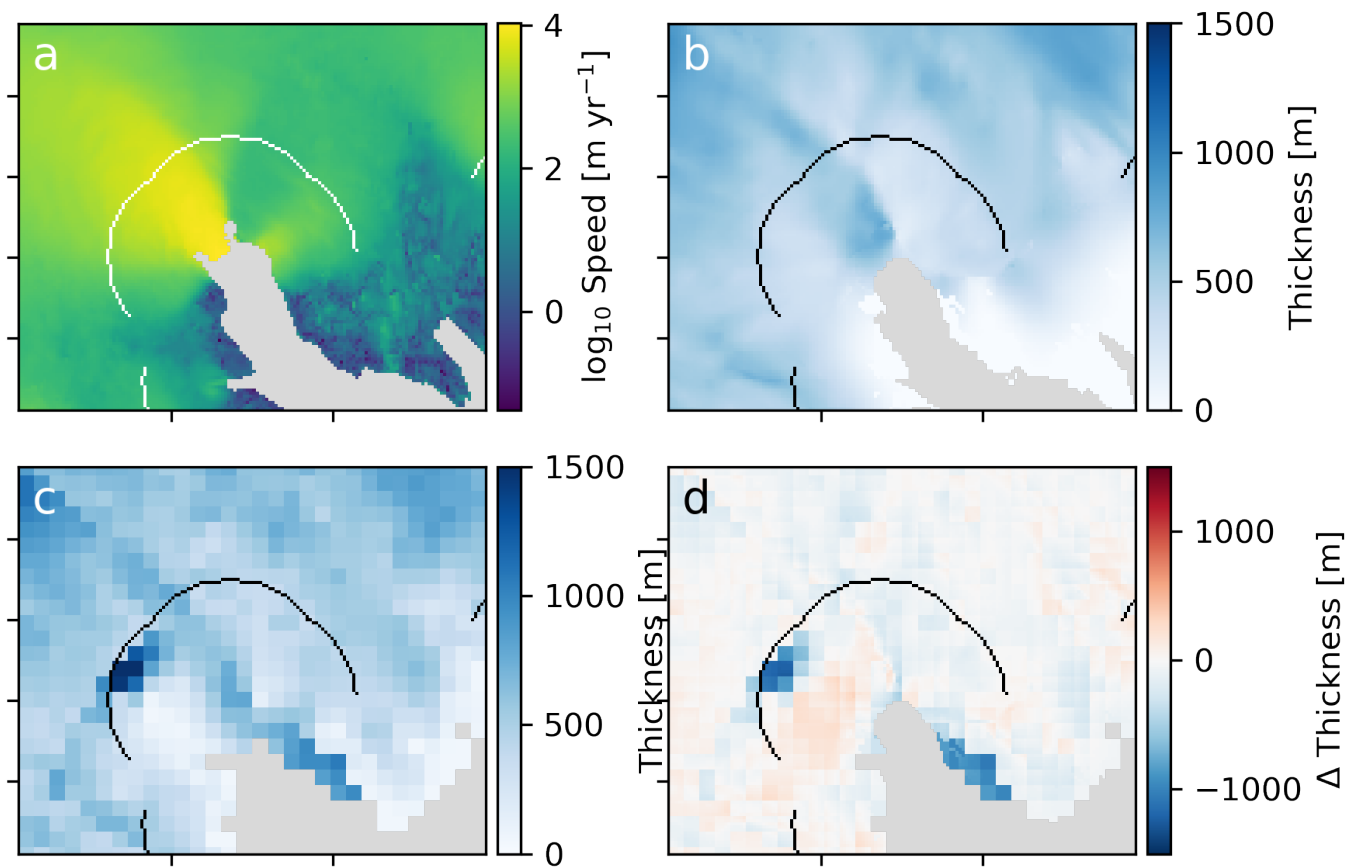


Figure B1. Differences between BedMachine ([Morlighem et al., 2017b](#)) and Bamber et al. (2013) near Køge Bugt. Panel (a) is baseline ice speed, (b) BedMachine thickness, (c) Bamber et al. (2013) thickness, and (d) difference computed as BedMachine - Bamber. Curved line is gate used in this work.

~~Regional Discharge with logarithmic y-axis Same as Fig. 5 but with logarithmic y-axis so that NE, NO, and SW sectors are more visible~~

Appendix C: Sentinel-1 ice velocity maps

We use ESA Sentinel-1 synthetic aperture radar (SAR) data to derive ice velocity maps covering the Greenland Ice Sheet margin using offset tracking (Strozzi et al., 2002) assuming surface parallel flow using the digital elevation model from the Greenland Ice Mapping Project (GIMP DEM, NSIDC 0645) by Howat et al. (2014, 2015). The operational interferometric post processing (IPP) chain (Dall et al., 2015; Kusk et al., 2018), developed at the Technical University of Denmark (DTU) Space and upgraded with offset tracking for ESA's Climate Change Initiative (CCI) Greenland project, was employed to derive the surface movement. The Sentinel-1 satellites have a repeat cycle of 12 days, and due to their constellation, each track has a six-day repeat cycle. We produce a Greenland wide product that spans two repeat cycles of Sentinel-1 A. The product is a mosaic of all the ice velocity maps based on 12 day pairs produced from all the tracks from Sentinel-1 A and B covering Greenland during those two cycles. The product thus has a total time span of 24 days. Six day pairs are also included in each mosaic from track 90, 112 and 142 covering the ice sheet margin in the south as well as other tracks on an irregular basis in order to increase the spatial resolution. (Rathmann et al., 2017) and Vijay et al. (2019) have exploited the high temporal resolution of the product to investigate dynamics of glaciers. The maps are available from 2016-09-13 and onward, are updated regularly, and are freely available from <http://promice.dk>.

Appendix D: ~~Catchments and Sectors~~

~~Catchment outlines of 260 glaciers are determined using ice flow direction from velocity and from topographic slope. In areas of flow greater than 100 m/yr, we use a composite ice velocity map (Mouginot et al., 2017), and, in slow-moving areas, we use surface slope to get the direction of the flow (GIMP, Howat et al. (2014, 2017)) smoothed over a spatially variable distance of 10 ice thicknesses to remove short-wavelength undulations of the surface. Glacier catchments are regrouped in 7 large regions, which were defined based on ice flow regime, and the need to divide the ice sheet into areas comparable in size and discharge with relatively homogeneous climate conditions.~~

Appendix D: Software

This work was performed ~~primarily using~~ using only open-source software, primarily GRASS GIS (Neteler et al., 2012) ; ~~Python (Van Rossum and Drake Jr, 1995), and and IPythonPython (Pérez and Granger, 2007)(Van Rossum and Drake Jr, 1995),~~ in particular the Jupyter (Kluyver et al., 2016), pandas (McKinney, 2010), numpy (Oliphant, 2006), statsmodel
5 (Seabold and Perktold, 2010), x-array (Hoyer and Hamman, 2017), and Matplotlib (Hunter, 2007) ~~libraries~~packages. The entire work was performed in Emacs using Org Mode (Schulte et al., 2012). The parallel (Tange, 2011) tool was used to speed up processing. We used proj4 (PROJ contributors, 2018) to compute the errors in the EPSG 3413 projection. All code used in this work is available in the Supplemental Material.

6 Revised Document

Greenland Ice Sheet solid ice discharge from 1986 through 2017

Kenneth D. Mankoff¹, Willam Colgan¹, Anne Solgaard¹, Nanna B. Karlsson¹, Andreas P. Ahlstrøm¹, Dirk van As¹, Jason E. Box¹, Shfaqat Abbas Khan², Kristian K. Kjeldsen¹, Jeremie Mouginot³, and Robert S. Fausto¹

¹Department of Glaciology and Climate, Geological Survey of Denmark and Greenland (GEUS), Copenhagen, Denmark

²DTU Space, National Space Institute, Department of Geodesy, Technical University of Denmark, Kgs. Lyngby, Denmark

³Department of Earth System Science, University of California, Irvine, CA, USA

Correspondence: Ken Mankoff (kdm@geus.dk)

Abstract. We present a 1986 through 2017 estimate of Greenland Ice Sheet ice discharge. Our data include all discharging ice that flows faster than 100 m yr^{-1} and are generated through an automatic and adaptable method, as opposed to conventional hand-picked gates. We position gates near the present-year termini and estimate problematic bed topography (ice thickness) values where necessary. In addition to using annual time-varying ice thickness, our time series uses velocity maps that begin with sparse spatial and temporal coverage and ends with near-complete spatial coverage and six-day updates to velocity. The 2010 through 2017 average ice discharge through the flux-gates is $\sim 488 \pm 49 \text{ Gt yr}^{-1}$. The 10 % uncertainty stems primarily from uncertain ice bed location (ice thickness). We attribute the $\sim 50 \text{ Gt yr}^{-1}$ differences among our results and previous studies to our use of updated bed topography from BedMachine v3. Discharge is approximately steady from 1986 to 2000, increases sharply from 2000 to 2005, then is approximately steady again. However, regional and glacier variability is more pronounced, with recent decreases at most major glaciers and in all but one region offset by increases in the NW region. As part of the journal's living archive option, all input data, code, and results from this study will be updated when new input data are accessible and made freely available at doi:10.22008/promice/data/ice_discharge.

1 Introduction

The mass of the Greenland ice sheet is decreasing (e.g. Fettweis et al. (2017); van den Broeke et al. (2017); Wiese et al. (2016); Khan et al. (2016)). Most ice sheet mass loss – as iceberg discharge, submarine melting, and meltwater runoff – enters the fjords and coastal seas, and therefore ice sheet mass loss directly contributes to sea-level rise (WCRP Global Sea Level Budget Group, 2018; Moon et al., 2018; Nerem et al., 2018; Chen et al., 2017). Greenland's total ice loss can be estimated through a variety of independent methods, for example 'direct' mass change estimates from GRACE (Wiese et al., 2016) or by using satellite altimetry to estimate surface elevation change, which is then converted into mass change (using a firn model, e.g. Khan et al. (2016)). However, partitioning the mass loss between ice discharge (D) and surface mass balance (SMB) remains challenging (c.f. Rignot et al. (2008) and Enderlin et al. (2014)). Correctly assessing mass loss, as well as the attribution of this loss (SMB or D) is critical to understanding the process-level response of the Greenland ice sheet to climate change, and thus improving models of future ice-sheet changes and associated sea-level rise (Moon et al., 2018).

The total mass of an ice-sheet, or a drainage basin, changes if the mass gain (SMB inputs, primarily snowfall) is not balanced by the mass loss (D and SMB outputs, the latter generally meltwater runoff). This change is typically termed ice-sheet mass balance (MB) and the formal expression for this rate of change in mass is (e.g. Cuffey and Paterson (2010)),

$$\frac{dM}{dt} = \rho \int_A b dA - \int_g Q dg, \quad (1)$$

5 where ρ is the average density of ice, b is an area mass balance, and Q is the discharge flux. The left hand side of the equation is the rate of change of mass, the first term on the right hand side is the area A integrated surface mass balance (SMB), and the second term is the discharge D mass flow rate that drains through gate g . Equation 1 is often simplified to

$$MB = SMB - D \quad (2)$$

where MB is the mass balance, and referred to as the "input-output" method (e.g. Khan et al. (2015)). Virtually all studies agree on the trend of Greenland mass balance, but large discrepancies persist in both the magnitude and attribution. Magnitude discrepancies include, for example, Kjeldsen et al. (2015) reporting a mass imbalance of -250 ± 21 Gt yr⁻¹ during 2003 to 2010, Ewert et al. (2012) reporting -181 ± 28 Gt yr⁻¹ during 2003 to 2008, and Rignot et al. (2008) reporting a mass imbalance of -265 ± 19 Gt yr⁻¹ during 2004 to 2008. Some of these differences may be due to different ice sheet area masks used in the studies. Attribution discrepancies include, for example, Enderlin et al. (2014) attributing the majority (64 %) of mass loss to changes in SMB during the 2005 to 2009 period but Rignot et al. (2008) attributing the majority (85 %) of mass loss to changes in D during the 2004 to 2008 period.

Discharge may be calculated through several methods, including mass flow rate through gates (e.g. Enderlin et al. (2014); King et al. (2018)), or solving as a residual from independent mass balance terms (e.g. Kjær et al. (2012); Kjeldsen et al. (2015)). The gate method that we use in this study incorporates ice thickness and an estimated vertical velocity profile from the observed surface velocity to calculate the discharge. A typical formulation of discharge across a gate D_g is,

$$D_g = \rho V H w, \quad (3)$$

where ρ is the average density of ice, V is depth-average gate-perpendicular velocity, H is the ice thickness, and w is the gate width. Uncertainties in V and H naturally influence the estimated discharge. At fast-flowing outlet glaciers, V is typically assumed to be equal at all ice depths, and observed surface velocities can be directly translated into depth-averaged velocities (as in Enderlin et al. (2014); King et al. (2018)). To minimize uncertainty from SMB or basal mass balance corrections downstream of a flux gate, the gate should be at the grounding line of the outlet glacier. Unfortunately, uncertainty in bed elevation (translating to ice thickness uncertainty) increases toward the grounding line.

Conventional methods of gate selection involve hand-picking gate locations, generally as linear features (e.g. Enderlin et al. (2014)) or visually approximating ice-orthogonal gates at one point in time (e.g. King et al. (2018)). Manual gate definition

is sub-optimal. For example, the largest discharging glaciers draw from an upstream radially-diffusing region that may not easily be represented by a single linear gate. Approximately flow-orthogonal curved gates may not be flow-orthogonal on the multi-decade time scale due to changing flow directions. Manual gate selection makes it difficult to update gate locations, corresponding with glacier termini retreat or advance, in a systematic and reproducible fashion. We therefore adopt an algorithmic approach to generate gates based on a range of criteria.

Here, we present a discharge dataset based on gates selected in a reproducible fashion by a new algorithm. Relative to previous studies, we employ ice velocity observation over a longer period with higher temporal frequency and denser spatial coverage. We use ice velocity from 1986 through 2017 including six-day velocities for the last ~500 days of the time series, and discharge at 200 m pixel resolution capturing all ice flowing faster than 100 m yr^{-1} that crosses glacier termini into fjords.

2 Input data

Historically, discharge gates were selected along well-constrained flight-lines of airborne radar data (Enderlin et al., 2014). Recent advances in ice thickness estimates through NASA Operation IceBridge (Millan et al., 2018), NASA Oceans Melting Greenland (OMG; Fenty et al. (2016)), fjord bathymetry (Tinto et al., 2015), and methods to estimate thickness from surface properties (e.g. McNabb et al. (2012); James and Carrivick (2016)) have been combined into digital bed elevation models such as BedMachine v3 (Morlighem et al., 2017b, a) or released as independent datasets (Millan et al., 2018). From these advances, digital bed elevation models have become more robust at tidewater glacier termini and grounding lines. The incorporation of flight-line ice thickness data into higher-level products that include additional methods and data means gates are no longer limited to flight-lines (e.g. King et al. (2018)).

Ice velocity data are available with increasing spatial and temporal resolution (e.g. Vijay et al. (2019)). Until recently, ice velocity mosaics were limited to once per year during winter (Joughin et al., 2010), and they are still temporally limited, often to annual resolution, prior to 2000 (e.g. Mouginot et al. (2018b, c)). Focusing on recent times, ice-sheet wide velocity mosaics from the Sentinel 1A & 1B are now available every six days (<http://PROMICE.org>). The increased availability of satellite data has improved ice velocity maps both spatially and temporally thereby decreasing the need to rely on spatial and temporal interpolation of velocities from annual/winter mosaics (Andersen et al., 2015; King et al., 2018).

The discharge gates in this study are generated using only surface speed and an ice mask. We use the MEaSURES Greenland Ice Sheet Velocity Map from InSAR Data, Version 2 (Joughin et al., 2010, 2015, updated 2018), hereafter termed "MEaSURES 0478" due to the National Snow and Ice Data Center (NSIDC) data set ID number. We use the BedMachine v3 (Morlighem et al., 2017b, a) ice mask.

For ice thickness estimates, we use surface elevation from GIMP (Howat et al. (2014, 2017); NSIDC data set ID 0715), adjusted through time with surface elevation change from Khan et al. (2016) and bed elevations from BedMachine v3 replaced by Millan et al. (2018) where available. Ice sector and region delineation is from Mouginot and Rignot (2019). Ice velocity data are obtained from a variety of products including Sentinel 1A & 1B derived by PROMICE (see Appendix), MEaSURES 0478, MEaSURES 0646 (Howat, 2017), Mouginot et al. (2018b), and Mouginot et al. (2018c). Official glacier names come

from Bjørk et al. (2015). Other glacier names come from Mouginot and Rignot (2019). See Table 1 for an overview of data sets used in this work.

This work uses 308 different velocity maps, biased toward the last 500 days of the time series when six-day ice velocities become available from the Sentinel-1 satellites. The temporal distribution is 1 to a few velocity map per year from 1986 to 2000, 9 to 13 velocity maps per year from 2000 through 2015, 24 in 2016, and 55 in 2017.

Table 1. Summary of data sources used in this work.

Property	Name used in this paper	Reference
Basal Topography	BedMachine	Morlighem et al. (2017b, a)
Basal Topography for Southeast		Millan et al. (2018)
Surface Elevation	GIMP 0715	Howat et al. (2014, 2017)
Surface Elevation Change	Surface Elevation Change	Khan et al. (2016)
Baseline Velocity	MEaSURES 0478	Joughin et al. (2015, updated 2018)
Velocity	Sentinel	Appendix
Velocity	MEaSURES 0646	Howat (2017)
Velocity	pre-2000	Mouginot et al. (2018b, c)
Sectors & Regions	Sectors & Regions	Mouginot and Rignot (2019)
Names		Bjørk et al. (2015); Mouginot and Rignot (2019)

3 Methods

3.1 Terminology

We use the following terminology, most displayed in Fig. 1:

- "Pixels" are individual 200 m x 200 m raster discharge grid cells. We use the nearest neighbor when combining data sets that have different grid properties.
- "Gates" are contiguous (including diagonal) clusters of pixels.
- "Sectors" are spatial areas that have 0, 1, or > 1 gate(s) plus any upstream source of ice that flows through the gate(s), and come from Mouginot and Rignot (2019).
- "Regions" are groups of sectors, also from Mouginot and Rignot (2019), and labeled by approximate geographic region.
- The "baseline" period is the average 2015, 2016, and 2017 winter velocity from MEaSURES 0478.
- "Coverage" is the percentage of total, region, sector, or gate discharge observed at any given time. By definition coverage is 100 % during the baseline period. From the baseline data, the contribution to total discharge of each pixel is calculated,

and coverage is reported for all other maps that have missing observations (Fig. A2). Total estimated discharge is always reported because missing pixels are gap-filled (see "Missing and invalid data" section below).

- "Fast-flowing ice" is defined as ice that flows more than 100 m yr^{-1} .
- Names are reported using the official Greenlandic names from Bjørk et al. (2015) if a nearby name exists, then Mougnot and Rignot (2019) in parentheses.

Although we refer to solid ice discharge, and it is in the solid phase when it passes the gates and eventually reaches the termini, submarine melting does occur at the termini and some of the discharge enters the fjord as liquid water (Enderlin and Howat, 2013).

3.2 Gate location

Gates are algorithmically generated for fast-flowing ice (greater than 100 m yr^{-1}) close to the ice sheet terminus determined by the baseline-period data. We apply a 2D inclusive mask to the baseline data for all ice flowing faster than 100 m yr^{-1} . We then select the mask edge where it is near the BedMachine ice mask (not including ice shelves), which effectively provides grounding line termini. We buffer the termini 5000 m in all directions creating ovals around the termini and once again down-select to fast-flowing ice pixels. This procedure results in gates 5000 m upstream from the baseline terminus that bisect the baseline fast-flowing ice. We manually mask some land- or lake-terminating glaciers which are initially selected by the algorithm due to fast flow and mask issues.

We select a 100 m yr^{-1} speed cutoff because slower ice, taking longer to reach the terminus, is more influenced by SMB. For the influence of this threshold on our results see the Discussion section and Fig. 2.

We select gates at 5000 m upstream from the baseline termini, which means that gates are likely $> 5000 \text{ m}$ from the termini further back in the historical record (Murray et al., 2015; Wood et al., 2018). The choice of a 5000 m buffer follows from the fact that it is near-terminus and thus avoids the need for (minor) SMB corrections downstream, yet is not too close to the terminus where discharge results are sensitive to the choice of distance-to-terminus value (Fig. 2), which may be indicative of bed (ice thickness) errors.

3.3 Thickness

We derive thickness from surface and bed elevation. We use GIMP 0715 surface elevations in all locations, and the BedMachine bed elevations in most locations, except southeast Greenland where we use the Millan et al. (2018) bed. The GIMP 0715 surface elevations are all time-stamped per pixel. We adjust the surface through time by linearly interpolating elevation changes from Khan et al. (2016), which covers the period from 1995 to 2016. We use the average of the first and last three years for earlier and later times, respectively. Finally, from the fixed bed and temporally varying surface, we calculate the time-dependent ice thickness at each gate pixel.

3.4 Missing or invalid data

The baseline data provides velocity at all gate locations by definition, but individual non-baseline velocity maps often have missing or invalid data. Also, thickness provided by BedMachine is clearly incorrect in some places (e.g. fast-flowing ice that is 10 m thick, Fig. 3). We define invalid data and fill in missing data as described below.

5 3.4.1 Invalid velocity

We flag invalid (outlier) velocities by treating each pixel as an individual time series, applying a 30 point rolling window, flagging values more than 2 standard deviations outside the mean, and repeating this filter three times. We also drop the 1972 to 1985 years from Mouginot et al. (2018b) because there is low coverage and extremely high variability when using our algorithm.

10 This outlier detection method appears to correctly flag outliers (see Appendix for un-filtered time series graphs), but likely also flags some true short-term velocity increases. The effect of this filter is a $\sim 1\%$ reduction in discharge most years, but more in years with high discharge – a reduction of 3.2 % in 2013, 4.3 % in 2003, and more in the 1980s when the data is noisy. Any analysis using this data and focusing on individual glaciers or short-term changes (or lack there-of) should re-evaluate the upstream data sources.

15 3.4.2 Missing velocity

We generate an ice speed time series by assigning the PROMICE, MEaSURES 0478, MEaSURES 0646, and pre-2000 products to their respective reported time stamps (even though these are time-span products), or to the middle of their time span when they cover a long period such as the annual maps from Mouginot et al. (2018b, c). We ignore that any individual velocity map or pixel has a time span, not a time stamp. Velocities are sampled only where there are gate pixels. Missing pixel velocities
20 are linearly interpolated in time, except for missing data at the beginning of the time series which are back- and forward-filled with the temporally-nearest value for that pixel (Fig. A2). We do not spatially interpolate missing velocities because the spatial changes around a missing data point are most likely larger than the temporal changes. We visually represent the discharge contribution of directly observed pixels, termed coverage (Fig. A2) as time series graphs and opacity of dots and error bars in the figures. Therefore, the gap-filled discharge contribution at any given time is equal to 100 minus the coverage. Discharge is
25 always reported as estimated total discharge even when coverage is less than 100 %.

3.4.3 Invalid thickness

The thickness data appear to be incorrect in some locations. For example, many locations have fast-flowing ice, but report ice thickness as 10 m or less (Fig. 3, left panel). We accept all ice thickness greater than 20 m and construct from this a thickness versus \log_{10} speed relationship. For all ice thickness less than or equal to 20 m thick we adjust thickness based this relationship
30 (Fig. 3, right panel). We selected the 20 m thickness cutoff after visually inspecting the velocity distribution (Fig. 3, left panel). This thickness adjustment adds 20 Gt yr^{-1} to our baseline-period discharge estimate with no adjustment. In the Appendix and

Table A2 we discuss the discharge contribution of these adjusted pixels, and a comparison among this and other thickness adjustments.

3.5 Discharge

We calculate discharge per pixel using density (917 kg m^{-3}), filtered and filled ice speed, projection-corrected pixel width, and adjusted ice thickness derived from time-varying surface elevation and a fixed bed elevation (Eq. 3). We assume that any change in surface elevation corresponds to a change in ice thickness and thereby neglect basal uplift, erosion, and melt, which combined are orders of magnitude less than surface melting (e.g. Cowton et al. (2012); Khan et al. (2007)). We also assume depth-averaged ice velocity is equal to the surface velocity.

We calculate discharge using the gate-orthogonal velocity at each pixel and at each timestamp – all velocity estimates are gate-orthogonal at all times, regardless of gate position, orientation, or changing glacier velocity direction over time.

Annual averages are calculated by linearly interpolating to daily, then estimating annual. The difference between this method and averaging only the observed samples is $\sim 3\%$ median (5% average, and a maximum of 10% when examining the entire ice sheet and all years in our data). It is occasionally larger at individual glaciers when a year has few widely-space samples of highly variable velocity.

3.5.1 Discharge Uncertainty

A longer discussion related to our and others treatments of errors and uncertainty is in the Appendix, but here we describe how we estimate the uncertainty related to the ice discharge following a simplistic approach. This yields an uncertainty of the total ice discharge of approximately 10% throughout the time series.

At each pixel we estimate the maximum discharge, D_{\max} , from

$$D_{\max} = \rho(V + \sigma_V)(H + \sigma_H)W, \quad (4)$$

and minimum discharge, D_{\min} , from

$$D_{\min} = \rho(V - \sigma_V)(H - \sigma_H)W, \quad (5)$$

where ρ is ice density, V is baseline velocity, σ_V is baseline velocity error, H is ice thickness, σ_H is ice thickness error, and W is the width at each pixel. Included in the thickness term is surface elevation change through time (dH/dt) and its uncertainty ($\sigma_{dH/dt}$). When data sets do not come with error estimates we treat the error as 0.

We use $\rho = 917 \text{ kg m}^{-3}$ because the gates are near the terminus in the ablation zone and ice thickness estimates should not include snow or firn, although regionally ice density may be $< 917 \text{ kg m}^{-3}$ due to crevasses. We ignore the velocity error σ_V and the elevation change error σ_H because the proportional thickness error (σ_H/H) is an order of magnitude larger than

the proportional velocity error (σ_V/V) yet both contribute linearly to the discharge. Similarly, $\sigma_H \gg \sigma_{dH/dt}$. W is location-dependent due to the errors between our working map projection (EPSG 3413) and a more accurate spheroid model of the earth surface. We adjust linear gate width by up to ~4% in the north and ~-2.5% in the south of Greenland (area errors are up to 8%). On a pixel by pixel basis we used the provided thickness uncertainty for each dataset. Where we modified the thickness ($H < 20$ m), we prescribe an uncertainty of 0.5 times the adjusted thickness. Subsequently, the uncertainty on individual glacier-, sector-, region-, or ice sheet scale is obtained by summarizing, but not reducing by the square of the sums, the uncertainty related to each pixel. We are conservative with our thickness error estimates, by assuming the uncertainty range is from D_{\min} to D_{\max} and not reducing by the sum-of-squares of sectors or regions.

4 Results

4.1 Gates

Our gate placement algorithm generates 6002 pixels making up 276 gates, assigned to 176 ice-sheet sectors from Mouginot and Rignot (2019). Previous similar studies have used 230 gates (King et al., 2018) and 178 gates (Enderlin et al., 2014).

The widest gate (~47 km) is Sermersuaq (Humboldt Gletsjer), the 2nd widest (~34 km) is Sermeq Kujalleq (Jakobshavn Isbræ). 23 additional glaciers have gate lengths longer than 10 km. The minimum gate width is 3 pixels (600 m) by definition in the algorithm.

The average unadjusted thickness gates is 405 m with a standard deviation of 260. The average thickness after adjustment is 439 m with a standard deviation of 225. A histogram of unadjusted and adjusted thickness at all gate locations is shown in Fig. 3.

4.2 Discharge

Our ice discharge dataset (Fig. 4) reports a total discharge of 438 ± 43 Gt in 1986, has a minimum of 421 ± 42 Gt in 1995, increases to 452 ± 45 in 2000, further to 504 ± 49 Gt/yr in 2005, after which annual discharge remains approximately steady at 484 to $503 \pm \sim 50$ Gt/yr during the 2005 to 2017 period. Annual maxima in ice discharged occurred in 2005 (504 ± 49 Gt/yr), 2011 (499 ± 50 Gt/yr), and 2014 (503 ± 51 Gt/yr).

At the region scale, the SE glaciers (see Fig. 1 for regions) are responsible for 139 to 167 (± 11 %) Gt yr⁻¹ of discharge (30 to 34 % of ice-sheet wide discharge) over the 1986 to 2017 period. By comparison, the predominantly land-terminating NO, NE and SW together were also responsible for 131 to 168 of discharge (~31 % of ice-sheet wide discharge) during this time (Fig. 5). The discharge from most regions has been approximately steady or declining for the past decade. The NW is the only region exhibiting a persistent increase in discharge – From ~89 to 113 Gt yr⁻¹ (21 % increase) over the 1998 through 2017 period (+ ~1 Gt yr⁻¹ or + ~1 % yr⁻¹). This persistent increase in NW discharge offsets declining discharge from other regions. The largest contributing region, SE, contributed a high of 167 ± 19 Gt in 2005, but dropped to $149 (155) \pm 18$ Gt in 2016 (2017).

Focusing on the top eight contributors (mean of last year) at the individual sector or glacier scale (Fig. 6), Sermeq Kujalleq (Jakobshavn Isbræ) has slowed down from an annual average high of $\sim 52 \text{ Gt yr}^{-1}$ in 2012 to $\sim 45 \text{ Gt yr}^{-1}$ in 2016 and $\sim 38 \text{ Gt yr}^{-1}$ in 2017, likely due to ocean cooling (Khazendar et al., 2019). We exclude Ikertivaq from the top 8 because that gate spans multiple sectors and outlets, while the other top dischargers are each a single outlet. The 2013 to 2016 slowdown of Sermeq Kujalleq (Fig. 6) is compensated by the many glaciers that make up the NW region (Fig. 5). The large 2017 reduction in discharge at Sermeq Kujalleq is partially offset by a large increase in the 2nd largest contributor, Helheim Gletsjer (Fig. 6).

5 Discussion

Different ice discharge estimates among studies likely stem from three categories: 1) changes in true discharge, 2) different input data (ice thickness and velocity), and 3) different assumptions and methods used to analyze data. Improved estimates of true discharge is the goal of this and many other studies, but changes in true discharge (category 1) can happen only when a work extends a time series into the future because historical discharge is fixed. Thus, any inter-study discrepancies in historical discharge must be due to category 2 (different data) or category 3 (different methods). Most studies use both updated data and new or different methods, but do not always provide sufficient information to disentangle the two. This is inefficient. To more quantitatively discuss inter-study discrepancies, it is imperative to explicitly consider all three potential causes of discrepancy. Only when results are fully reproducible – meaning all necessary data and code are available (c.f. Mankoff and Tulaczyk (2017); Rezvanbehbahani et al. (2017)) – can new works confidently attribute discrepancies relative to old works. Therefore, in addition to providing new discharge estimates, we attempt to examine discrepancies among our estimates and other recent estimates. Without access to code and data from previous studies, it is challenging to take this examination beyond a qualitative discussion.

The algorithm-generated gates we present offer some advantages over traditional hand-picked gates. Our gates are shared publicly, are generated by code that can be audited by others, and are easily adjustable within the algorithmic parameter space. This allows both sensitivity testing of gate location (Fig. 2) and allows gate positions to systematically evolve with glacier termini (not done here). The total ice discharge we estimate is $\sim 10 \%$ less than the total discharge of two previous estimates (Enderlin et al., 2014; Rignot et al., 2008), and similar to that of King et al. (2018), who attributes their discrepancy with Enderlin et al. (2014) to the latter using only summer velocities, which have higher annual average values than seasonally-comprehensive velocity products. The gate locations also differ among studies, and glaciers with baseline velocity less than 100 m yr^{-1} are not included in our study due to our velocity cutoff threshold, but this should not lead to substantially different discharge estimates (Fig. 2).

Our gate selection algorithm also does not place gates in northeast Greenland at Storstrømmen, Bredebræ, or their confluence, because during the baseline period that surge glacier was in a slow phase. We do not manually add gates at these glaciers. The last surge ended in 1984 (Reeh et al., 1994; Mouginot et al., 2018a), prior to the beginning of our time series, and these glaciers are therefore not likely to contribute substantial discharge even in the early period of discharge estimates.

We instead attribute the majority of our discrepancy with Enderlin et al. (2014) to the use of differing bed topography in southeast Greenland. When we compare our top ten highest discharging glaciers in 2000 with those reported by Enderlin et al. (2014), we find that the Køge Bugt discharge reported by Enderlin et al. (2014) is ~31 Gt, but our estimate is only ~16 Gt (and ~17 Gt in King et al. (2018)). The Bamber et al. (2013) bed elevation dataset that likely uses the same bed data employed by Enderlin et al. (2014) has a major depression in the central Køge Bugt bed. This region of enhanced ice thicknesses is not present in the BedMachine dataset that we and King et al. (2018) employ (Fig. B1). If the Køge Bugt gates of Enderlin et al. (2014) are in this location, then those gates overlie Bamber et al. (2013) ice thicknesses that are about twice those reported in BedMachine v3. With all other values held constant, this results in roughly twice the discharge. Although we do not know whether BedMachine or Bamber et al. (2013) is more correct, conservation of mass suggests that a substantial subglacial depression should be evident as either depressed surface elevation or velocity (Morlighem et al., 2016).

We are unable to attribute the remaining discrepancy between our discharge estimates and those by Enderlin et al. (2014). It is likely a combination of differing seasonal velocity sampling (King et al., 2018), our evolving surface elevation from Khan et al. (2016), or other previously-unpublished algorithmic or data differences, of which many possibilities exist.

Our ice discharge estimates agree well with the most recently published discharge estimate (King et al., 2018), except that our discharge is slightly less. We note that our uncertainty estimates include the King et al. (2018) estimates, but the opposite does not appear to be true. The minor differences are likely due to different methods. King et al. (2018) use seasonally varying ice thicknesses, derived from seasonally varying surface elevations, and a Monte Carlo method to temporally interpolate missing velocity data to produce discharge estimates. In comparison, we use linear interpolation of both yearly surface elevation estimates and temporal data gaps. It is not clear whether linear or higher-order statistical approaches are best-suited for interpolation as annual cycles begin to shift, as is the case with Sermeq Kujalleq (Jakobshavn Isbræ) after 2015. There are benefits and deficiencies with both methods. Linear interpolation may alias large changes if there are no other observations nearby in time. Statistical models of past glacier behavior may not be appropriate when glacier behavior changes.

It is unlikely that discharge estimates using gates that are only approximately flow-orthogonal and time-invariant (King et al., 2018) have large errors due to this, because it is unlikely that glacier flow direction changes significantly, but our gate-orthogonal treatment may be the cause of some differences among our approach and other works. Discharge calculated using non-orthogonal methodology would overestimate true discharge.

6 Data availability

This work in its entirety is available at [doi:10.22008/promice/data/ice_discharge](https://doi.org/10.22008/promice/data/ice_discharge) (Mankoff, 2019a). The glacier-scale, sector, region, and Greenland summed ice sheet discharge dataset is available at [doi:10.22008/promice/data/ice_discharge/d/v0.0.1](https://doi.org/10.22008/promice/data/ice_discharge/d/v0.0.1) (Mankoff, 2019c), where it will be updated as more velocity data become available. The gates can be found at [doi:10.22008/promice/data/ice_discharge/gates/v0.0.1](https://doi.org/10.22008/promice/data/ice_discharge/gates/v0.0.1) (Mankoff, 2019d), the code at [doi:10.22008/promice/data/ice_discharge/code/v0.0.1](https://doi.org/10.22008/promice/data/ice_discharge/code/v0.0.1) (Mankoff, 2019b), and the surface elevation change at [doi:10.22008/promice/data/DTU/surface_elevation_change/v1.0.0](https://doi.org/10.22008/promice/data/DTU/surface_elevation_change/v1.0.0) (Khan, 2017).

7 Conclusions

We have presented a novel dataset of flux gates and 1986 through 2017 glacier-scale ice discharge estimate for the Greenland ice sheet. These data are underpinned by an algorithm that both selects gates for ice flux and then computes ice discharges.

Our results are similar to the most recent discharge estimate (King et al., 2018) but begin in 1986 - although there is low coverage and few samples prior to 2000. From our discharge estimate we show that over the past ~30 years, ice sheet discharge was ~430 Gt yr⁻¹ prior to 2000, rose to over 500 Gt yr⁻¹ from 2000 to 2005, and has held roughly steady since 2005 at near 500 Gt yr⁻¹. However, when viewed at a region or sector scale, the system appears more dynamic with spatial and temporal increases and decreases canceling each other out to produce the more stable ice sheet discharge. We note that there does not appear to be any dynamic connection among the regions, and any increase in one region that was offset by a decrease in another has likely been due to chance. If in coming years when changes occur the signals have matching signs, then ice sheet discharge would decrease or increase, rather than remain fairly steady.

The application of our flux-gate algorithm shows that ice-sheet wide discharge varies by ~30 Gt yr⁻¹ due only to gate position, or ~40 Gt due to gate position and cutoff velocity (Fig. 2). This variance is approximately equal to the uncertainty associated with ice-sheet wide discharge estimates reported in many studies (e.g. Rignot et al. (2008); Andersen et al. (2015); Kjeldsen et al. (2015)). We highlight a major discrepancy with the ice discharge data of Enderlin et al. (2014) and we suspect this discharge discrepancy – most pronounced in southeast Greenland – is associated with the choice of digital bed elevation model, specifically a deep hole in the bed at Køge Bugt.

Transparency in data and methodology are critical to move beyond a focus of estimating discharge quantities, towards more operational mass loss products with realistic errors and uncertainty estimates. The convention of devoting a paragraph, or even page, to methods is insufficient given the complexity, pace, and importance of Greenland ice sheet research. Therefore the flux gates, discharge data, and the algorithm used to generate the gates, discharge, and all figures from this manuscript are freely available. We hope that the flux gates, data, and code we provide here is a step toward helping others both improve their work and discover the errors in ours.

Acknowledgements. Author Contribution: KDM conceived of the algorithm approach, and wrote the code. KDM, WIC, and RSF iterated over the algorithm results and methods. ASO provided the velocity data. SAK supplied the surface elevation change data. All authors contributed to the scientific discussion, writing, and editing of the manuscript. The authors declare that they have no conflict of interest. Data from the Programme for Monitoring of the Greenland Ice Sheet (PROMICE) were provided by the Geological Survey of Denmark and Greenland (GEUS) at <http://www.promice.org>. Parts of this work were funded by the INTAROS project under the European Union's Horizon 2020 research and innovation program under grant agreement No. 727890.

References

- Andersen, M. L., Stenseng, L., Skourup, H., Colgan, W., Khan, S. A., Kristensen, S. S., Andersen, S. B., Box, J. E., Ahlstrøm, A. P., Fettweis, X., and Forsberg, R.: Basin-scale partitioning of Greenland ice sheet mass balance components (2007 – 2011), *Earth and Planetary Science Letters*, 409, 89–95, <https://doi.org/10.1016/j.epsl.2014.10.015>, 2015.
- 5 Bamber, J. L., Griggs, J. A., Hurkmans, R. T. W. L., Dowdeswell, J. A., Gogineni, S. P., Howat, I., Mouginot, J., Paden, J., Palmer, S., Rignot, E., and Steinhage, D.: A new bed elevation dataset for Greenland, *The Cryosphere*, 7, 499–510, <https://doi.org/10.5194/tc-7-499-2013>, 2013.
- Bjørk, A. A., Kruse, L. M., and Michaelsen, P. B.: Brief Communication: Getting Greenland’s glaciers right – a new dataset of all official Greenlandic glacier names, *The Cryosphere*, 9, 2215–2218, <https://doi.org/10.5194/tc-9-2215-2015>, 2015.
- 10 Chen, X., Zhang, X., Church, J. A., Watson, C. S., King, M. A., Monselesan, D., Legresy, B., and Harig, C.: The increasing rate of global mean sea-level rise during 1993–2014, *Nature Climate Change*, 7, 492–495, <https://doi.org/10.1038/nclimate3325>, <http://dx.doi.org/10.1038/nclimate3325>, 2017.
- Cowton, T., Nienow, P., Bartholomew, I. D., Sole, A., and Mair, D. W. F.: Rapid erosion beneath the Greenland ice sheet, *Geology*, 40, 343–346, <https://doi.org/10.1130/G32687.1>, 2012.
- 15 Cuffey, K. M. and Paterson, W. S. B.: *The physics of glaciers*, Academic Press, fourth edn., 2010.
- Dall, J., Kusk, A., Nielsen, U., and Merryman Boncori, J. P.: Ice velocity mapping using TOPS SAR data and offset tracking, in: *FRINGE* 2015, vol. 731, 2015.
- Enderlin, E. M. and Howat, I. M.: Submarine melt rate estimates for floating termini of Greenland outlet glaciers (2000 – 2010), *Journal of Glaciology*, 59, 67–75, <https://doi.org/10.3189/2013JoG12J049>, 2013.
- 20 Enderlin, E. M., Howat, I. M., Jeong, S., Noh, M.-J., van Angelen, J. H., and van den Broeke, M. R.: An improved mass budget for the Greenland Ice Sheet, *Geophysical Research Letters*, 41, 866–872, <https://doi.org/10.1002/2013GL059010>, 2014.
- Ewert, H., Groh, A., and Dietrich, R.: Volume and mass changes of the Greenland ice sheet inferred from ICESat and GRACE, *Journal of Geodynamics*, 59-60, 111–123, <https://doi.org/10.1016/j.jog.2011.06.003>, <http://dx.doi.org/10.1016/j.jog.2011.06.003>, 2012.
- Fenty, I., Willis, J., Khazendar, A., Dinardo, S., Forsberg, R., Fukumori, I., Holland, D., Jakobsson, M., Moller, D., Morison, J., Münchow, A., Rignot, E. J., Schodlok, M. P., Thompson, A. F., Tinto, K., Rutherford, M., and Trenholm, N.: Oceans Melting Greenland: Early Results from NASA’s Ocean-Ice Mission in Greenland, *Oceanography*, 29, 72–83, <https://doi.org/10.5670/oceanog.2016.100>, 2016.
- 25 Fettweis, X., Box, J. E., Agosta, C., Amory, C., Kittel, C., Lang, C., Van As, D., Machguth, H., and Gallée, H.: Reconstructions of the 1900–2015 Greenland ice sheet surface mass balance using the regional climate MAR model, *The Cryosphere*, 11, 1015–1033, <https://doi.org/10.5194/tc-11-1015-2017>, <http://dx.doi.org/10.5194/tc-11-1015-2017>, 2017.
- 30 Howat, I.: MEaSUREs Greenland Ice Velocity: Selected Glacier Site Velocity Maps from Optical Images, Version 2, <https://doi.org/10.5067/VM5DZ20MYF5C>, used all subsets; Accessed 2018-11-15. NASA National Snow and Ice Data Center Distributed Active Archive Center, 2017.
- Howat, I., Negrete, A., and Smith, B.: MEaSUREs Greenland Ice Mapping Project (GIMP) Digital Elevation Model, Version 1, <https://doi.org/10.5067/NV34YUIXLP9W>, used all subsets; Access date unknown. NASA National Snow and Ice Data Center Distributed
- 35 Active Archive Center, 2015.

- Howat, I., Negrete, A., and Smith, B.: MEaSURES Greenland Ice Mapping Project (GIMP) Digital Elevation Model from GeoEye and WorldView Imagery, Version 1, <https://doi.org/10.5067/H0KUYVF53Q8M>, used all subsets; Accessed 2018-10-28. NASA National Snow and Ice Data Center Distributed Active Archive Center, 2017.
- Howat, I. M., Negrete, A., and Smith, B. E.: The Greenland Ice Mapping Project (GIMP) land classification and surface elevation data sets, *The Cryosphere*, 8, 1509–1518, <https://doi.org/10.5194/tc-8-1509-2014>, <http://dx.doi.org/10.5194/tc-8-1509-2014>, 2014.
- Hoyer, S. and Hamman, J. J.: xarray: N-D labeled Arrays and Datasets in Python, *Journal of Open Research Software*, 5, <https://doi.org/10.5334/jors.148>, <http://dx.doi.org/10.5334/jors.148>, 2017.
- Hunter, J. D.: Matplotlib: A 2D graphics environment, *Computing In Science & Engineering*, 9, 90–95, 2007.
- James, W. H. M. and Carrivick, J. L.: Automated modelling of spatially-distributed glacier ice thickness and volume, *Computers & Geosciences*, <https://doi.org/10.1016/j.cageo.2016.04.007>, 2016.
- Joughin, I., Smith, B., Howat, I., and Scambos, T.: MEaSURES Greenland Ice Sheet Velocity Map from InSAR Data, Version 2, <https://doi.org/10.5067/OC7B04ZM9G6Q>, used all subsets; Accessed 2019-03-10. NASA National Snow and Ice Data Center Distributed Active Archive Center, 2015, updated 2018.
- Joughin, I., Smith, B. E., and Howat, I.: Greenland Ice Mapping Project: ice flow velocity variation at sub-monthly to decadal timescales, *The Cryosphere*, 12, 2211–2227, <https://doi.org/10.5194/tc-12-2211-2018>, <http://dx.doi.org/10.5194/tc-12-2211-2018>, 2018.
- Joughin, I. R., Smith, B., Howat, I. M., Scambos, T. A., and Moon, T.: Greenland flow variability from ice-sheet-wide velocity mapping, *Journal of Glaciology*, 56, 415–430, <https://doi.org/10.3189/002214310792447734>, 2010.
- Khan, S. A.: Greenland Ice Sheet Surface Elevation Change, https://doi.org/10.22008/promice/data/DTU/surface_elevation_change/v1.0.0, submitted. GEUS Data Center, 2017.
- Khan, S. A., Wahr, J., Stearns, L. A., Hamilton, G. S., van Dam, T., Larson, K. M., and Francis, O.: Elastic uplift in southeast Greenland due to rapid ice mass loss, *Geophysical Research Letters*, 34, <https://doi.org/10.1029/2007gl031468>, <http://dx.doi.org/10.1029/2007GL031468>, 2007.
- Khan, S. A., Aschwanden, A., Bjørk, A. A., Wahr, J., Kjeldsen, K. K., and Kjær, K. H.: Greenland ice sheet mass balance: a review, *Reports on Progress in Physics*, 78, 046 801, <https://doi.org/10.1088/0034-4885/78/4/046801>, <http://dx.doi.org/10.1088/0034-4885/78/4/046801>, 2015.
- Khan, S. A., Sasgen, I., Bevis, M., van Dam, T., Bamber, J. L., Wahr, J., Willis, M., Kjær, K. H., Wouters, B., Helm, V., Csatho, B., Fleming, K., Bjørk, A. A., Aschwanden, A., Knudsen, P., and Munneke, P. K.: Geodetic measurements reveal similarities between post-Last Glacial Maximum and present-day mass loss from the Greenland ice sheet, *Science Advances*, 2, e1600931–e1600931, <https://doi.org/10.1126/sciadv.1600931>, <http://dx.doi.org/10.1126/sciadv.1600931>, 2016.
- Khazendar, A., Fenty, I. G., Carroll, D., Gardner, A., Lee, C. M., Fukumori, I., Wang, O., Zhang, H., Seroussi, H., Moller, D., Noël, B. P. Y., van den Broeke, M. R., Dinardo, S., and Willis, J.: Interruption of two decades of Jakobshavn Isbrae acceleration and thinning as regional ocean cools, *Nature Geoscience*, 12, 277–283, <https://doi.org/10.1038/s41561-019-0329-3>, <http://dx.doi.org/10.1038/s41561-019-0329-3>, 2019.
- King, M. D., Howat, I. M., Jeong, S., Noh, M. J., Wouters, B., Noël, B., and van den Broeke, M. R.: Seasonal to decadal variability in ice discharge from the Greenland Ice Sheet, *The Cryosphere*, 12, 3813–3825, <https://doi.org/10.5194/tc-12-3813-2018>, <http://dx.doi.org/10.5194/tc-12-3813-2018>, 2018.

- Kjeldsen, K. K., Korsgaard, N. J., Bjørk, A. A., Khan, S. A., Box, J. E., Funder, S., Larsen, N. K., Bamber, J. L., Colgan, W., Broeke, M. v. d., Siggaard-Andersen, M.-L., Nuth, C., Schomacker, A., Andresen, C. S., Willerslev, E., and Kjær, K. H.: Spatial and temporal distribution of mass loss from the Greenland Ice Sheet since AD 1900, *Nature*, 528, 396–400, <https://doi.org/10.1038/nature16183>, 2015.
- 5 Kjær, K. H., Khan, S. A., Korsgaard, N. J., Wahr, J., Bamber, J. L., Hurkmans, R., Van Den Broeke, M. R., Timm, L. H., Kjeldsen, K. K., Bjørk, A. A., Larsen, N. K., Jørgensen, L. T., Færch-Jensen, A., and Willerslev, E.: Aerial Photographs Reveal Late20th-Century Dynamic Ice Loss in Northwestern Greenland, *Science*, 337, 569 – 573, <https://doi.org/10.1126/science.1220614>, 2012.
- Kluyver, T., Ragan-Kelley, B., Pérez, F., Granger, B., Bussonnier, M., Frederic, J., Kelley, K., Hamrick, J., Grout, J., Corlay, S., Ivanov, P., Avila, D., Abdalla, S., and Willing, C.: Jupyter Notebooks – a publishing format for reproducible computational workflows, 2016.
- Kusk, A., Boncori, J. P. M., and Dall, J.: An automated System for Ice Velocity Measurement from SAR, in: EUSAR 2018; 12th European
10 Conference on Synthetic Aperture Radar, pp. 1–4, VDE, 2018.
- Mankoff, K. D.: Greenland Ice Sheet Discharge 2000 to 2018: All Data, https://doi.org/10.22008/promice/data/ice_discharge, submitted. GEUS Data Center, 2019a.
- Mankoff, K. D.: Greenland Ice Sheet Discharge 2000 to 2018: Code, https://doi.org/10.22008/promice/data/ice_discharge/code/v0.0.1, submitted. GEUS Data Center, 2019b.
- 15 Mankoff, K. D.: Greenland Ice Sheet Discharge 2000 to 2018: Discharge, https://doi.org/10.22008/promice/data/ice_discharge/d/v0.0.1, submitted. GEUS Data Center, 2019c.
- Mankoff, K. D.: Greenland Ice Sheet Discharge 2000 to 2018: Gates, https://doi.org/10.22008/promice/data/ice_discharge/gates/v0.0.1, submitted. GEUS Data Center, 2019d.
- Mankoff, K. D. and Tulaczyk, S. M.: The past, present, and future viscous heat dissipation available for Greenland subglacial conduit
20 formation, *The Cryosphere*, 11, 303–317, <https://doi.org/10.5194/tc-11-303-2017>, 2017.
- McKinney, W.: Data Structures for Statistical Computing in Python, in: Proceedings of the 9th Python in Science Conference, edited by van der Walt, S. and Millman, J., pp. 51 – 56, 2010.
- McNabb, R. W., Hock, R., O’Neel, S., Rasmussen, L. A., Ahn, Y., Braun, M., Conway, H., Herreid, S., Joughin, I. R., Pfeffer, W. T., Smith, B., and Truffer, M.: Using surface velocities to calculate ice thickness and bed topography: a case study at Columbia Glacier, Alaska,
25 USA, *Journal of Glaciology*, 58, 1151–1164, <https://doi.org/10.3189/2012JoG11J249>, 2012.
- Millan, R., Rignot, E., Mouginot, J., Wood, M., Bjørk, A. A., and Morlighem, M.: Vulnerability of Southeast Greenland glaciers to warm Atlantic Water from Operation IceBridge and Ocean Melting Greenland data., *Geophysical Research Letters*, 45, 2688–2696, <https://doi.org/10.1002/2017gl076561>, <http://dx.doi.org/10.1002/2017GL076561>, 2018.
- Moon, T., Ahlstrøm, A., Goelzer, H., Lipscomb, W., and Nowicki, S.: Rising Oceans Guaranteed: Arctic Land Ice Loss and Sea Level Rise,
30 Current Climate Change Reports, <https://doi.org/10.1007/s40641-018-0107-0>, <http://dx.doi.org/10.1007/s40641-018-0107-0>, 2018.
- Morlighem, M., Rignot, E., and Willis, J.: Improving Bed Topography Mapping of Greenland Glaciers Using NASA’s Oceans Melting Greenland (OMG) Data, *Oceanography*, 29, 62–71, <https://doi.org/10.5670/oceanog.2016.99>, 2016.
- Morlighem, M., Williams, C., Rignot, E., An, L., Arndt, J. E., Bamber, J., Catania, G., Chauché, N., Dowdeswell, J. A., Dorschel, B., Fenty, I., Hogan, K., Howat, I., Hubbard, A., Jakobsson, M., Jordan, T. M., Kjeldsen, K. K., Millan, R., Mayer, L., Mouginot, J., Noël, B.,
35 O’Cofaigh, C., Palmer, S. J., Rysgaard, S., Seroussi, H., Siegert, M. J., Slabon, P., Straneo, F., van den Broeke, M. R., Weinrebe, W., Wood, M., and Zinglensen, K.: IceBridge BedMachine Greenland, Version 3, <https://doi.org/10.5067/2CIX82HUV88Y>, used all subsets; Accessed 2018-10-28, 2017a.

- Morlighem, M., Williams, C. N., Rignot, E., An, L., Arndt, J. E., Bamber, J. L., Catania, G., Chauché, N., Dowdeswell, J. A., Dorschel, B., Fenty, I., Hogan, K., Howat, I. M., Hubbard, A., Jakobsson, M., Jordan, T. M., Kjeldsen, K. K., Millan, R., Mayer, L., Mouginot, J., Noël, B. P. Y., Cofaigh, C. Ó., Palmer, S., Rysgaard, S., Seroussi, H., Siegert, M. J., Slabon, P., Straneo, F., van den Broeke, M. R., Weinrebe, W., Wood, M., and Zinglensen, K. B.: BedMachine v3: Complete bed topography and ocean bathymetry mapping of Greenland from multi-beam echo sounding combined with mass conservation, *Geophysical Research Letters*, <https://doi.org/10.1002/2017gl074954>, 2017b.
- Mouginot, J. and Rignot, E.: Glacier catchments/basins for the Greenland Ice Sheet, <https://doi.org/10.7280/d1wt11>, <https://dash.lib.uci.edu/stash/dataset/doi:10.7280/D1WT11>, 2019.
- Mouginot, J., Bjørk, A. A., Millan, R., Scheuchl, B., and Rignot, E.: Insights on the Surge Behavior of Storstrømmen and L. Bistrup Bræ, Northeast Greenland, Over the Last Century, *Geophysical Research Letters*, 45, 11,197–11,205, <https://doi.org/10.1029/2018gl079052>, 2018a.
- Mouginot, J., Rignot, E., Millan, R., Wood, M., and Scheuchl, B.: Annual Ice Velocity of the Greenland Ice Sheet (1972-1990), <https://doi.org/10.7280/d1mm37>, <https://dash.lib.uci.edu/stash/dataset/doi:10.7280/D1MM37>, v5, 2018b.
- Mouginot, J., Rignot, E., Scheuchl, B., Millan, R., and Wood, M.: Annual Ice Velocity of the Greenland Ice Sheet (1991-2000), <https://doi.org/10.7280/d1gw91>, <https://dash.lib.uci.edu/stash/dataset/doi:10.7280/D1GW91>, v6, 2018c.
- Murray, T., Scharrer, K., Selmes, N., Booth, A. D., James, T. D., Bevan, S. L., Bradley, J., Cook, S., Llana, L. C., Drocourt, Y., and et al.: Extensive retreat of Greenland tidewater glaciers, 2000–2010, *Arctic, Antarctic, and Alpine Research*, 47, 427–447, <https://doi.org/10.1657/aaar0014-049>, <http://dx.doi.org/10.1657/AAAR0014-049>, 2015.
- Nerem, R. S., Beckley, B. D., Fasullo, J. T., Hamlington, B. D., Masters, D., and Mitchum, G. T.: Climate-change–driven accelerated sea-level rise detected in the altimeter era, *Proceedings of the National Academy of Sciences*, 115, 2022–2025, <https://doi.org/10.1073/pnas.1717312115>, <http://dx.doi.org/10.1073/pnas.1717312115>, 2018.
- Neteler, M., Bowman, M. H., Landa, M., and Metz, M.: GRASS GIS: a multi-purpose Open Source GIS, *Environmental Modelling & Software*, 31, 124–130, <https://doi.org/10.1016/j.envsoft.2011.11.014>, 2012.
- Oliphant, T. E.: A guide to NumPy, vol. 1, Trelgol Publishing USA, 2006.
- PROJ contributors: PROJ coordinate transformation software library, Open Source Geospatial Foundation, <https://proj4.org/>, 2018.
- Rathmann, N. M., Hvidberg, C. S., Solgaard, A. M., Grinsted, A., Gudmundsson, G. H., Langen, P. L., Nielsen, K. P., and Kusk, A.: Highly temporally resolved response to seasonal surface melt of the Zachariae and 79N outlet glaciers in northeast Greenland, *Geophysical Research Letters*, 44, 9805–9814, <https://doi.org/10.1002/2017gl074368>, <http://dx.doi.org/10.1002/2017GL074368>, 2017.
- Reeh, N., Bøggild, C., and Oerter, H.: Surge of Storstrømmen, a large outlet glacier from the Inland Ice of North-East Greenland, *Grønlands Geologiske Undersøgelse Rapport 162*, pp. 201–209, 1994.
- Rezvanbehbahani, S., Stearns, L. A., Kadivar, A., Walker, J. D., and van der Veen, C. J.: Predicting the Geothermal Heat Flux in Greenland: A Machine Learning Approach, *Geophysical Research Letters*, 44, 12,271–12,279, <https://doi.org/10.1002/2017gl075661>, <http://dx.doi.org/10.1002/2017GL075661>, 2017.
- Rignot, E. J., Box, J. E., Burgess, E. W., and Hanna, E.: Mass balance of the Greenland ice sheet from 1958 to 2007, *Geophysical Research Letters*, 35, <https://doi.org/10.1029/2008GL035417>, 2008.
- Schulte, E., Davison, D., Dye, T., and Dominik, C.: A multi-language computing environment for literate programming and reproducible research, *Journal of Statistical Software*, 46, 1–24, 2012.
- Seabold, S. and Perktold, J.: Statsmodels: Econometric and statistical modeling with python, in: 9th Python in Science Conference, 2010.

- Strozzi, T., Luckman, A., Murray, T., Wegmuller, U., and Werner, C.: Glacier motion estimation using SAR offset-tracking procedures, *IEEE Transactions on Geoscience and Remote Sensing*, 40, 2384–2391, <https://doi.org/10.1109/tgrs.2002.805079>, <http://dx.doi.org/10.1109/TGRS.2002.805079>, 2002.
- Tange, O.: GNU Parallel - The Command-Line Power Tool, *login: The USENIX Magazine*, 36, 42–47, <https://doi.org/10.5281/zenodo.16303>, <http://www.gnu.org/s/parallel>, 2011.
- 5 <https://doi.org/10.5281/zenodo.16303>, <http://www.gnu.org/s/parallel>, 2011.
- Tinto, K. J., Bell, R. E., Cochran, J. R., and Münchow, A.: Bathymetry in Petermann fjord from Operation IceBridge aerogravity, *Earth and Planetary Science Letters*, 422, 58–66, <https://doi.org/10.1016/j.epsl.2015.04.009>, 2015.
- van den Broeke, M., Box, J., Fettweis, X., Hanna, E., Noël, B., Tedesco, M., Van As, D., Van De Berg, W. J., and Van Kampenhout, L.: Greenland Ice Sheet Surface Mass Loss: Recent Developments in Observation and Modeling, *Current Climate Change Reports*, <https://doi.org/10.1007/s40641-017-0084-8>, <http://dx.doi.org/10.1007/s40641-017-0084-8>, 2017.
- 10 <https://doi.org/10.1007/s40641-017-0084-8>, <http://dx.doi.org/10.1007/s40641-017-0084-8>, 2017.
- Van Rossum, G. and Drake Jr, F. L.: Python reference manual, Centrum voor Wiskunde en Informatica Amsterdam, 1995.
- Vijay, S., Khan, S. A., Kusk, A., Solgaard, A. M., Moon, T., and Bjørk, A. A.: Resolving seasonal ice velocity of 45 Greenlandic glaciers with very high temporal details, *Geophysical Research Letters*, <https://doi.org/10.1029/2018gl081503>, <http://dx.doi.org/10.1029/2018GL081503>, 2019.
- 15 WCRP Global Sea Level Budget Group: Global sea-level budget 1993–present, *Earth System Science Data*, 10, 1551–1590, <https://doi.org/10.5194/essd-10-1551-2018>, <http://dx.doi.org/10.5194/essd-10-1551-2018>, 2018.
- Wiese, D. N., Yuan, D.-N., Boening, C., Landerer, F. W., and Watkins, M. M.: JPL GRACE Mascon Ocean, Ice, and Hydrology Equivalent HDR Water Height RL05M.1 CRI Filtered Version 2, <https://doi.org/10.5067/TEMSC-2LCR5>, dataset accessed [2017-12-14], 2016.
- Wood, M., Rignot, E., Fenty, I., Menemenlis, D., Millan, R., Morlighem, M., Mouginot, J., and Seroussi, H.: Ocean-induced melt triggers glacier retreat in Northwest Greenland, *Geophysical Research Letters*, <https://doi.org/10.1029/2018gl078024>, <http://dx.doi.org/10.1029/2018GL078024>, 2018.
- 20 <https://doi.org/10.1029/2018gl078024>, <http://dx.doi.org/10.1029/2018GL078024>, 2018.
- Zwally, H. J., Giovinetto, M. B., Beckley, M. A., and Saba, J. L.: Antarctic and Greenland Drainage Systems, http://icesat4.gsfc.nasa.gov/cryo_data/ant_grm_drainage_systems.php, GSFC Cryospheric Sciences Laboratory, 2012.

Figures

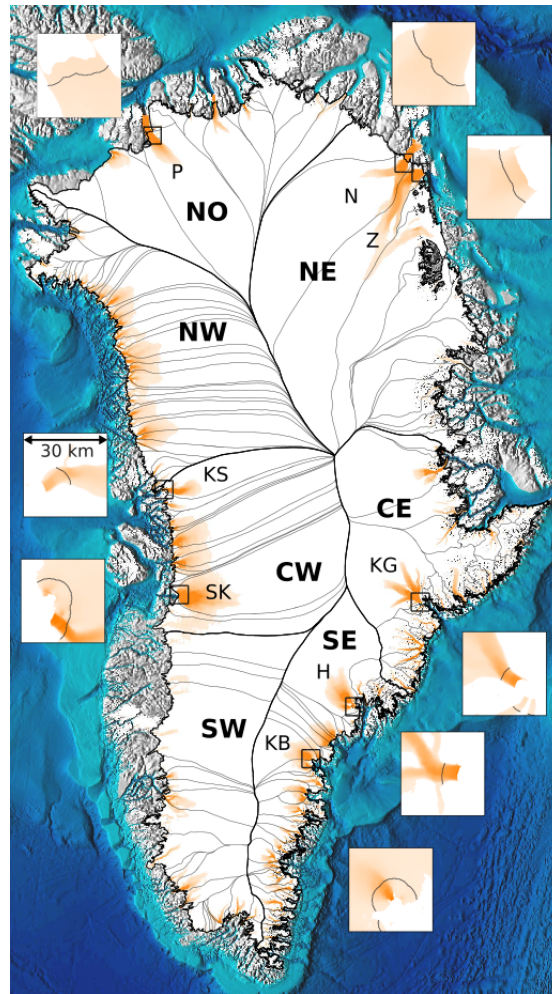


Figure 1. Overview showing fast-flowing ice (orange, greater than 100 m yr^{-1}) and the gates for the top eight discharging glaciers (Fig. 6). Gates are shown as black lines in inset images. Each inset is $30 \times 30 \text{ km}$ and all have the same color scaling, but different than the main map. Insets pair with nearest label and box. On the main map, regions from Mouginit and Rignot (2019) are designated by thicker black lines and large bold labels. Sectors (same source) are delineated with thinner gray lines, and the top discharging glaciers are labeled with smaller font. H = Helheim Gletsjer, KB = (Køge Bugt), KG = Kangerlussuaq Gletsjer, KS = Kangilliup Sermia (Rink Isbræ), N = (Nioghalvfjærdsbræ), P = Petermann Gletsjer, SK = Sermeq Kujalleq (Jakobshavn Isbræ), and Z = Zachariae Isstrøm. Basemap terrain (gray), ocean bathymetry (blues), and ice mask (white) come from BedMachine.

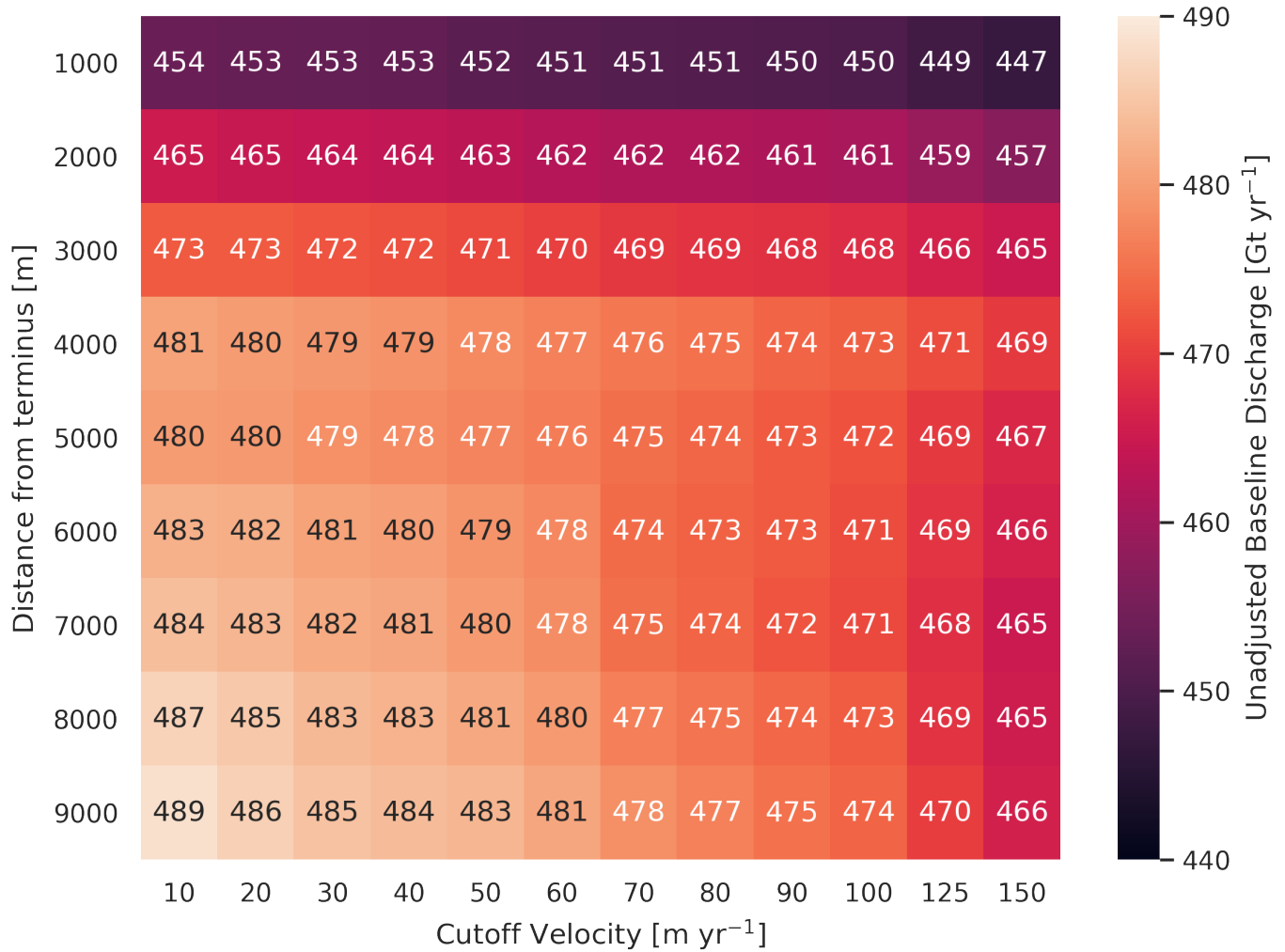


Figure 2. Heatmap and table showing ice sheet discharge as a function of gate buffer distance and ice speed cutoff. The colors of the numbers change for readability.

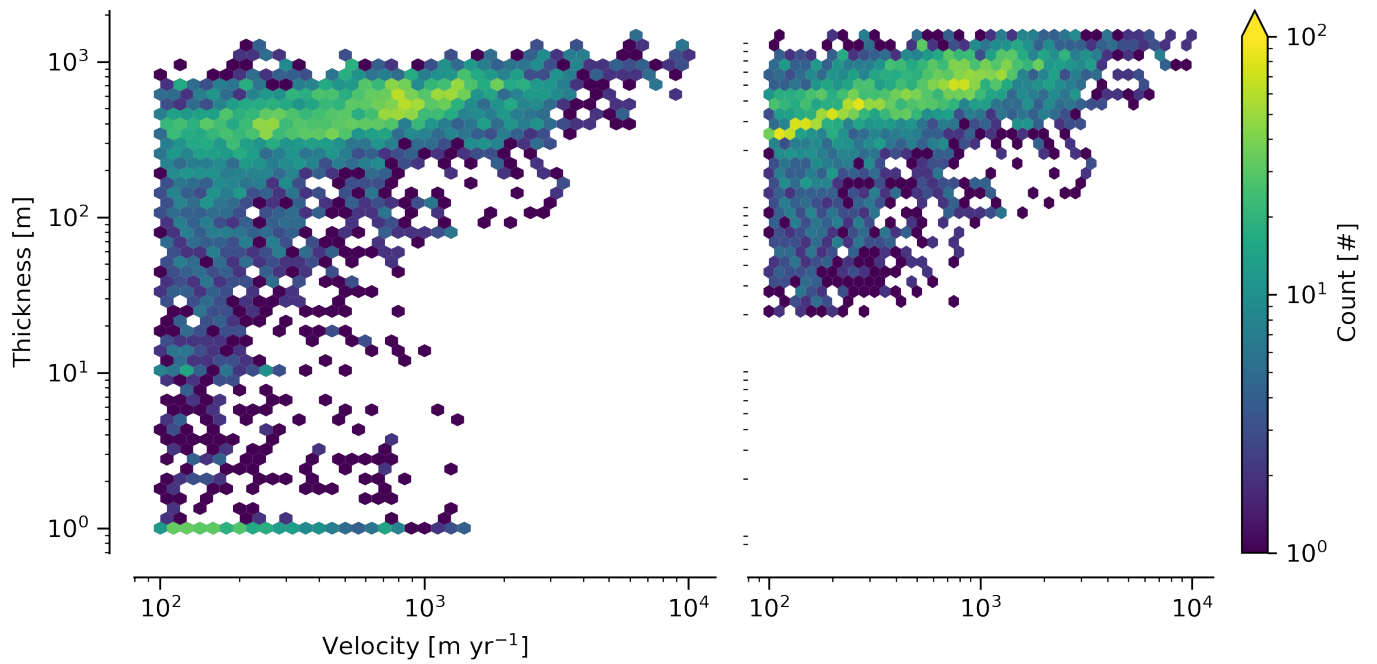


Figure 3. 2D histogram of velocity and thickness at all gate pixels. Left panel: Unadjusted (BedMachine & Millan et al. (2018)) thickness. Right panel: Adjusted (as described in the text) thickness.

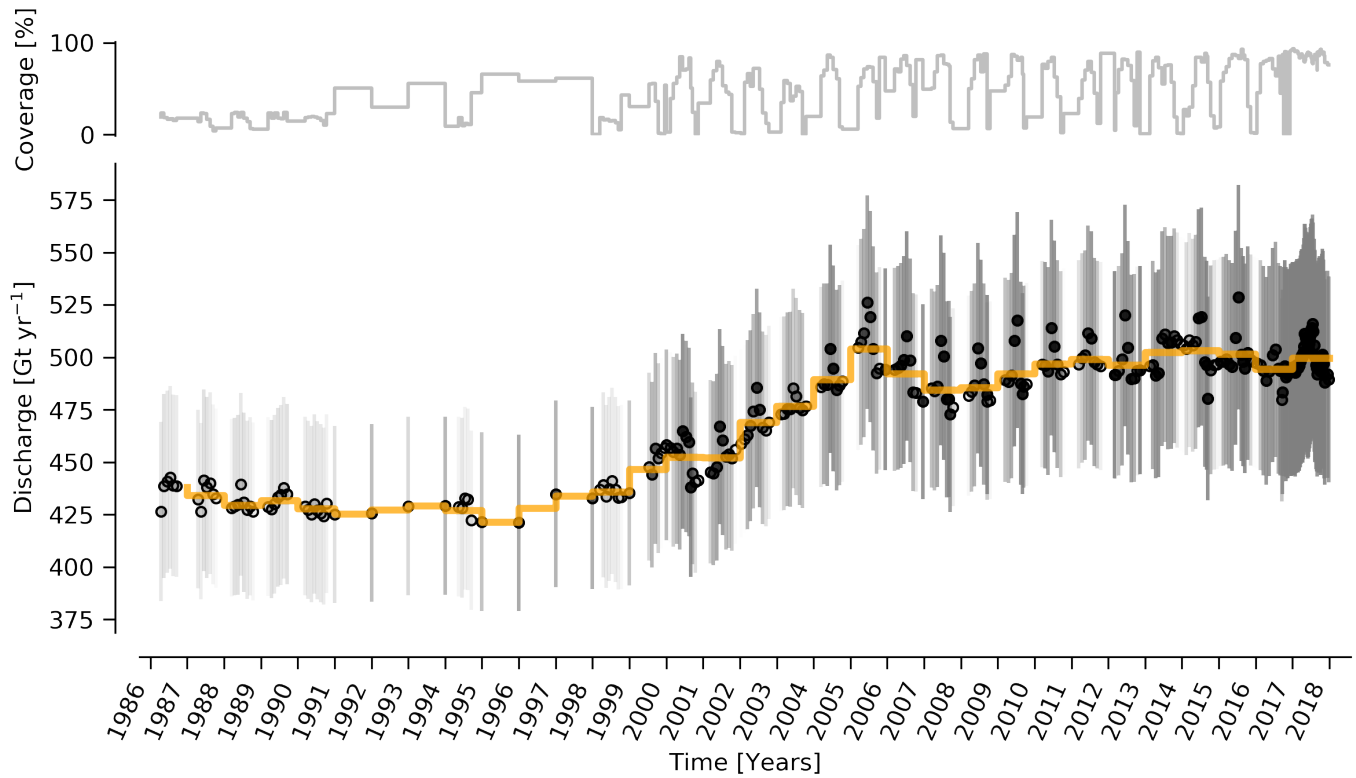


Figure 4. Bottom panel: Time series of ice discharge from the Greenland ice sheet. Dots represent when observations occurred. Orange stepped line is annual average. Coverage (percentage of total discharge observed at any given time) is shown in top panel, and also by opacity of dot interior and error bars on lower panel. When coverage is < 100 %, total discharge is estimated and shown.

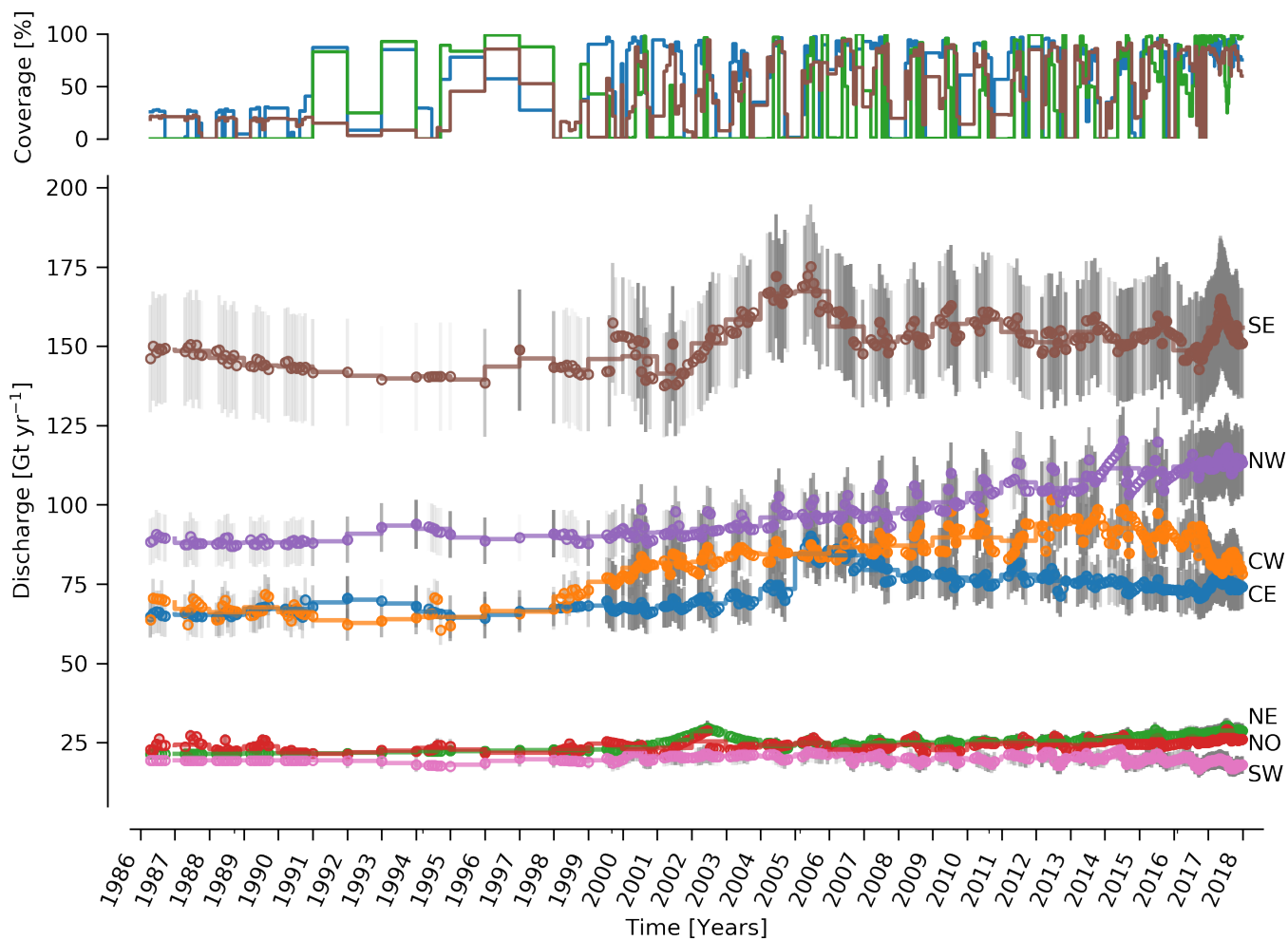


Figure 5. Bottom panel: Time series of ice discharge by region. Same graphical properties as Fig. 4. Top panel: The region with highest coverage (CE), lowest coverage (NE), and coverage for the region with highest discharge (SE) are shown. Coverage for other regions not shown to reduce clutter.

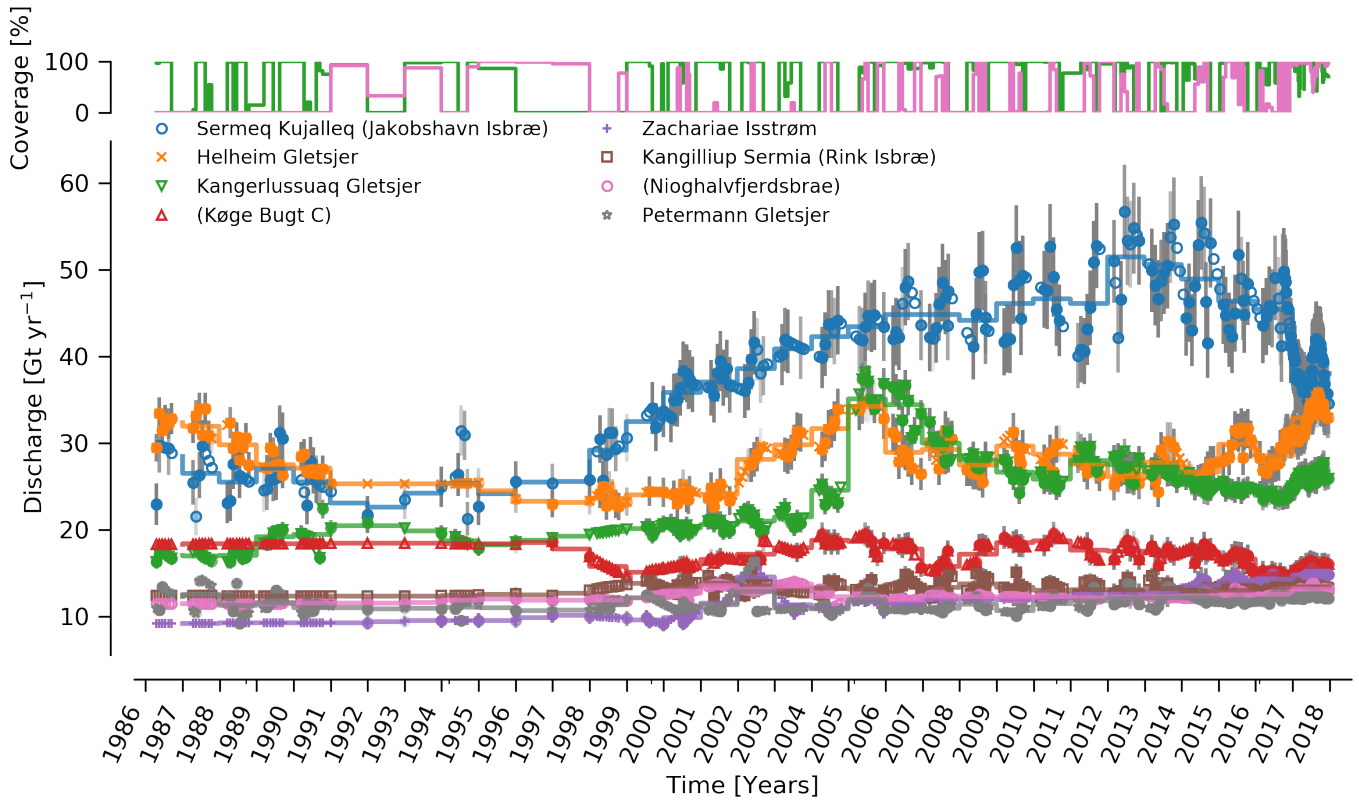


Figure 6. Bottom panel: Time series of ice discharge showing top eight (mean of last year) discharging glaciers. Same graphical properties as Fig. 4. Only an example high (Kangerlussuaq Gletsjer) and low (Nioghalvfjærdsbræ) coverage shown to reduce clutter.

Appendix A: Errors and Uncertainties

Here we describe our error and uncertainty treatments. We begin with a brief philosophical discussion of common uncertainty treatments, our general approach, and then the influence of various decisions made throughout our analysis, such as gate location and treatments of unknown thicknesses.

5 Traditional and mathematically valid uncertainty treatments divide errors into two classes: systematic (bias) and random. The primary distinction is that systematic errors do not decrease with more samples, and random errors decrease as the number of samples or measurements increases. The question is then which errors are systematic and which are random. A common treatment is to decide that errors within a region are systematic, and among regions are random. This approach has no physical basis - two glaciers a few 100 m apart but in different regions are assumed to have random errors, but two glaciers 1000s of
10 km apart but within the same region are assumed to have systematic errors. It is more likely the case that all glaciers less wide than some width or more deep than some depth have systematic errors even if they are on opposite sides of the ice sheet, if ice thickness is estimated with the same method (i.e. the systematic error is likely caused by the sensor and airplane, not the location of the glacier).

The decision to have R random samples (where R is the number of regions, usually ~ 18 based on Zwally et al. (2012)) is
15 also arbitrary. Mathematical treatment of random errors means that even if the error is 50 %, 18 measurements reduces it to only 11.79 %.

This reduction is unlikely to be physically meaningful. Our 176 sectors, 276 gates and 6002 pixels means that even if errors were 100 % for each, we could reduce it to 7.5, 6.0, or 1.3 % respectively. We note that the area error introduced by the common EPSG:3413 map projection is -5 % in the north and +8 % in the south. While this error is mentioned in some other works (e.g.
20 Joughin et al. (2018)) it is often not explicitly mentioned.

We do not have a solution for the issues brought up here, except to discuss them explicitly and openly so that those, and our own, error treatments are clearly presented and understood to likely contain errors themselves.

A1 Invalid Thickness

We assume ice thicknesses < 20 m are incorrect where ice speed is > 100 m yr⁻¹. Of 6002 pixels, 5366 have valid thickness,
25 and 636 (12 %) have invalid thickness. However, the speed at the locations of the invalid thicknesses is generally much less (and therefore the assumed thickness is less), and the influence on discharge is less than an average pixel with valid thickness (Table A1).

When aggregating by gate, there are 276 gates. Of these, 187 (68 %) have no bad pixels and 89 (32 %) have some bad pixels, 65 have > 50 % bad pixels, and 61 (22 %) are all bad pixels.

30 We adjust these thickness using a poor fit (correlation coefficient: 0.3) of the \log_{10} of the ice speed to thickness where the relationship is known (thickness > 20 m). We set errors equal to one half the thickness (i.e. $\sigma_H = \pm 0.5 H$). We also test the sensitivity of this treatment to simpler treatments, and have the following five categories:

NoAdj No adjustments made. Assume BedMachine thickness are all correct.

Table A1. Statistics of pixels with and without valid thickness. Numbers represent speed [m yr^{-1}] except for the "count" row.

	Good Pixels	Bad Pixels
count	5366	636
mean	821	266
std	1040	235
min	100	101
25%	230	129
50%	487	171
75%	972	281
max	10044	1423

NoAdj+Millan Same as NoAdj, but using Millan et al. (2018) bed where available.

300 If a gate has some valid pixel thicknesses, set the invalid thicknesses to the minimum of the valid thicknesses. If a gate has no valid thickness, set the thickness to 300 m.

400 Set all thickness < 50 m to 400 m

5 **Fit** Use the thickness v. speed relationship described above.

Table A2 shows the estimated baseline discharge to these four treatments:

Table A2. Effect of different thickness adjustments on baseline discharge

Treatment	Discharge [Gt]
NoAdj	472 ± 49
NoAdj+Millan	480 ± 49
300	488 ± 49
400	495 ± 51
Fit	492 ± 51

Finally, Figure A1 shows the geospatial locations, concentration, and speed of gates with and without bad pixels.

A2 Missing Velocity

We estimate discharge at all pixel locations for any time when there exists any velocity product. Not every velocity product provides velocity estimates at all locations, and we fill in where there are gaps by linear interpolating velocity at each pixel in time. We calculate coverage, the discharge-weighted percent of observed velocity at any given time (Figure A2), and display coverage as 1) line plots over the time series graphs, 2) opacity of the error bars and 3) opacity of the infilling of time series dots. Linear interpolation and discharge-weighted coverage is illustrated in Figure A2, where pixel A has a velocity value at

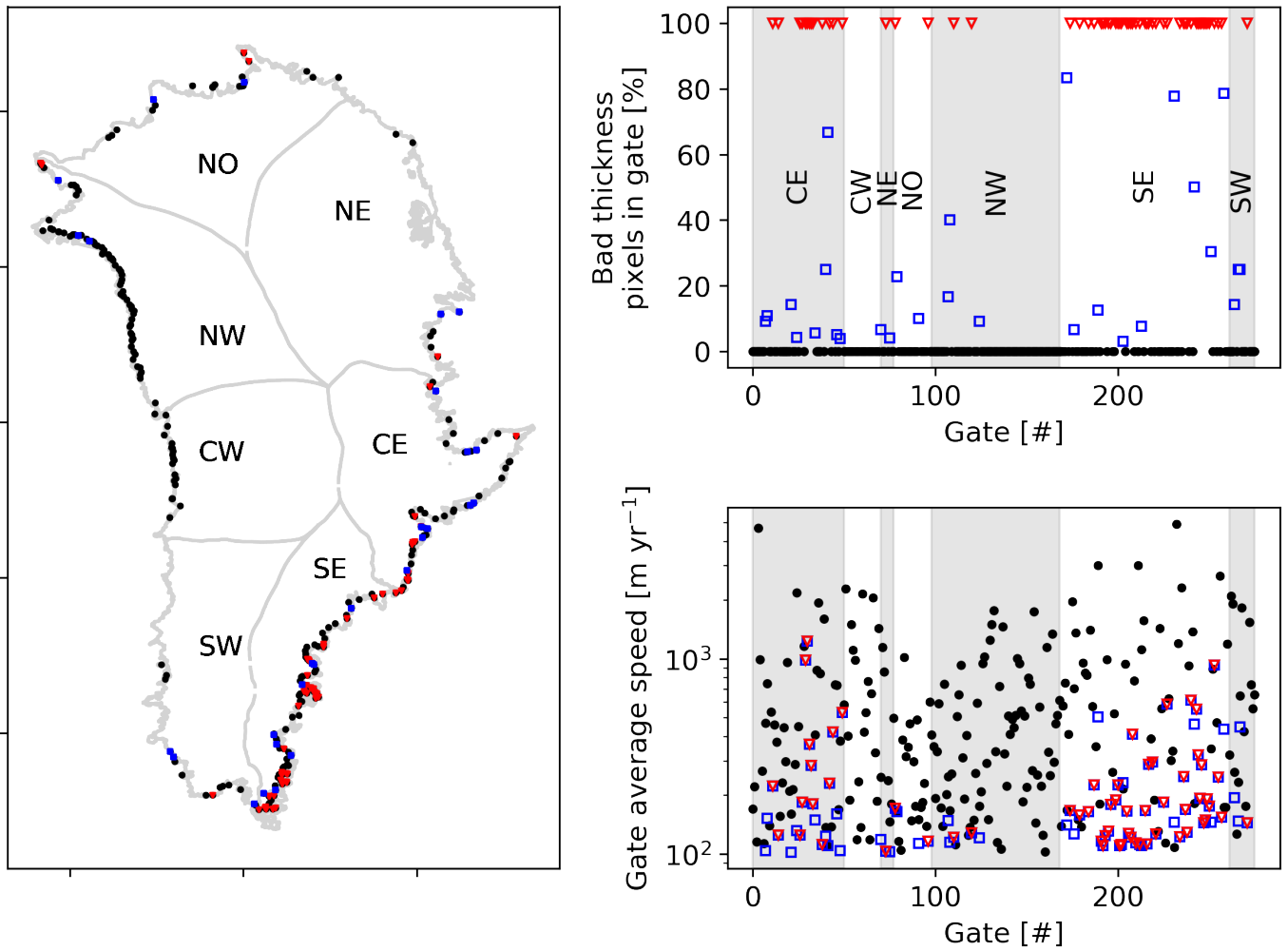


Figure A1. Gate locations and thickness quality. Left: locations of all gates. Black dots represent gates with 100 % valid thickness pixels, blue with partial, and red with none. Top right: Percent of bad pixels in each of the 276 gates, arranged by region. Bottom panel: Average speed of gates. Color same as left panel.

all three times, but pixel B has a filled gap at time t_3 . The concentration of valid pixels is 0.5, but the weighted concentration, or coverage, is $9/11$ or ~ 0.82 . When displaying these three discharge values, t_1 and t_4 would have opacity of 1 (black), and t_3 would have opacity of 0.82 (dark gray).

This treatment is applied at the pixel level and then weight-averaged to the gate, sector, region, and ice sheet results.

5 A3 Filtered Velocity

Here we show the same time series as in Figs. 4, 5, and 6 but without any velocity filtering applied.

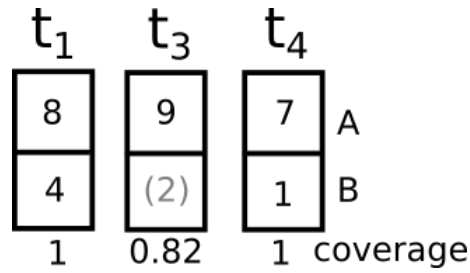


Figure A2. Schematic demonstrating coverage. Velocities are filled with linear interpolation in time, and coverage is weighted by discharge. t columns represent the same two gate pixels (A & B) at three time steps, where t_n are linearly spaced, but t_2 is not observed anywhere on the ice sheet and therefore not included. Numbers in boxes represents example discharge values. Gray parenthetical number is filled, not sampled, in pixel B at time t_3 . Weighted filling computes the coverage as $9/11 = 0.8\bar{1}$, instead of 0.5 (half of the pixels at time t_3 have observations).

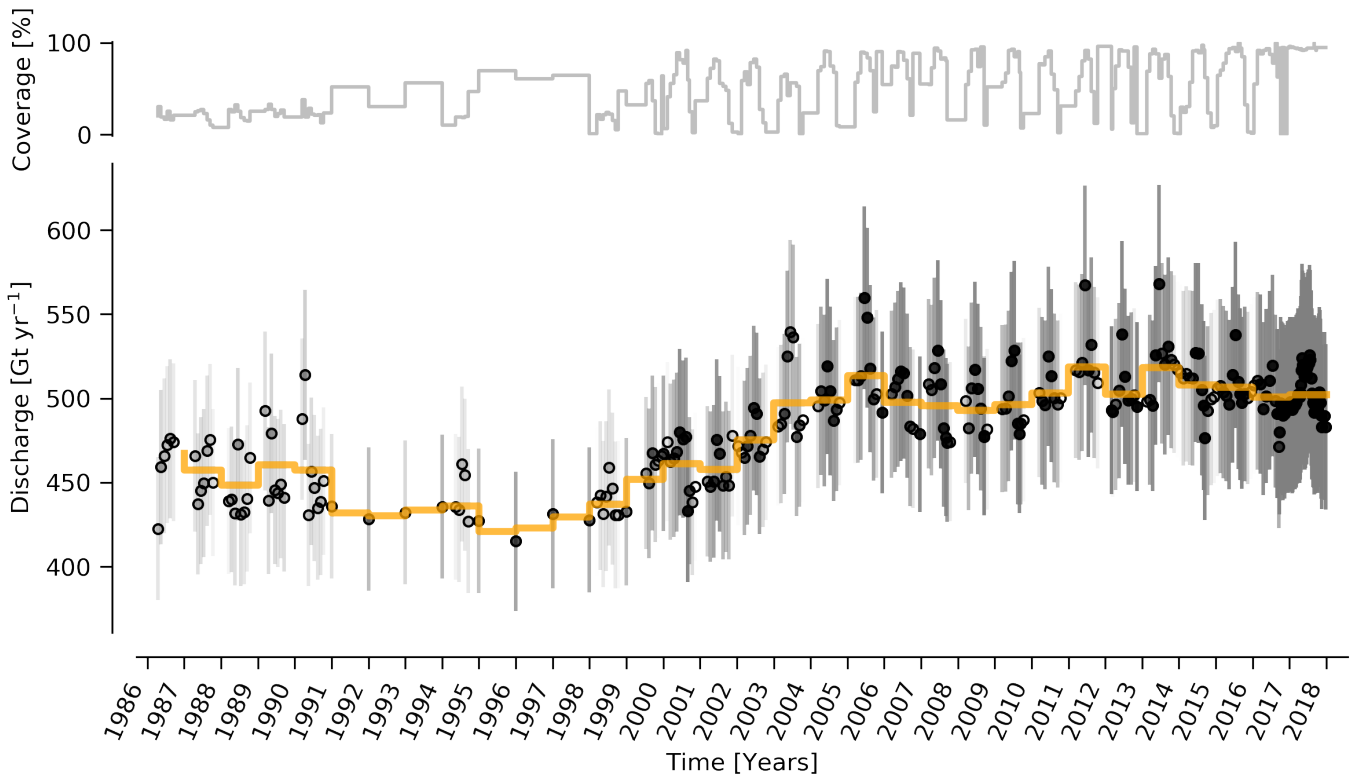


Figure A3. Same as Fig. 4 but without the velocity filter. Note different y-axis

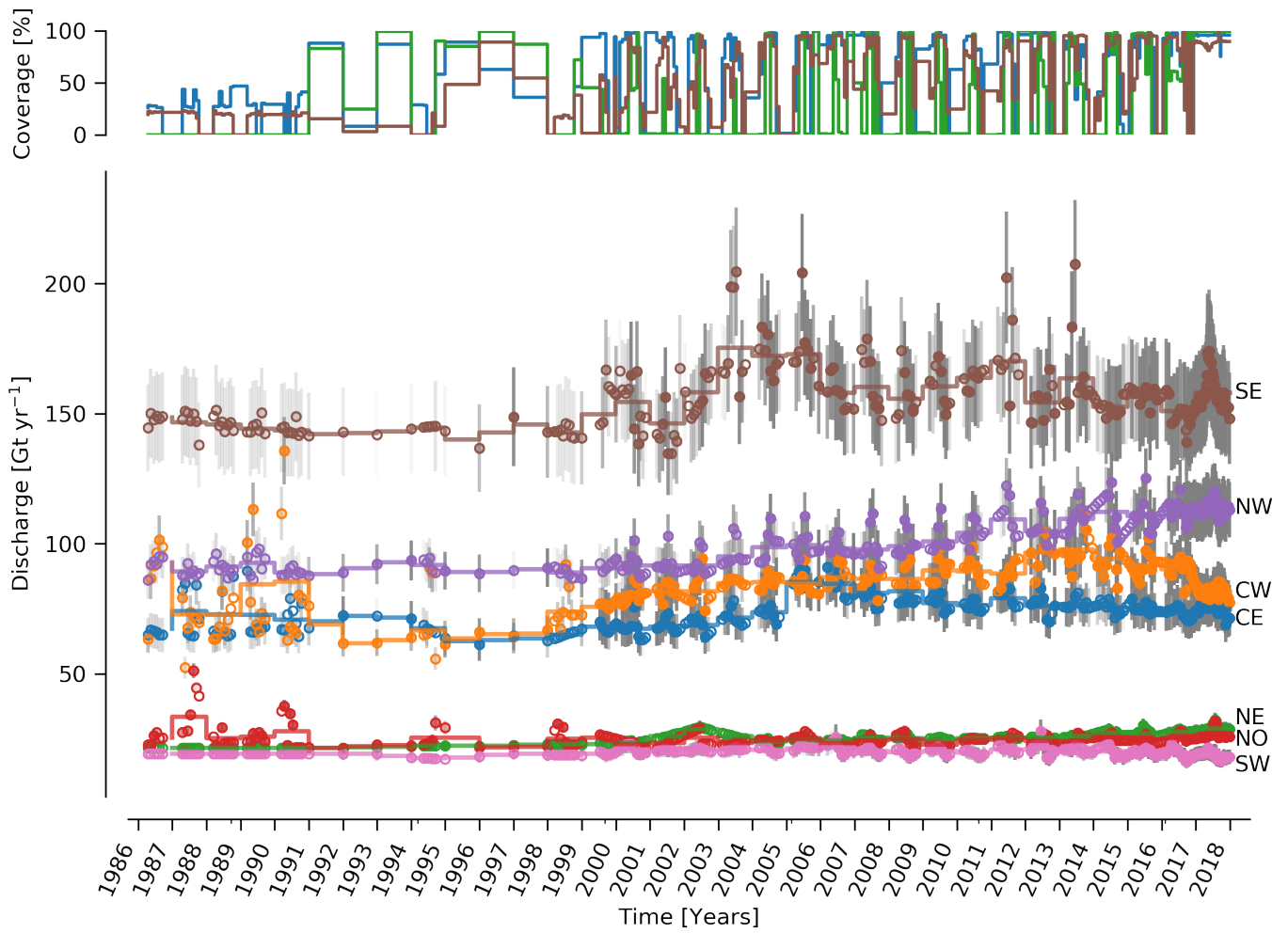


Figure A4. Same as Fig. 5 but without the velocity filter. Note different y-axis

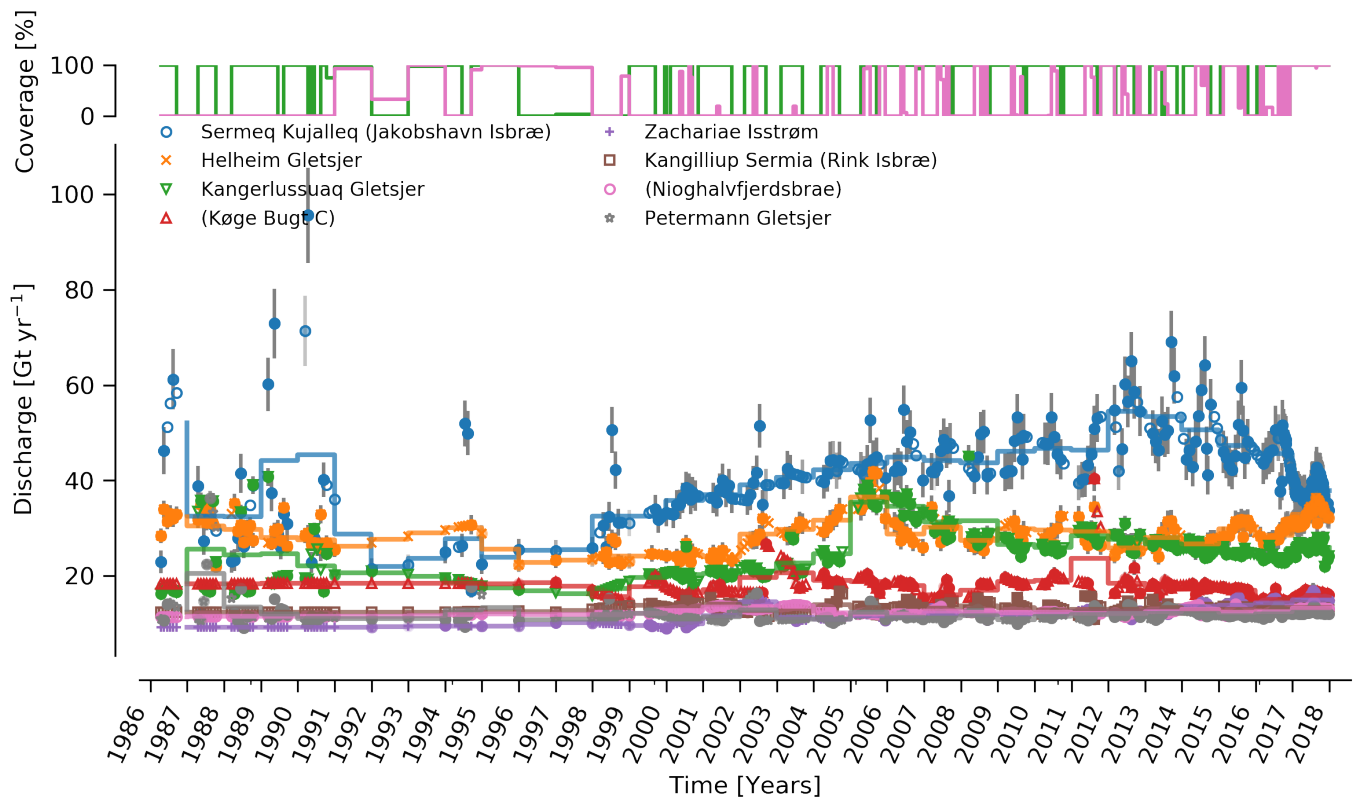


Figure A5. Same as Fig. 6 but without the velocity filter. Note different y-axis

Appendix B: Køge Bugt Bed Change between Bamber et al. (2013) and Morlighem et al. (2017b)

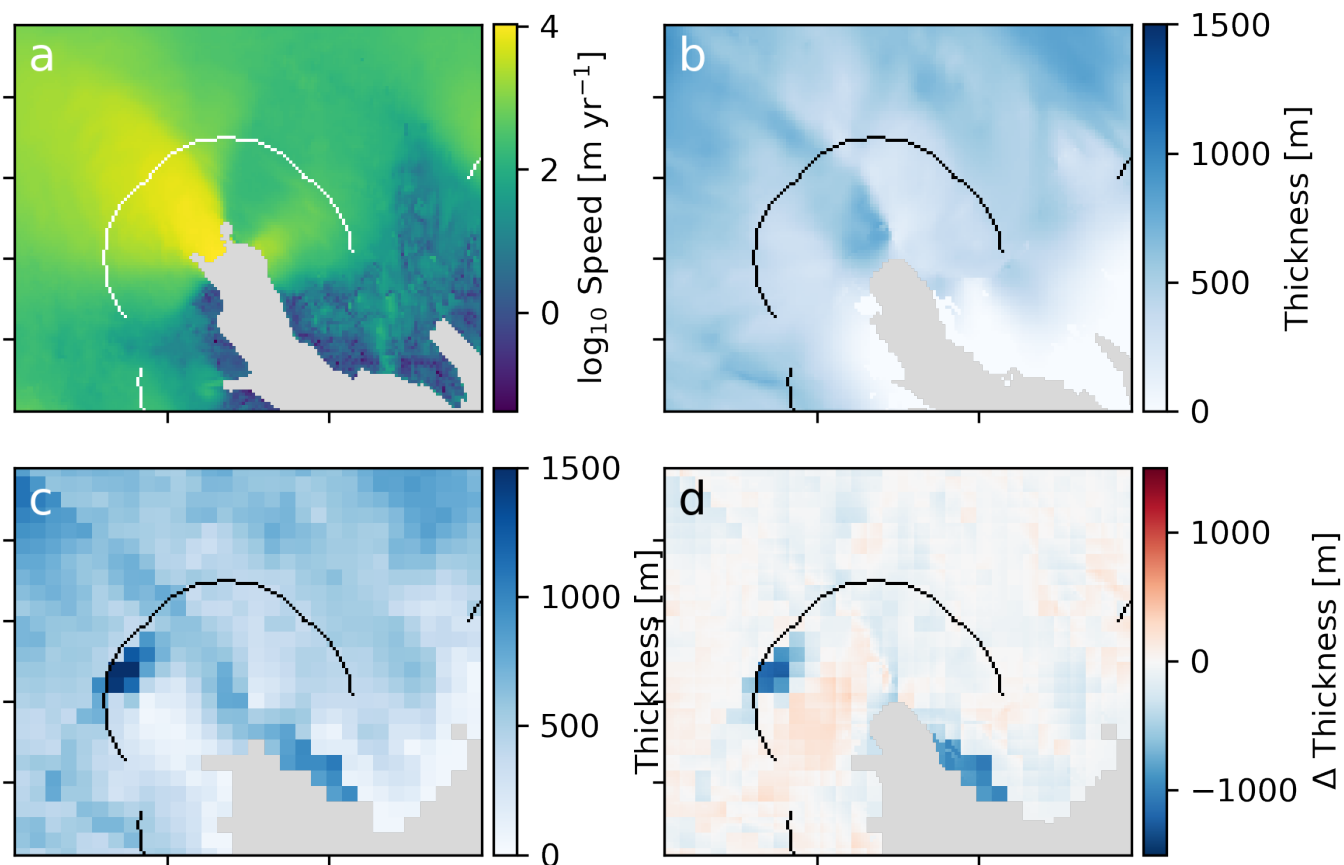


Figure B1. Differences between BedMachine (Morlighem et al., 2017b) and Bamber et al. (2013) near Køge Bugt. Panel (a) is baseline ice speed, (b) BedMachine thickness, (c) Bamber et al. (2013) thickness, and (d) difference computed as BedMachine - Bamber. Curved line is gate used in this work.

Appendix C: Sentinel-1 ice velocity maps

We use ESA Sentinel-1 synthetic aperture radar (SAR) data to derive ice velocity maps covering the Greenland Ice Sheet margin using offset tracking (Strozzi et al., 2002) assuming surface parallel flow using the digital elevation model from the Greenland Ice Mapping Project (GIMP DEM, NSIDC 0645) by Howat et al. (2014, 2015). The operational interferometric post processing (IPP) chain (Dall et al., 2015; Kusk et al., 2018), developed at the Technical University of Denmark (DTU) Space and upgraded with offset tracking for ESA's Climate Change Initiative (CCI) Greenland project, was employed to derive the surface movement. The Sentinel-1 satellites have a repeat cycle of 12 days, and due to their constellation, each track has a six-day repeat cycle. We produce a Greenland wide product that spans two repeat cycles of Sentinel-1 A. The product is a mosaic of all the ice velocity maps based on 12 day pairs produced from all the tracks from Sentinel-1 A and B covering Greenland during those two cycles. The product thus has a total time span of 24 days. Six day pairs are also included in each mosaic from track 90, 112 and 142 covering the ice sheet margin in the south as well as other tracks on an irregular basis in order to increase the spatial resolution. (Rathmann et al., 2017) and Vijay et al. (2019) have exploited the high temporal resolution of the product to investigate dynamics of glaciers. The maps are available from 2016-09-13 and onward, are updated regularly, and are freely available from <http://promice.dk>.

Appendix D: Software

This work was performed using only open-source software, primarily GRASS GIS (Neteler et al., 2012) and Python (Van Rossum and Drake Jr, 1995), in particular the Jupyter (Kluyver et al., 2016), pandas (McKinney, 2010), numpy (Oliphant, 2006), statsmodel (Seabold and Perktold, 2010), x-array (Hoyer and Hamman, 2017), and Matplotlib (Hunter, 2007) packages. The entire work was performed in Emacs using Org Mode (Schulte et al., 2012). The parallel (Tange, 2011) tool was used to speed up processing. We used proj4 (PROJ contributors, 2018) to compute the errors in the EPSG 3413 projection. All code used in this work is available in the Supplemental Material.